UNIVERSITÀ DELLA CALABRIA

Dipartimento di Fisica

Dottorato di Ricerca in

Scienze e Tecnologie Fisiche, Chimiche e dei Materiali

Ciclo

XXXIV

Hunting stabilization effects of the high-energy resummation at the LHC

Settore Scientifico Disciplinare
FIS/02 - Fisica Teorica, Modelli e Metodi Matematici

Coordinatore: Prof.ssa Gabriella CIPPARRONE

Firma ____ Firma oscurata in base alle linee guida del Garante della privacy

Supervisore: Prof. Ale[redacted]

Firma ____ Firma oscurata in base alle linee guida del Garante della privacy

Dottorando: Dott. Mohammed Maher Abdelrahim MOHAMMED

*Firma*____ Firma oscurata in base alle linee guida del Garante della privacy ____

Abstract

Studying semi-hard processes in the large center-of-mass energy limit gives us an opportunity to further test perturbative QCD in an unexplored kinematical configuration, contributing to a better understanding of the dynamics of strong interactions. For semi-hard reactions in kinematics at large center-of-mass energy $\sqrt{s}$, the BFKL resummation of energy logarithms comes into play, since large energy logarithms compensate the smallness of QCD coupling α_s and must therefore be accounted for to all perturbative orders.

Tracing the path toward performing precision calculations via BFKL resummation of high-energy logarithms, in this thesis we present phenomenological analyses for distinct inclusive processes, highlighting the recognized problem of instabilities under higher-order corrections and energy-scales variations, that would abort any possibility to investigate semi-hard reactions with high-precision at natural energy-scales. At the same time, we present new reactions that seem to act as fair stabilizers of the high-energy series.

First, the inclusive production at the LHC of a charged light hadron and of a jet, featuring a wide separation in rapidity, is presented making use of optimization methods to fix energy-scale. We report some predictions, tailored on the CMS and CASTOR acceptances, for the cross section averaged over the azimuthal angle between the identified jet and hadron and for azimuthal correlations. Then, we propose as a novel probe channel for the manifestation of the BFKL dynamics, the inclusive hadroproduction of a Higgs boson and of a jet, featuring large transverse momenta and well

separated in rapidity. We present predictions for azimuthal Higgs-jet correlations and other observables, to be possibly compared with typical experimental analyses at the LHC. Finlay, we propose the inclusive semi-hard production, in proton-proton collisions, of two bottom-flavored hadrons, as well as of a single bottom-flavored hadron accompanied by a light jet, as novel channels for targeting stabilization effects of the high-energy resummation under higher-order corrections. Moreover, we propose the study of double differential distributions in the transverse momenta of the two final-state particles as a common basis to investigate the interplay of different resummation approaches.

Sintesi in lingua italiana

Lo studio dei processi semiduri nel limite di alta energia nel centro di massa ci offre l'opportunità di testare ulteriormente la QCD perturbativa in una configurazione cinematica finora inesplorata, contribuendo a una migliore comprensione della dinamica delle interazioni forti. Per le reazioni semidure in cinematica a grande energia del centro di massa $\sqrt{s}$, entra in gioco la risommazione BFKL dei logaritmi di energia, poiché i logaritmi di grande energia compensano la piccolezza dell'accoppiamento QCD α_s e devono quindi essere calcolati a tutti gli ordini perturbativi.

Tracciando il percorso verso l'esecuzione di calcoli di precisione tramite la risommazione BFKL dei logaritmi ad alta energia, in questa tesi presentiamo analisi fenomenologiche per diversi processi inclusivi, evidenziando il noto problema delle instabilità sotto correzioni di ordine superiore e variazioni delle scale energetiche, che annullerebbero ogni possibilità per studiare reazioni semi-dure con alta precisione alle scale energetiche naturali per quei processi. Allo stesso tempo, presentiamo nuove reazioni che sembrano fungere da corretti stabilizzatori della serie ad alta energia.

In primo luogo, viene presentata la produzione inclusiva ad LHC di un adrone leggero carico e di un getto, caratterizzati da un'ampia separazione in rapidità, utilizzando metodi di ottimizzazione per fissare la scala energetica. Riportiamo alcune previsioni, adattate alle accettanze di CMS e CASTOR, per la sezione trasversale mediata sull'angolo azimutale tra getto e adrone identificati e per le correlazioni azimutali. Quindi, proponiamo come nuovo canale sonda per la manifestazione della dinamica BFKL, l'adroproduzione inclusiva di un bosone di Higgs e di un getto, caratterizzati

da grandi momenti trasversali e ben separati in rapidità. Presentiamo previsioni per le correlazioni azimutali di Higgs-jet e altre osservabili, da confrontare eventualmente con analisi sperimentali ad LHC. Infine, proponiamo la produzione semi-dura inclusiva, nelle collisioni protone-protone, di due adroni con sapore "bottom", nonché di un singolo adrone con sapore "bottom" accompagnato da un getto, come nuovi canali per studiare gli effetti di stabilizzazione ad alta energia sotto correzioni di ordine superiore. Proponiamo anche lo studio delle doppie distribuzioni differenziali nei momenti trasversi delle due particelle di stato finale come base comune per investigare l'interazione tra diversi approcci alla risommazione.

Contents

List of Figures

Introduction

The standard model (SM) of particle physics represents a unified description of the fundamental interactions that govern the dynamical behavior of the elementary particles at sub-atomic scale. The validity of SM has been leaned on a long history of theoretical speculations and experimental measurements, crowned with the discovery of the Higgs boson [1, 2], at the Large Hadron Collider (LHC). With more data to be collected at the LHC, the study of semi-hard processes[1] in the large center-of-mass energy limit allows us to further test perturbative QCD (pQCD) in unexplored kinematical configurations thus contributing to a better understanding of the dynamics of strong interactions. Within pQCD computations, reducing theoretical uncertainties coming from higher-order corrections is required to have a reliable estimate of the production rate. At high energies, the validity of the perturbative expansion, truncated at a certain order in the strong coupling α_s, is spoiled. This is due to the appearance of large logarithms of the center-of-mass energy squared, s, associated with the perturbative calculations and it is needed to resum them to all orders in α_s. The most powerful framework to perform this resummation is the Balitsky–Fadin–Kuraev–Lipatov (BFKL) [4–9] approach, initially developed at the so-called leading logarithmic approximation (LLA), where it prescribes how to resum all terms proportional to $(\alpha_s \ln s)^n$. To improve the obtained results at LLA, the so-called next-to-leading logarithmic approximation (NLA) was considered [10, 11], where also all

[1]Semi-hard processes [3] are those with center-of-mass energy squared s is substantially larger than one or more hard scales Q_i^2, $s \gg Q_i^2 \gg \Lambda_{QCD}^2$, with Λ_{QCD} is the QCD scale.

terms proportional to $\alpha_s(\alpha_s \ln s)^n$, were resumed. A significant question for collider phenomenology is highlighting at which energies the BFKL dynamics becomes significant and cannot be overlooked. Typical BFKL observables that can be studied at the LHC are the azimuthal coefficients of the Fourier expansion of the cross section differential in the variables of the tagged objects over the relative azimuthal-angle. They take a certain factorization form given as the convolution of a universal BFKL Green's function with process-dependent impact factors, the latter describing the transition from each colliding proton to the respective final-state identified object. The BFKL Green's function obeys an integral equation, whose kernel is known at the next-to-leading order (NLO) [10–14]. In order to confront the theoretical prediction with the observed data, we need the NLO corrections to impact factors, so as to treat different processes with consistent accuracy. So far the available impact factors calculated at NLO order are: 1) colliding-parton (quarks and gluons) impact factors [15,16], which represents the basis for constructing the 2) forward-jet impact factor [17–22] and 3) forward charged-light hadron one [23], 4) the impact factor describing the γ^* to light-vector-meson (LVM) leading twist transition [24], 5) the one detailing the $\gamma^* \to \gamma^*$ subprocess [25–30], and 6) the one for the production of a forward Higgs boson in the infinite top-mass limit [31,32].

Over last years, pursuing the goal of identifying observables that fit the data where BFKL approach is distinct, and other possible resummations approaches fail, a number of reactions have been proposed for different collider environments: the exclusive diffractive leptoproduction of two light vector mesons [33–37], the inclusive hadroproduction of two jets featuring large transverse momenta and well separated in rapidity (Mueller–-Navelet channel [38]), for which several phenomenological studies have appeared so far (see, *e.g.*, Refs. [20, 22, 39–50]), the inclusive detection of two light-charged rapidity-separated hadrons [51–53], three- and four-jet hadroproduction [54–62], J/Ψ-plus-jet [63], hadron-plus-jet [64], Higgs-plus-jet [65,66], heavy-

light dijet system [67,68] and forward Drell–Yan dilepton production with a possible backward-jet tag [69].

In phenomenological analyses of inclusive processes with a theoretical setup based on the BFKL resummation, a significant issue was recognized that NLA corrections both to the BFKL Green's function and impact factors turn out to be of the same size and with opposite sign of pure LLA contributions, that making the perturbative series highly unstable. This behavior manifests as a large uncertainty arising from the renormalization (and factorization) scale choice, which by its turn calls for some optimization procedure to make reliable predictions.

Recently, a new direction toward restoring the stability of the BFKL series at natural scales was initiated, via the analysis of semi-hard reactions with detected objects featuring large transverse masses, for example, the inclusive production of a Higgs in association with a jet [65,66], which bring evidence that high-energy resummed distributions in rapidity and transverse momentum exhibit solid stability under higher-order corrections. A relevant step in this direction was taken in [67,68,70], where a hybrid formalism combining the BFKL resummation and collinear factorization was adopted.

Aware of the importance to pursue the phenomenological paths toward looking for signals of stabilization of the high-energy resummation under higher-order corrections and energy-scale variation, we will study and discuss two distinct classes of semi-hard reactions, according to the necessity for stabilizing the (scale optimization) procedure of the perturbative series. The first type of processes we are interested in, are the reactions that show sensitivity to the renormalization/factorization scale choice, and cannot be studied at a "natural" scale, while the second processes are characterized by natural energy scales provided by the nature of the large transverse masses and kinematics configurations of the final detected particles, where there is no need to use scale optimization procedures.

The thesis is organized as follows: In Chapter 1, we present briefly the basic building blocks of BFKL formalism, such as the gluon Reggeization, the BFKL factorization structure of the amplitudes at LLA and NLA, and the definition of impact factors at both LLA and NLA. In Chapter 2, we will sketch a general framework used to describe inclusive processes at the hand of BFKL resummation, and investigate the Hadron-jet production channel, by addressing the previously mentioned issues of the unsuitability effects under choosing different energy-scales values. In Chapter 3, we present studies on Higgs-plus-jet and Bottom-flavored inclusive emissions as stabilizers of the high-energy resummation. In Chapter 4, we will make general conclusions and point to possible future outlooks.

The results presented in this thesis, specifically in chapter 3 and section 2.2 of chapter 2, are the subject of three publications:

- A.D. Bolognino, F.G. Celiberto, D.Yu. Ivanov, M.M.A. Mohammed, A. Papa, Eur. Phys. J. C **78** (2018) no.9, 772 [arXiv:1808.05483 [hep-ph]].
- F.G. Celiberto, D.Yu. Ivanov, M.M.A. Mohammed, A. Papa, Eur. Phys. J. C **81** (2021), 293 [arXiv:2008.00501 [hep-ph]].
- F.G. Celiberto, M. Fucilla, D.Yu. Ivanov, M.M.A. Mohammed, A. Papa, Phys. Rev. D. **104** (2021), 114007 [arXiv:2109.11875 [hep-ph]].

Chapter 1

Basics of the BFKL approach

The BFKL approach goes back to the middle of the 70-th of the last century, as an attempt to answer the question, what is the structure of the Pomeron in the gauge field theories, in particular, what is the perturbative QCD (pQCD) Pomeron. In pQCD, for scattering of particles at high center-of-mass (c.o.m) energy $\sqrt{s}$, and fixed transfer momentum t (i.e. not growing with s), the amplitude is dominated by Reggeized gluons exchanges in the t-channel, and goes like $s^{j(t)}$ within BFKL approach. This chapter is devoted to showing the main building blocks used in the derivation of BFKL equation which determines the behavior pQCD amplitudes at high-energies in which vacuum quantum numbers are exchanged in the t-channel, by resumming order by order terms proportional to powers of large energy logarithms that appear in the perturbative series. A pedagogical derivation of the BFKL equation in momentum space can be found in the textbooks [71–73], our presentation focuses on those points which will be relevant for the rest of this thesis. In the first section, we discuss Gluon Reggeization, the second and third sections are dedicated to presenting the BFKL approach in both leading (LLA) and next-to-leading (NLA) approximations, respectively. Finally, the derivation of the BFKL amplitude in multi-Regge kinematics, and the definition of the impact factors are presented.

1.1 Gluon Reggeization

The cornerstone of the BFKL approach is the gluon Reggeization, the notion of Reggeization of elementary particles in perturbation theory dates back to the work of Gell-Mann and his collaborators [74–76]. The Reggeization of a given elementary particle of spin j and mass m usually means that the amplitude of a scattering process with exchange of the quantum numbers of that particle in the t-channel goes like $s^{j(t)}$, in the limit $s \gg |t|$ (Regge limit). The function $j(t)$ is called the Regge trajectory of the given particle and takes the value of the spin of that particle when t is equal to its squared mass. In perturbative QCD, the notion of gluon Reggeization means that for a scattering process in a dynamical regime with large $\sqrt{s}$ and fixed transfer momentum t (i.e. not growing with s), the leading contribution in each order of perturbation theory to the process amplitude is given by the Reggeized gluon. The Reggeization of the gauge boson was checked in both QED and QCD, where in the former case only the electron does Reggeize in perturbation theory [76], but the photon remains elementary [77], and in the latter case all elementary particles of the theory are Reggeize (eg.gluons [5,6], [8,78,79], as well as quark [80–82]). The gluon Reggeization is very important at high-energy processes since the exchanges of the gluon in the t-channel provide nondecrease of cross sections with energy, where the Reggeized gluon is a gluon with a modified propagator of the form

$$D_{\mu\nu}(s, q^2) = -i\frac{q_{\mu\nu}}{q^2}\left(\frac{s}{s_0}\right)^{\alpha_g(q^2)-1}, \tag{1.1}$$

where $\alpha_g(q^2) = 1 + \omega(t)$ is the gluon trajectory.

The simplest realization of the gluon Reggeization is in the elastic process $A + B \to A' + B'$ (Fig 1.1), with an exchange of gluon quantum numbers in the t-channel. Gluon Reggeization means that in the Regge kinematical region $s \simeq -u \to \infty$, t fixed (i.e.

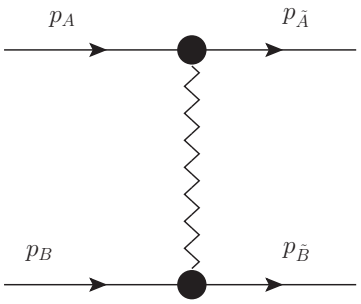

Figure 1.1: **The process $A + B \to A' + B'$ with colour octet in the t channel and negative signature. The zigzag line represent Reggeized gluon exchange.**

not growing with s), the amplitude of this process takes the Regge form

$$(A_8)^{A'B'}_{AB} = \Gamma^c_{AA'} \frac{s}{t} \left[\left(\frac{s}{-t} \right)^{\omega(t)} + \left(\frac{-s}{-t} \right)^{\omega(t)} \right] \Gamma^c_{BB'}, \tag{1.2}$$

which is valid in the LLA as well as in the NLA. Here, c is a colour index, and $\Gamma^c_{pp'}$ are the particle-particle-Reggeon (PPR) vertices[1], not depending on s, and $\omega(t)$ is the Reggeized gluon trajectory, at 1-loop is determined by the s-channel discontinuity of the amplitudes. It reads

$$\omega^{(1)}(t) = \frac{g^2 N_c t}{2(2\pi)^{D-1}} \int \frac{d^{D-2} q_1}{\vec{q_1}^{\,2} (\vec{q} - \vec{q_1})^2} \simeq -\frac{g^2 N_c \Gamma(1-\epsilon)}{(4\pi)^{2+\epsilon}} \frac{2}{\epsilon} \left(\vec{q}^{\,2} \right)^{\epsilon}. \tag{1.3}$$

The space-time dimension $D = 4 + 2\epsilon$ is taken different from 4 to regularize infrared divergencies.

1.2 BFKL in LLA

If we consider inelastic amplitude for the process $A + B \to A' + B' + n$ (see Fig 1.2), where n is a system of produced particles with momenta k_i ($i = 1, ..., n$). In the

[1] At leading-order PPR vertices are determined by the Born amplitudes

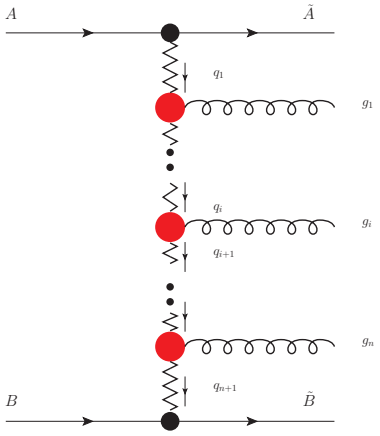

Figure 1.2: **Diagrammatical representation of the production amplitude $A_{AB}^{A'B'+n}$ in LLA.**

LLA the main contributions to the unitarity relations come from the multi-Regge kinematics (MRK)[2], where the real part of the production amplitude can be written in the factorized form

$$(A_8)_{AB}^{A'B'+n} = 2s\Gamma_{AA'}^{c_1}\left[\prod_{i=1}^{n}\gamma_{c_ic_i+1}^{P_i}(q_i,q_{i+1})\,\frac{1}{t_i}\left(\frac{s_i}{s_R}\right)^{\omega_i}\right]\frac{1}{t_{n+1}}\left(\frac{s_{n+1}}{s_R}\right)^{\omega_{n+1}}\Gamma_{BB'}^{c_{n+1}}, \qquad (1.4)$$

where $\gamma_{c_ic_i+1}^{P_i}(q_i,q_{i+1})$ are the gauge invariant effective vertices of two t-channel gluons (Reggeon) with color indices $c_{i,i+1}$ and momenta $q_{i,i+1}$, to a produced s-channel gluons of momenta $k_i = q_i - q_{i+1}$, $q_0 \equiv p_A$, $q_{n+1} \equiv -p_B$, $s_i = (k_{i-1}+k_i)^2$, $k_0 \equiv p_{\tilde{A}}$, $k_{n+1} \equiv p_{\tilde{B}}$, and ω_i stand for $\omega(t_i)$, with $t_i = q_i^2$. The elastic amplitude for the process $A + B \to A' + B'$ at high-energies can be obtained from the previous expression for the production

[2]When rapidities of the produced particles are strongly ordered and their transverse momenta do not grow with s.

amplitudes by using s-channel unitarity, and reads

$$A_{AB}^{A'B'} = \frac{is}{(2\pi)^{D-2}} \int \frac{d^{D-2}q_1}{\vec{q}^2{}_1 \vec{q}_1'^2} \frac{d^{D-2}q_2}{\vec{q}^2{}_2 \vec{q}_2'^2} \int_{\delta-i\infty}^{\delta+i\infty} \frac{d\omega}{\sin(\pi\omega)} \sum_{R,\nu} \Phi_{AA'}^{(R,\nu)}(\vec{q}_1;\vec{q};s_0) \times \left[\left(\frac{s}{s_0}\right)^{\omega} - \tau \left(\frac{-s}{s_0}\right)^{\omega} \right] G_{\omega}^{(R)}(\vec{q}_1,\vec{q}_2;\vec{q}) \Phi_{BB'}^{(R,\nu)}(-\vec{q}_2;-\vec{q};s_0). \quad (1.5)$$

The quantities $\Phi_{PP'}^{(R,\nu)}$ are the so-called impact factors in the t-channel color state (R,ν), they are process dependent parts, describing the transition $A \to A'$ and $B \to B'$, the summation is over the color group irreducible representations R, which are contained in the product of two adjoint representations and over its states ν. The function $G_{\omega}^{(R)}$ represents the Mellin transform of the Green's functions for Reggeon-Reggeon scattering and obeys the following iterated equation:

$$\omega G_{\omega}^{(R)}(\vec{q}_1,\vec{q}_2;\vec{q}) = \vec{q}_1^2 \vec{q}_1^{2\prime} \delta^{D-2}(\vec{q}_1-\vec{q}_2) + \int \frac{d^{D-2}\vec{q}_r}{\vec{q}_r^2 \vec{q}_r^{2\prime}} K^{(R)}(\vec{q}_1,\vec{q}_r;\vec{q}) G_{\omega}^{(R)}(\vec{q}_r,\vec{q}_2;\vec{q}), \quad (1.6)$$

whose integral kernel is

$$K^{(R)}(\vec{q}_1,\vec{q}_2;\vec{q}) = \left[\omega(-\vec{q}_1^2) + \omega(-\vec{q}_1^{2\prime})\right] \delta^{D-2}(\vec{q}_1-\vec{q}_2) + K_r^{(R)}(\vec{q}_1,\vec{q}_2;\vec{q}), \quad (1.7)$$

where the first term related to the gluon trajectory corresponds to the virtual corrections, while the second one corresponds to the real ones. The BFKL equation is the integral equation given in Eq (1.6), and is valid for $t = 0$ and singlet ($R = 0$) quantum numbers in the t-channel.

1.3 BFKL in NLA

The ingredients used to compute BFKL equation at NLA [83], were the 2-loop gluon Regge trajectory [84,85], the 1-loop vertex for production of one gluon in the collision

of two Reggeons (the Lipatov effective vertex [86]),the -Born level- vertices for two gluon emission [87,88] and for the production of a quark-antiquark pair [89].

In the NLA the unitarity relations must be modified from two perspectives: the first one due to the 1-loop corrections in effective vertex for the production of the particles P_i, and the particle-particle-Reggeon vertices, these set of corrections is realized by performing one of the following replacements in the production amplitudes 1.4:

$$\omega^{(1)} \to \omega^{(2)}, \quad \Gamma^{C(Born)}_{P'P} \to \Gamma^{C(1-loop)}_{P'P}, \gamma^{G_i(Born)}_{c_i c_{i+1}} \to \gamma^{G_i(1-loop)}_{c_i c_{i+1}}.$$

The second set of modifications is consists of allowing the emission of one pair of particles with rapidities of the same order of magnitude, both in the central or in the fragmentation region, this means performing one of the following replacements in the production amplitudes 1.4:

$$\Gamma^{C(Born)}_{P'P} \to \Gamma^{C(Born)}_{\{f\}P}, \gamma^{G_i(Born)}_{c_i c_{i+1}} \to \gamma^{Q\bar{Q}(Born)}_{c_i c_{i+1}}, \quad \gamma^{G_i(Born)}_{c_i c_{i+1}} \to \gamma^{GG(Born)}_{c_i c_{i+1}},$$

where $\Gamma_{\{f\}P}$ stands for the all intermediate states in the fragmentation region of particle P scattering off Reggeon, and $\gamma^{Q\bar{Q}}, \gamma^{GG}$ are the effective vertices for the production of a quark-antiquark pair and of a two-gluon pair, respectively.

At NLA the terms proportional to β_0, that account for the inclusion of the running of the coupling, introduce a logarithmic dependence in momentum space representation, thus the positiveness of cross sections is not always ensured. Moreover, the NLL corrections to the BFKL Green's function are known to be very large and negative [90], and all that led to many ways to improve the convergence of the perturbative series [91–96].

1.4 The BFKL amplitude

To draw a general scheme about how to study different processes within NLA BFKL approach (which depends on the available NLO impact factors), let us consider the following process which involves the exchange of the vacuum quantum numbers in the t-channel: $A + B \to A' + B'$.

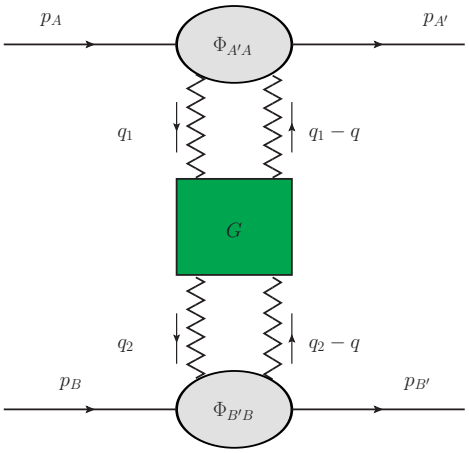

Figure 1.3: **Diagrammatic representation of the imaginary part of amplitude for the process** $A + B \to A' + B'$.

Using the optical theorem [97–99], the total cross-section of this process reads

$$\sigma_{AB}(s) = \frac{\mathrm{Im}_s A_{AB}^{A'B'}}{s}. \tag{1.8}$$

Within BFKL approach, the imaginary part expression of the amplitude can be factorized [83] as a convolution of the Green's function of two interacting Reggeized gluons with the impact factors[3] (vertices $\Phi_{A\to A'}$ and $\Phi_{B\to B'}$) of the colliding particles

[3]Which are practically the couplings of the pomeron to the hadrons.

$[\Phi_{A\to A'} \otimes G \otimes \Phi_{B\to B'}]$, and it is given as

$$\mathrm{Im}_s A_{AB}^{A'B'} = \frac{s}{(2\pi)^{D-2}} \int \frac{d^{D-2}q_1}{\overrightarrow{q}_1} \Phi_A(\overrightarrow{q}_1, s_0) \int_{\delta-i\infty}^{\delta+i\infty} \frac{d\omega}{2\pi i} \left(\frac{s}{s_0}\right)^{\omega} G_\omega(\overrightarrow{q}_1, \overrightarrow{q}_2) \times \int \frac{d^{D-2}q_2}{\overrightarrow{q}_2} \Phi_B(-\overrightarrow{q}_2, s_0), \quad (1.9)$$

where $\overrightarrow{q}_1$, $\overrightarrow{q}_2$ are the transverse momenta of the Reggeized gluons, s the squared center-of-mass energy and s_0 are arbitrary energy scale parameter. The Green's function $G_\omega(\overrightarrow{q}_1, \overrightarrow{q}_2)$ is process independent and obeys the BFKL equation,

$$\omega G_\omega(\overrightarrow{q}_1, \overrightarrow{q}_2) = \delta^{D-2}(\overrightarrow{q}_1 - \overrightarrow{q}_2) + \int d^{D-2}\overrightarrow{q} K(\overrightarrow{q}_1, \overrightarrow{q}) G_\omega(\overrightarrow{q}, \overrightarrow{q}_2), \quad (1.10)$$

with $K(\overrightarrow{q}_1, \overrightarrow{q})$ the BFKL kernel. The BFKL kernel determines the energy dependence of scattering amplitudes. The vertices (impact factors $\Phi_{A\to A'}, \Phi_{B\to B'}$) depend on the particular process under analysis, they are known in NLA for a few processes, in particular, the impact factors for colliding-parton (quarks and gluons) impact factors [15,16], which represent the common basis for the calculation of the forward-jet impact factor [17–22], and of the forward light-charged hadron one [23]; the impact factor describing the γ^* to light-vector-meson leading twist transition [24], and the γ^* to γ^* transition [25–30], and recently, the one for the production of a forward Higgs boson in the infinite top-mass limit [31,32].

Now to derive the general form for the amplitude in the so-called (ν, n)-representation, it is favorable to work within the transverse momentum representation, which is defined as,

$$\hat{\overrightarrow{q}} \,|\, \overrightarrow{q}_i\rangle = \overrightarrow{q}_i \,|\, \overrightarrow{q}_i\rangle\,, \quad \langle \overrightarrow{q}_1 | \overrightarrow{q}_2\rangle = \delta^{(2)}(\overrightarrow{q}_1 - \overrightarrow{q}_2),$$
$$\langle A|B\rangle = \langle A|\overrightarrow{k}\rangle\langle\overrightarrow{k}|B\rangle = \int d^2k A(\overrightarrow{k}) B(\overrightarrow{k}). \quad (1.11)$$

The BFKL kernel $K(\overrightarrow{q}_1, \overrightarrow{q}_2)$ becomes

$$K(\overrightarrow{q}_1, \overrightarrow{q}_2) = \langle \overrightarrow{q}_1 | \hat{K} | \overrightarrow{q}_2 \rangle , \tag{1.12}$$

and the equation (1.10) reads

$$\omega \langle \overrightarrow{q}_1 | \hat{G}_\omega | \overrightarrow{q}_2 \rangle = \langle \overrightarrow{q}_1 | \overrightarrow{q}_2 \rangle + \int d^2 \overrightarrow{q} \, \langle \overrightarrow{q}_1 | \hat{K} | \overrightarrow{q} \rangle \langle \overrightarrow{q} | \hat{G}_\omega | \overrightarrow{q}_2 \rangle ,$$

$$\omega \langle \overrightarrow{q}_1 | \hat{G}_\omega | \overrightarrow{q}_2 \rangle - \langle \overrightarrow{q}_1 | \hat{K}\hat{G}_\omega | \overrightarrow{q}_2 \rangle = \langle \overrightarrow{q}_1 | \overrightarrow{q}_2 \rangle ,$$

$$\langle \overrightarrow{q}_1 | (\omega - \hat{k})\hat{G}_\omega | \overrightarrow{q}_2 \rangle = \langle \overrightarrow{q}_1 | \overrightarrow{q}_2 \rangle , \tag{1.13}$$

which has the solution

$$\hat{G}_\omega = (\omega - \hat{k})^{-1}. \tag{1.14}$$

The kernel expanded in terms of the strong coupling, given as

$$\hat{K} = \bar{\alpha}_S \hat{K}^0 + \bar{\alpha}_S^2 \hat{K}^1, \tag{1.15}$$

with $\bar{\alpha}_S = \alpha_S N_c/\pi$, and N_c the number of colours, $\hat{K}^0$ and $\hat{K}^1$ are BFKL kernel in LLA and NLA accuracy, respectively. Using this kernel expansion we can rewrite the Green function operator $\hat{G}_\omega$ with NLA accuracy as

$$\hat{G}_\omega = (\omega - \bar{\alpha}_S \hat{K}^0)^{-1} + (\omega - \bar{\alpha}_S \hat{K}^0)^{-1}(\bar{\alpha}_s^2 \hat{K}^1)(\omega - \bar{\alpha}_S \hat{K}^0)^{-1} + \mathcal{O}\left[(\bar{\alpha}_s^2 \hat{K}^1)^2\right]. \tag{1.16}$$

In this representation the amplitude (1.9) takes the form

$$Im_s A_{AB}^{A'B'} = \frac{s}{(2\pi)^{D-2}} \int_{\delta - i\infty}^{\delta + i\infty} \frac{d\omega}{2\pi i} \left(\frac{s}{s_0}\right)^\omega \langle \frac{\Phi_A}{\overrightarrow{q}_1} | \hat{G}_\omega | \frac{\Phi_B}{\overrightarrow{q}_2} \rangle . \tag{1.17}$$

The basis of the eigenfunction of $\hat{K}^0$, with $\chi(\nu, n)$ LLA BFKL trajectory,

$$\hat{K}^0 \left|\nu, n\right\rangle = \chi(\nu, n) \left|\nu, n\right\rangle, \quad \chi(\nu, n) = 2\psi(1) - \psi(\frac{n}{2} + \frac{1}{2} + i\nu) - \psi(\frac{n}{2} + \frac{1}{2} - i\nu), \tag{1.18}$$

with $\psi(x) = \Gamma'(x)/\Gamma(x)$, is the logarithmic derivative of the Euler gamma function; is given by the set of functions bellow

$$\left\langle \overrightarrow{q} \right|\left.\nu, n\right\rangle = \frac{1}{\pi\sqrt{2}}(\overrightarrow{q}^2)^{i\nu - 1/2} e^{in\phi}, \tag{1.19}$$

where ϕ is the azimuthal angle of $\overrightarrow{q}$. So, the orthonormality and completeness conditions, respectively read

$$\left\langle \nu', n' \right|\left.\nu, n\right\rangle = \int \frac{d^2q}{2\pi^2}(\overrightarrow{q}^2)^{i\nu - i\nu' - 1} e^{i(n-n')\phi} = \delta(\nu - \nu')\delta_{nn'}. \tag{1.20}$$

$$\hat{1} = \sum_{n=-\infty}^{+\infty} \int_{-\infty}^{+\infty} d\nu \left|\nu, n\right\rangle \left\langle \nu, n\right|. \tag{1.21}$$

Using (1.21) twice in (1.17) we will end up with

$$Im_s A_{AB}^{A'B'} = \frac{s}{(2\pi)^{D-2}} \sum_{n=-\infty}^{+\infty} \int_{-\infty}^{+\infty} d\nu \sum_{n'=-\infty}^{+\infty} \int_{-\infty}^{+\infty} d\nu' \int_{\delta - i\infty}^{\delta + i\infty} \frac{d\omega}{2\pi i} \left(\frac{s}{s_0}\right)^{\omega}$$

$$\times \left\langle \frac{\Phi_A}{\overrightarrow{q}_1} \right|\left.\nu, n\right\rangle \left\langle \nu, n\right| \hat{G}_\omega \left|\nu', n'\right\rangle \left\langle \nu', n'\right| \left.\frac{\Phi_B}{\overrightarrow{q}_2}\right\rangle, \tag{1.22}$$

where $\left\langle \frac{\Phi_1}{\overrightarrow{q}_1} \right|\left.\nu, n\right\rangle$ and $\left\langle \nu', n'\right| \left.\frac{\Phi_2}{\overrightarrow{q}_2}\right\rangle$ are projections of the impact factors onto the eigenfunctions of LO BFKL, and are given as

$$\left\langle \frac{\Phi_A}{\overrightarrow{q}_1} \right|\left.\nu, n\right\rangle \equiv \int d^2q_1 \frac{\Phi_A(\overrightarrow{q}_1)}{\overrightarrow{q}_1^2} \frac{1}{\pi\sqrt{2}}(\overrightarrow{q}_1^2)^{i\nu - \frac{1}{2}} e^{in\phi_1}. \tag{1.23}$$

$$\langle \nu, n | \frac{\Phi_B}{\overrightarrow{q}_2} \rangle \equiv \int d^2 q_2 \frac{\Phi_B(\overrightarrow{-q}_2)}{\overrightarrow{q}_2^2} \frac{1}{\pi\sqrt{2}} (\overrightarrow{q}_2^2)^{-i\nu-\frac{1}{2}} e^{-in\phi_2}. \tag{1.24}$$

The action of the full NLO BFKL kernel on the set of functions Eq (1.19) is expressed as follows:

$$\hat{K} |\nu, n\rangle = \bar{\alpha}_s(\mu_R)\chi(\nu, n) |\nu, n\rangle + \bar{\alpha}_s^2(\mu_R)\Big(\chi^{(1)}(\nu, n) + \frac{\beta_0}{4N_c}\chi(\nu, n)\ln(\mu_R^2)\Big) |\nu, n\rangle$$

$$+ \bar{\alpha}_s^2 \frac{\beta_0}{4N_c}\chi(\nu, n)\Big(i\frac{\partial}{\partial\nu}\Big) |\nu, n\rangle , \tag{1.25}$$

where μ_R is the renormalization scale; the first term represents the action of LO kernel, while the second and the third ones stand for the diagonal and the non-diagonal parts of the NLO kernel,

$$\beta_0 = \frac{11}{3}N_c - \frac{2}{3}n_f, \tag{1.26}$$

is the first coefficient of the QCD β-function, where n_f is the number of active flavors.

Knowing the action of the kernel (as in Eq. (1.18)), we can use Eq. (1.16) to write the matrix element $\langle \nu, n | \hat{G}_\omega |\nu', n'\rangle$ of the BFKL Green's function in NLA,

$$\langle n, \nu | \hat{G}_\omega |n, \nu'\rangle = \delta_{nn'}\delta(\nu - \nu')\Big[\frac{1}{\omega - \overline{\alpha}_s\chi(n, \nu)} + \frac{1}{(\omega - \overline{\alpha}_s\chi(n, \nu))^2}$$

$$\times \Big(\overline{\alpha}_s^2\Big(\chi^{(1)}(n, \nu) + \frac{\beta_0}{4N_c}\chi(n, \nu)\ln(\mu_R)^2\Big)\Big)\Big]$$

$$+ \frac{\overline{\alpha}_s^2 \frac{\beta_0}{4N_c}\chi(n, \nu')\delta_{nn'}}{(\omega - \overline{\alpha}_s\chi(n, \nu))(\omega - \overline{\alpha}_s\chi(n, \nu'))}\Big(i\frac{\partial}{\partial\nu'}\delta(\nu - \nu')\Big), \tag{1.27}$$

where the first part is LLA contribution, while other remaining terms are due to the diagonal and the non-diagonal parts of NLO kernel $\hat{K}^1$, the function $\chi^{(1)}(\nu, n)$ for general conformal spin n,has been calculated in Ref. [100], and conveniently given by

$$\chi^{(1)}(\nu, n) = -\frac{\beta_0}{8N_c}\Big(\chi^2(\nu, n) - \frac{10}{3}\chi(\nu, n) - i\chi'(\nu, n)\Big) + \bar{\chi}(\nu, n), \tag{1.28}$$

where

$$\bar{\chi}(\nu,n) = -\frac{1}{4}\Big[\frac{\pi^2-4}{3}\chi(\nu,n) - 6\zeta(3) - \chi''(\nu,n) + 2\phi(\nu,n) + 2\phi(-\nu,n)$$

$$+ \frac{\pi^2\sinh(\pi\nu)}{2\nu\cosh^2(\pi\nu)}\Big(\Big(3+\Big(1+\frac{n_f}{N_c^3}\Big)\frac{11+12\nu^2}{16(1+\nu^2)}\Big)\delta_{n0} - \Big(1+\frac{n_f}{N_c^3}\Big)\frac{1+4\nu^2}{32(1+\nu^2)}\delta_{n2}\Big)\Big], \tag{1.29}$$

$$\phi(\nu,n) = -\int_0^1 dz\frac{x^{-1/2+i\nu+n/2}}{1+x}\Big[\frac{1}{2}\Big(\psi'(\frac{n+1}{2}) - \zeta(2)\Big) + Li_2(x) + Li_2(-x)$$

$$+ \ln x\Big(\psi(n+1) - \psi(1) + \ln(1+x) + \sum_{k=1}^{\infty}\frac{(-x)^k}{k+n}\Big) + \sum_{k=1}^{\infty}\frac{x^k}{(k+n)^2}(1-(-1)^k)\Big]$$

$$= \sum_{k=1}^{\infty}\frac{(-1)^{k+1}}{k+(n+1)/2+i\nu}\Big[\psi'(k+n+1) - \psi'(k+1) + (-1)^{k+1}(\beta'(k+n+1)$$

$$+ \beta'(k+1) - \frac{1}{k+(n+1)/2+i\nu}(\psi(k+n+1) - \psi(k+1))\Big] \tag{1.30}$$

with

$$\beta'(z) = \frac{1}{4}\Big[\psi'\Big(\frac{z+1}{2}\Big) - \psi'\Big(\frac{z}{2}\Big)\Big], \qquad Li_2(x) = -\int_0^x dt\frac{\ln(1-t)}{t}. \tag{1.31}$$

The impact factors in Eqs. (1.23) and (1.24) expanded in terms of α_s, read

$$\Phi_{1,2} = \alpha_s(\mu_R)\Big(c_{1,2}(\nu,n) + \alpha_s(\mu_R)c_{1,2}^{(1)}(\nu,n)\Big), \tag{1.32}$$

where $c_{1,2}(\nu,n)$ and $c_{1,2}^{(1)}(\nu,n)$ are the LO and NLO impact factors in the (ν,n)-representation, respectively.

Substituting Eq (1.28) in Eq (1.27), we can write the matrix element as

$$\langle n,\nu|\,\hat{G}_\omega\,|n,\nu'\rangle = \delta_{nn'}\delta(\nu-\nu')\Big[\frac{1}{\omega-\overline{\alpha}_s\chi(n,\nu)} + \frac{\overline{\alpha}_s^2}{(\omega-\overline{\alpha}_s\chi(n,\nu))^2}$$

$$\times\Big\{\overline{\chi}(n,\nu) + \frac{\beta_0}{4N_c}\chi(n,\nu)\Big(-\chi(n,\nu) + \frac{10}{3} + 2\ln(\mu_R)^2 + i\frac{\partial}{\partial\nu}\chi(n,\nu)\Big)\Big\}\Big]$$

$$+\frac{\overline{\alpha}_s^2\frac{\beta_0}{4N_c}\chi(n,\nu')\delta_{nn'}}{(\omega-\overline{\alpha}_s\chi(n,\nu))(\omega-\overline{\alpha}_s\chi(n,\nu'))}\Big(i\frac{\partial}{\partial\nu'}\delta(\nu-\nu')\Big). \tag{1.33}$$

It will be useful to write the following formulas, which appear latter on when we carry the integration over ω and one of the ν's variable in Eq (1.22)

$$\int_{\delta-i\infty}^{\delta+i\infty}\frac{d\omega}{2\pi i}\frac{\left(\frac{s}{s_0}\right)^{\omega}}{(\omega-\overline{\alpha}_s\chi(n,\nu))^2}=\ln\left(\frac{s}{s_0}\right)\left(\frac{s}{s_0}\right)^{\overline{\alpha}_s\chi(n,\nu)}, \tag{1.34}$$

$$\int_{-\infty}^{+\infty}d\nu'\Phi_A(n,\nu)\Big(i\frac{\partial}{\partial\nu'}\delta(\nu-\nu')\Big)\Phi_B(n,\nu')=\Phi_A(n,\nu)\Big(-i\frac{\partial\Phi_B(n,\nu)}{\partial\nu}\Big). \tag{1.35}$$

Using formulas (1.32),(1.33),(1.34), and (1.35) into (1.22), and after a few algebraic steps, we end up with the following final representation of the BFKL amplitude at NLA

$$Im_s A_{AB}^{A'B'}=\frac{s}{(2\pi)^{D-2}}\sum_{n=-\infty}^{+\infty}\int_{-\infty}^{+\infty}d\nu\left(\frac{\hat{s}}{s_0}\right)^{\bar{\alpha}_s(\mu_R)\chi(n,\nu)}\alpha_s^2(\mu_R)c_1(n,\nu)c_2(n,\nu)$$

$$\times\Big[1+\bar{\alpha}_s(\mu_R)\left(\frac{c_2^{(1)}(n,\nu)}{c_2(n,\nu)}\right)+\bar{\alpha}_s^2(\mu_R)\ln\frac{\hat{s}}{s_0}\Big\{\bar{\chi}(n,\nu)+\frac{\beta_0}{8N_c}\chi(n,\nu)$$

$$\times\Big(-\chi(n,\nu)+\frac{10}{3}+2\ln\mu_R^2+i\frac{d\ln(\frac{c_1(n,\nu)}{c_2(n,\nu)})}{d\nu}\Big)\Big\}\Big]. \tag{1.36}$$

1.5 Impact factors

The notion of the Impact factors has been introduced to account for the coupling of the Pomeron to the hadrons. We need NLO impact factos in NLA, which take contributions from virtual corrections (one-particle intermediate states) and real particle production (two-particle intermediate states). Although impact factors are process

dependent, they all share the following universal property

$$\Phi(k,q)\Big|_{k\to 0}^{k-q\to 0} \quad \to 0,$$

which guarantees the infra-red finiteness of the amplitude.

From the previous section 1.4, we can define the LO impact factor, which describes the transition $A \to A'$, as follows (see, *e.g.*, Ref. [101]):

$$\Phi^{(0)}_{A'A}(\vec{q}_R, \vec{q}) = \frac{1}{\sqrt{N_c^2-1}} \sum_{\{f\}} \int \frac{dM_a}{2\pi} \Gamma^{(0)}_{\{a\}A}(q_R) \Gamma^{(0)}_{\{a\}A'}(q'_R)^* d\rho_a, \tag{1.37}$$

where $\Gamma^{(0)}$ are vertices evaluated in Born approximation, the integration here is over the standard phase space $d\rho_a$ of an intermediate state $\{a\}$ as well as over its squared invariant mass M_a^2.

The phase space of a state a consisting of particles with momenta l_n is

$$d\rho_a = (2\pi)^D \delta\left(p_A - q_R - \sum_{n\in a} l_n\right) \prod_{n\in a} \frac{d^{D-1} l_n}{(2\pi)^{D-1} 2E_n}, \tag{1.38}$$

while the squared invariant mass of the state a

$$M_a^2 = (p_A - q_R)^2 = (p'_A - q'_R)^2.$$

At NLA the simple expression for the LLA impact factor must be modified from two perspectives. The first one due to the modifications in production vertices after including the radiative corrections, and the second is to account for the gluon emission in the central rapidity region. Therefore, the NLA definition of the impact factor reads

$$\Phi^{(1)}_{A'A}(\vec{q}_R, \vec{q} l s_0) = \frac{1}{\sqrt{N_c^2-1}} \sum_{\{f\}} \int \frac{dM_a^2}{2\pi} \Gamma^{(0)}_{\{a\}A}(q_R) \Gamma^{(0)}_{\{a\}A'}(q'_R)^* d\rho_a \theta(s_\Lambda - M_a^2)$$

$$-\frac{1}{2}\int \frac{d^{D-2}q_{R'}}{\vec{q}^2\vec{q}'^2_{R'}}\Phi^{(Born)}_{A'A}(\vec{q}_{R'},\vec{q})\left[K_r^{(Born)}(\vec{q}_{R'},\vec{q}_R;\vec{q})\ln\left(\frac{s_\Lambda^2}{(\vec{q}_{R'}-\vec{q}_R)^2 s_0}\right)\right.$$
$$\left.+\vec{q}'^2_{R'}\vec{q}^2_{R'}\delta(\vec{q}_R-\vec{q}_{R'})\left\{\omega(t_R)\ln\left(\frac{\vec{q}_R^2}{s_0}\right)+\omega(t'_R)\ln\left(\frac{\vec{q}'^2_R}{s_0}\right)\right\}\right], \tag{1.39}$$

where the intermediate parameter s_Λ should go to infinity, and the dependence on this parameter vanishes due to the cancellation between the first and second terms; the trajectory function $\omega(t)$ is the one defined at 1-loop in Eq (1.3).

Chapter 2

Hadron-jet production channel

2.1 General remarks

Inclusive processes at high-energies with tagged objects in the final state featuring large rapidity separation have been considered as a promising testfield for the search of BFKL dynamics in current and future colliders. The more the tagged objects are separated in rapidity, the deeper into the small-x region of collinear PDFs we enter. In this region, and because of the conservation of momentum, the cross section decreases as the rapidity gap increases. Recently, a number of probes for BFKL signals have been proposed for different collider environments: the diffractive leptoproduction of two light vector mesons [35, 102–104], the total cross section of two highly-virtual photons [105], the inclusive hadroproduction of two jets with large transverse momenta and well separated in rapidity (Mueller-Navelet channel [38]), for which several phenomenological studies have carried out so far (for more details see [106] and references therein), the inclusive detection of two light-charged hadrons [107–109], three- and four-jet hadroproduction [54–56, 58, 61, 62], J/Ψ-jet [110], hadron-jet [111–113], the inclusive production of rapidity-separated Λ-Λ or Λ-jet pairs [114], and recently, double Λ_c or of a Λ_c plus a light-flavored jet system [70], Drell-Yan–jet [115, 116] and heavy-quark pair photo- and hadroproduction [117–119].

This chapter is dedicated to give a description of inclusive semi-hard reactions

with full NLA accuracy, and to give the full NLA BFKL analysis for the cross-section and azimuthal-angle for the inclusive production at the LHC of a charged light hadron and of a jet, featuring a wide separation in rapidity, as suggested probe process for the investigation of the BFKL formalism of resummation of high-energy logarithms in the pQCD series. Moreover, we make use of optimization methods to set the values of the renormalization scale (μ_R) and study the effect of choosing different values for the factorization scale (μ_F), entering the theoretical description of this process.

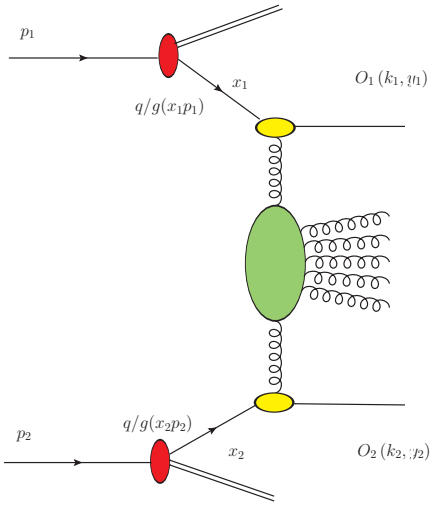

Figure 2.1: **Schematic representation of a generic semi-hard process**.

2.1.1 Theoretical setup

A generic expression of the inclusive hadroproduction processes of our considerations (see Fig 2.1):

$$\text{proton}(p_1) \;+\; \text{proton}(p_2) \;\to\; O_1(\vec{k}_1, y_1) \;+\; \text{X} \;+\; \text{O}_2(\vec{k}_2, y_2), \tag{2.1}$$

where $O_{1,2}$ are emitted objects with high transverse momenta of similar sizes $\vec{k}^2_{1,2}$, and wide rapidity separation $\Delta Y = |y_1 - y_2|$. The symbol X is stands for an undetected

system of hadrons. The colliding protons' momenta P_1 and P_2 are taken as Sudakov basis vectors satisfying $P_1^2 = P_2^2 = 0$ and $2(P_1 \cdot P_2) = s$, so that the momenta of detected objects can be decomposed as

$$k_{1,2} = x_{1,2}P_{1,2} + \frac{\vec{p}_{1,2}^{\,2}}{x_{1,2}s}P_{2,1} + k_{1,2\perp} \ , \quad k_{1,2\perp}^2 = -\vec{k}_{1,2}^{\,2} \tag{2.2}$$

The longitudinal-momentum fractions $x_{1,2}$ are related to their rapidities in the c.o.m. frame through the relation $y_{1,2} = \pm\frac{1}{2}\ln\frac{x_{1,2}^2 s}{\vec{k}_{1,2}^{\,2}}$, so that $dy_{1,2} = \pm\frac{dx_{1,2}}{x_{1,2}}$, and $\Delta Y = y_1 - y_2 = \ln\frac{x_1 x_2 s}{|\vec{k}_1||\vec{k}_2|}$, here the spatial part of the four-vector $k_{1\parallel}$ being taken positive.

In QCD collinear factorization, the processes can be viewed as initiated by two protons each emitting one parton, according to its parton distribution function (PDF) and ended with the detected object in the final state. In the case of hadrons in the final state, they are formulated according to their fragmentation functions (FFs). Within collinear factorization, a general formula for the processes of our interest, reads

$$\frac{d\sigma}{dx_1 dx_2 d^2k_1 d^2k_2} = \sum_{i,j=q,\bar{q},g} \int_0^1 dx_a \int_0^1 dx_b \, f_i(x_a,\mu_F) f_j(x_b,\mu_F) \frac{d\hat{\sigma}_{i,j}(\hat{s},\mu_F)}{dx_1 dx_2 d^2k_1 d^2k_2}, \tag{2.3}$$

where the i, j indices specify the parton types (quarks $q = u, d, s, c, b$; antiquarks $\bar{q} = \bar{u}, \bar{d}, \bar{s}, \bar{c}, \bar{b}$; or gluon g), $f_{i,j}\,(x_{a,b}, \mu_F)$ represent the initial proton PDFs and the; $x_{a,b}$ are the longitudinal fractions of the partons involved in the hard subprocess, while μ_F is the factorization scale; $d\hat{\sigma}_{i,j}\,(\hat{s})$ is the partonic cross section and $\hat{s} \equiv x_a x_b s$ is the squared center-of-mass energy of the parton-parton collision subprocess.

In the BFKL approach the cross section of the hard subprocesses can be presented as the Fourier sum of the azimuthal coefficients $\mathscr{C}_n$, having so

$$\frac{d\sigma}{dy_1 dy_2\, d|\vec{k}_1|\, d|\vec{k}_2| d\phi_1 d\phi_2} = \frac{1}{(2\pi)^2}\left[\mathscr{C}_0 + \sum_{n=1}^{\infty} 2\cos(n\phi)\,\mathscr{C}_n\right], \tag{2.4}$$

where $\phi = \phi_1 - \phi_2 - \pi$, with $\phi_{1,2}$ the emitted objects $O_{1,2}$ azimuthal angles, while $y_{1,2}$ and $\vec{p}_{1,2}$ are their rapidities and transverse momenta, respectively. The ϕ-averaged cross section $\mathscr{C}_0$ and the other coefficients $\mathscr{C}_{n\neq 0}$ are given by

$$\mathscr{C}_n \equiv \int_0^{2\pi} d\phi_1 \int_0^{2\pi} d\phi_2 \, \cos[n(\phi_1 - \phi_2 - \pi)] \, \frac{d\sigma}{dy_1 dy_2 \, d|\vec{p}_1| \, d|\vec{p}_2| d\phi_1 d\phi_2}$$

$$= \frac{e^{\Delta Y}}{s} \int_{-\infty}^{+\infty} d\nu \, \left(\frac{x_1 x_2 s}{s_0}\right)^{\bar{\alpha}_s(\mu_R)\left\{\chi(n,\nu)+\bar{\alpha}_s(\mu_R)\left[\bar{\chi}(n,\nu)+\frac{\beta_0}{8N_c}\chi(n,\nu)\left[-\chi(n,\nu)+\frac{10}{3}+2\ln\left(\frac{\mu_R^2}{\sqrt{\vec{k}_1^2\vec{k}_2^2}}\right)\right]\right]\right\}}$$

$$\times \alpha_s^2(\mu_R) c_1(n,\nu,|\vec{k}_1|,x_1)[c_2(n,\nu,|\vec{k}_2|,x_2)]^*$$

$$\times \left\{1 + \alpha_s(\mu_R)\left[\frac{c_1^{(1)}(n,\nu,|\vec{k}_1|,x_1)}{c_1(n,\nu,|\vec{k}_1|,x_1)} + \left[\frac{c_2^{(1)}(n,\nu,|\vec{k}_2|,x_2)}{c_2(n,\nu,|\vec{k}_2|,x_2)}\right]^*\right]\right.$$

$$\left. + \bar{\alpha}_s^2(\mu_R) \ln\left(\frac{x_1 x_2 s}{s_0}\right) \frac{\beta_0}{4N_c}\chi(n,\nu) f(\nu)\right\} \, . \tag{2.5}$$

Here $\bar{\alpha}_s(\mu_R) \equiv \alpha_s(\mu_R) N_c/\pi$, with N_c the number of colors, $\chi\,(n,\nu)$ is the LO BFKL characteristic function given in Eq 1.19, $c_{1,2}^{(1)}(n,\nu,|\vec{k}_{1,2}|,x_{1,2})$ are the LO forward /backward objects impact factors in the (n,ν)-representation, given as an integral in the partons fractions $x_{1,2}$, containing the PDFs of the gluon and of the different quark /antiquark flavors in the proton, and the FFs of the detected hadrons. The LO impact factor for the possible cases of our consideration, can be given in compact form as follows

$$c_i(n,\nu,|\vec{k}|,x) = 2\sqrt{\frac{C_F}{C_A}}(\vec{k}^2)^{i\nu-1/2} \int_x^1 d\beta \left(\frac{\beta}{x}\right)^{2i\nu-1}$$

$$\times \left[\frac{C_A}{C_F} f_g(\beta)\mathscr{S}_g(x,\beta) + \sum_{r=q,\bar{q}} f_r(\beta)\mathscr{S}_r(x,\beta)\right] \, , \tag{2.6}$$

where

$$\mathscr{S}_{g,r}(x,\beta) = \begin{cases} \dfrac{1}{\beta} D_{g,r}^{H_b}(x/\beta) \,, & i \equiv \text{hadron} \,; \\ \delta(\beta - x) \,, & i \equiv \text{jet} \,. \end{cases} \tag{2.7}$$

and the $f(\nu)$ function is defined by

$$i\frac{d}{d\nu} \ln\left(\frac{c_1}{[c_2]^*}\right) = 2\left[f(\nu) - \ln\left(\sqrt{|\vec{k}_1||\vec{k}_2|}\right)\right] \,. \tag{2.8}$$

The remaining objects are the NLO impact factors $c_{1,2}^{(1)}(n,\nu,|\vec{k}_{1,2}|,x_{1,2})$, for the hadron case, its expression given in Ref. [23], while the jet one is defined in Ref. [20].

2.1.2 BLM optimization scale setting

It is broadly perceived that the NLO corrections of both, impact factors and the BFKL kernel, in the MS renormalization scheme, are very large in absolute value, thus making the perturbative series highly unstable. For this reason we need some optimization procedure to make reliable predictions. To fix the arbitrarily chosen renormalization scale μ_R, we follow Ref. [44], which showed that, using Brodsky-Lepage-Mackenzie (BLM) optimization method, one can reduce the large uncertainties in the μ_R setting, by absorbing the non-conformal β_0-terms (which are present not only in the NLA BFKL kernel, but also in the expressions for the NLA impact factor) into the running coupling. This leads to a non-universality of the BLM scale and to its dependence on the energy of the process.

We first perform a finite renormalization from the $\overline{\text{MS}}$ to the physical MOM scheme, whose definition is related to the 3-gluon vertex being a key ingredient of the BFKL approach and get

$$\alpha_s^{\overline{\text{MS}}} = \alpha_s^{\text{MOM}}\left(1 + \frac{\alpha_s^{\text{MOM}}}{\pi} T\right) \,, \tag{2.9}$$

with $T = T^\beta + T^{\rm conf}$,

$$T^\beta = -\frac{\beta_0}{2}\left(1+\frac{2}{3}I\right)\,, \tag{2.10}$$

$$T^{\rm conf} = \frac{3}{8}\left[\frac{17}{2}I + \frac{3}{2}\left(I-1\right)\xi + \left(1-\frac{1}{3}I\right)\xi^2 - \frac{1}{6}\xi^3\right]\,,$$

where $I = -2\int_0^1 dx \frac{\ln(x)}{x^2-x+1} \simeq 2.3439$ and ξ is the gauge parameter of the MOM scheme, fixed at zero in the following. Then, the "optimal" BLM scale $\mu_R^{\rm BLM}$ is the value of μ_R that makes the β_0-dependent part in the expression for the observable of interest vanish.

Finally, the optimal scale $\mu_R^{\rm BLM}$ is the value of μ_R satisfies the condition

$$C_n^{\beta_0} \propto \int_{y_1^{\rm min}}^{y_1^{\rm max}} dy_1 \int_{y_2^{\rm min}}^{y_2^{\rm max}} dy_2 \int_{k_1^{\rm min}}^{k_1^{\rm max}} dk_1 \int_{k_2^{\rm min}}^{k_2^{\rm max}} dk_2 \int_{-\infty}^{\infty} d\nu\, e^{Y\bar{\alpha}_s^{\rm MOM}(\mu_R^{\rm BLM})\chi(n,\nu)} c_1(n,\nu)[c_2(n,\nu)]^*$$

$$\left[\frac{5}{3} + \ln\frac{(\mu_R^{\rm BLM})^2}{|\vec{k}_1||\vec{k}_2|} + f(\nu) - 2\left(1+\frac{2}{3}I\right)\right.$$

$$\left. + \bar{\alpha}_s^{\rm MOM}(\mu_R^{\rm BLM}) Y \frac{\chi(n,\nu)}{2}\left(-\frac{\chi(n,\nu)}{2} + \frac{5}{3} + \ln\frac{(\mu_R^{\rm BLM})^2}{|\vec{k}_1||\vec{k}_2|} + f(\nu) - 2\left(1+\frac{2}{3}I\right)\right)\right] = 0\,. \tag{2.11}$$

The first term in the r.h.s. of Eq. (2.11) originates from the NLA corrections to the hadron/jet vertices and the second one (proportional to $\alpha_s^{\rm MOM}$) from the NLA part of the kernel. We finally plug these scales into our expression for the integrated coefficients in the BLM scheme (for the derivation see Ref. [44]):

$$C_n = \int_{y_1^{\rm min}}^{y_1^{\rm max}} dy_1 \int_{y_2^{\rm min}}^{y_2^{\rm max}} dy_2 \int_{k_1^{\rm min}}^{k_1^{\rm max}} dk_1 \int_{k_2^{\rm min}}^{k_2^{\rm max}} dk_2 \int_{-\infty}^{\infty} d\nu \tag{2.12}$$

$$\frac{e^Y}{s}\, e^{Y\bar{\alpha}_s^{\rm MOM}(\mu_R^{\rm BLM})\left[\chi(n,\nu)+\bar{\alpha}_s^{\rm MOM}(\mu_R^{\rm BLM})\left(\bar{\chi}(n,\nu)+\frac{T^{\rm conf}}{3}\chi(n,\nu)\right)\right]} \left(\alpha_s^{\rm MOM}(\mu_R^{\rm BLM})\right)^2$$

$$\times c_1(n,\nu)[c_2(n,\nu)]^* \left\{ 1 + \bar{\alpha}_s^{\rm MOM}(\mu_R^{\rm BLM}) \left[\frac{\bar{c}_1^{(1)}(n,\nu)}{c_1(n,\nu)} + \left[\frac{\bar{c}_2^{(1)}(n,\nu)}{c_2(n,\nu)} \right]^* + \frac{2T^{\rm conf}}{3} \right] \right\} .$$

2.1.3 BFKL-sensitive observables

To explore different kinematic configurations, based on realistic one used at the LHC, we integrate the coefficients (2.5) over the phase space for the two emitted objects, $O_{1,2}(\vec{k}_{1,2}, y_{1,2})$, while their rapidity distance ΔY, is kept fixed

$$C_n(\Delta Y, s) = \int_{k_1^{\rm min}}^{k_1^{\rm max}} d|\vec{k}_1| \int_{k_2^{\rm min}}^{k_2^{\rm max}} d|\vec{k}_2| \int_{y_1^{\rm min}}^{y_1^{\rm max}} dy_1 \int_{y_2^{\rm min}}^{y_2^{\rm max}} dy_2 \delta\left(y_1 - y_2 - \Delta Y\right) \mathscr{C}_n \qquad (2.13)$$

Since that the typical BFKL observables at the LHC are the azimuthal angle ϕ correlations of tagged particles in the final state, which are separated in rapidity, a specific attention has been drawn to the behaviour of the so-called azimuthal correlation. In attempt to to find, less inclusive, observable to test high-energy logs resummation, we consider the ϕ-summed cross section, C_0, and the dependence on the relative azimuthal angle between the tagged particles in the final state, where the latter is defined to be

$$\langle \cos\left[n\left(\phi_1 - \phi_2 - \pi\right)\right] \rangle \equiv \frac{\mathscr{C}_n}{\mathscr{C}_0}, \quad \text{with} \quad n = 1, 2, 3 . \qquad (2.14)$$

The emission of multiple gluons manifests as a fast decrease of $\langle \cos\left[n\left(\phi_1 - \phi_2 - \pi\right)\right] \rangle$ with the difference rapidity between the final observed objects. However, even this observable suffer from a large collinear logs contamination, since the $n = 0$ moment is very sensitive to collinear dynamics, thus we need observable has less influence of the collinear region. A further step in this direction was to eliminate the $n = 0$ dependence, by proposing the so-called "conformal ratios" R_{nm} [120,121]:

$$\frac{\langle \cos\left[2\left(\phi_1 - \phi_2 - \pi\right)\right] \rangle}{\langle \cos\left(\phi_1 - \phi_2 - \pi\right) \rangle} \equiv \frac{\mathscr{C}_2}{\mathscr{C}_1} \equiv R_{21} , \; \frac{\langle \cos\left[3\left(\phi_1 - \phi_2 - \pi\right)\right] \rangle}{\langle \cos\left[2\left(\phi_1 - \phi_2 - \pi\right)\right] \rangle} \equiv \frac{\mathscr{C}_3}{\mathscr{C}_2} \equiv R_{32}. \qquad (2.15)$$

Further generalization for the conformal ratios has been suggested for recent proposed processes involving three and four-jets [54–58, 60–62] in the final states, as special Mueller-Navelet jets with central tagged jets.

2.2 Hadron-jet process

In this section we present, the inclusive production at the LHC of a charged light hadron and of a jet [64, 122, 123], with a wide separation in rapidity,

$$\text{proton}(p_1) + \text{proton}(p_2) \to \text{hadron}(k_1, y_1) + \text{X} + \text{jet}(k_2, y_2) \ , \tag{2.16}$$

as suggested probe channel for the investigation of the BFKL mechanism of resummation of high-energy logarithms in the pQCD series. We present a numerical predictions, tailored, as in previous section, for both the CMS and CASTOR detectors, for the cross section averaged over the azimuthal angle between the tagged jet and hadron and for azimuthal correlations coefficients. Here, a charged light hadron: $\pi^{\pm}, K^{\pm}, p\,(\bar{p})$ and a jet with high transverse momenta, separated by a large interval of rapidity, are produced together with an undetected hadronic system X (see Fig. 2.2). The process (3.1) has many common features with the inclusive J/Ψ-meson plus backward jet production, considered in Ref. [63]. From the theoretical point of view, J/Ψ-meson process, has more uncertainties in comparison to the Hadron-jet one. First the impact factor for J/Ψ-meson production was considered in LO. Instead, impact factor for the light hadron is known up to NLO accuracy. Previous studies with BFKL calculations for various processes at LHC show that the account of NLO corrections to the impact factors reduce the theoretical uncertainties. The motivations for building a numerical predictions for this process are summarized in the following points:

- Hadron-jet process is fully describable within NLO BFKL, thus it can be used to test the specific BFKL factorization structure experimentally.
- The process we are considering here is naturally imposed asymmetry cuts due to the different nature of the two tagged objects.
- The different nature of the two detected objects should simplify the detection of these events out of the minimum-bias ones.
- From the theoretical point of view one can use this process to compare and constrain collinear FFs, handling the linear expressions as in the di-hadron process. And/or to compare different models for jet algorithms which are not quadratic as it would be in the Mueller-Navelet jet case.

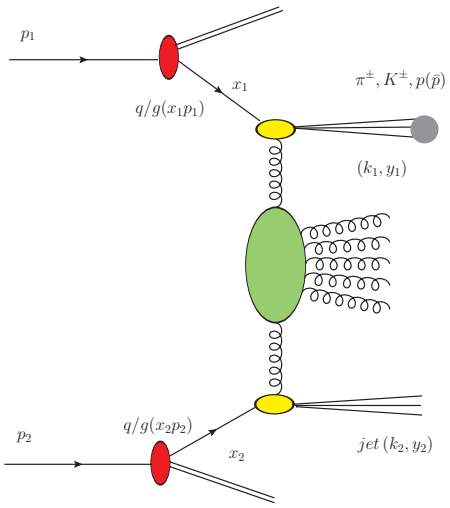

Figure 2.2: **Schematic presentation for the Hadron-jet process.**

2.2.1 Theoretical framework

In the considered process (2.2), both identified hadron and jet have high transverse momenta, $\vec{k}_J^2 \sim \vec{k}_H^2 \geq \Lambda_{QCD}^2$ and large separation in rapidity $Y = y_1 - y_2$, which

makes the BFKL re-summation come into play. The momenta of hadron and jet can be written using the Sudakov vector decomposition form:

$$k_H = x_H p_1 + \frac{\vec{k}_H^2}{x_H s} p_2 + k_{H\perp} \ , \quad k_{H\perp}^2 = -\vec{k}_H^2 \ ,$$

$$k_J = x_J p_2 + \frac{\vec{k}_J^2}{x_J s} p_1 + k_{J\perp} \ , \quad k_{J\perp}^2 = -\vec{k}_J^2 \ . \tag{2.17}$$

where x_H,x_J are the longitudinal momentum fractions for hadron and jet respectively and the connections between them and the rapidities are given through the relations:

$$y_H = \frac{1}{2} \ln \frac{x_H^2 s}{\vec{k}_H^2}, \quad y_J = \frac{1}{2} \ln \frac{\vec{k}_J^2}{x_J^2 s}. \tag{2.18}$$

In this process the vertices describing the dynamics in the proton fragmentation region is combination of proton -to- identified hadron vertex and proton-to-jet vertex. The LO impact factor in the ν -representation for the identified hadron, written in expression contains the PDFs of the gluon and of the different quark/anti-quark flavors in the proton, and the FFs of the detected hadron, reads:

$$c_H(n, \nu, |\vec{k}_H|, x_H) = 2\sqrt{\frac{C_F}{C_A}} (\vec{k}_H^2)^{i\nu - 1/2} \int_{x_H}^1 \frac{dx}{x} \left(\frac{x}{x_H} \right)^{2i\nu - 1} \tag{2.19}$$

$$\times \left[\frac{C_A}{C_F} f_g(x) D_g^h \left(\frac{x_H}{x} \right) + \sum_{r=q,\bar{q}} f_r(x) D_r^h \left(\frac{x_H}{x} \right) \right] \ , \tag{2.20}$$

and $c_J(n, \nu)$ is the LO forward jet vertex in the ν-representation,

$$c_J(n, \nu, |\vec{k}_J|, x_J) = 2\sqrt{\frac{C_F}{C_A}} (\vec{k}_J^2)^{i\nu - 1/2} \left(\frac{C_A}{C_F} f_g(x_J) + \sum_{s=q,\bar{q}} f_s(x_J) \right) . \tag{2.21}$$

The differential cross-section can be presented as Fourier sum of the azimuthal

coefficients C_n, as below:

$$\frac{d\sigma}{dy_H dy_J\, d|\vec{k}_H|\, d|\vec{k}_J| d\phi_H d\phi_J} = \frac{1}{(2\pi)^2}\left[C_0 + \sum_{n=1}^{\infty} 2\cos(n\phi)\, C_n\right], \tag{2.22}$$

where $\phi_{1,2}$ are hadron/jet azimuthal angles, and C_0 the differential cross-section integrated over $\phi_{1,2}$. The C_n coefficients are $\phi_{1,2}$ independent, they depend just on the transverse momenta, rapidities and the re-normalization, factorization and energy scale parameters.

It is useful to introduce the variable

$$Y_0 = \ln\left(\frac{s_0}{|\overrightarrow{k_H}||\overrightarrow{k_J}|}\right), \tag{2.23}$$

in such a way that

$$Y - Y_0 = \ln\left(\frac{x_H x_J s}{s_0}\right), \tag{2.24}$$

where $Y = y_1 - y_2 = \ln\left(\frac{x_H x_J s}{|\overrightarrow{k_H}||\overrightarrow{k_J}|}\right)$, is the rapidity gap.

Using all formulas above, the coefficients C_n in the so-called exponentiated representation are given by

$$C_n \equiv \int_0^{2\pi} d\phi_H \int_0^{2\pi} d\phi_J\, \cos[n(\phi_H - \phi_J - \pi)]\, \frac{d\sigma}{dy_H dy_J\, d|\vec{k}_H|\, d|\vec{k}_J| d\phi_H d\phi_J}$$

$$= \frac{e^Y}{s}\int_{-\infty}^{+\infty} d\nu\, \left(\frac{x_H x_J s}{s_0}\right)^{\bar{\alpha}_s(\mu_R)\left\{\chi(n,\nu)+\bar{\alpha}_s(\mu_R)\left[\bar{\chi}(n,\nu)+\frac{\beta_0}{8N_c}\chi(n,\nu)\left[-\chi(n,\nu)+\frac{10}{3}+2\ln\left(\frac{\mu_R^2}{\sqrt{\vec{k}_H^2\vec{k}_J^2}}\right)\right]\right]\right\}}$$

$$\times\, \alpha_s^2(\mu_R) c_H(n,\nu,|\vec{k}_H|,x_H)[c_J(n,\nu,|\vec{k}_J|,x_J)]^*$$

$$\times\left\{1 + \alpha_s(\mu_R)\left[\frac{c_H^{(1)}(n,\nu,|\vec{k}_H|,x_H)}{c_H(n,\nu,|\vec{k}_H|,x_H)} + \left[\frac{c_J^{(1)}(n,\nu,|\vec{k}_J|,x_J)}{c_J(n,\nu,|\vec{k}_J|,x_J)}\right]^*\right]\right. \tag{2.25}$$

$$+\bar{\alpha}_s^2(\mu_R)\ln\left(\frac{x_H x_J s}{s_0}\right)\frac{\beta_0}{4N_c}\chi(n,\nu)f(\nu)\Bigg\}\ .$$

Here $\bar{\alpha}_s^2(\mu_R) \equiv \alpha_s^2(\mu_R)N_c/\pi$,with N_c the number of colours, β_0 is the first coefficient of the QCD β-function, and $c_{H,J}^{(1)}(n,\nu,|\vec{k}_{H,J}|,x_{H,J})$ are the hadron/jet NLO impact factor corrections in (ν,n)-representation, their expressions being given in Appendix (A).

2.2.2 Phenomenological analysis

With the theoretical setup described in 2.2.1, in this section we give an interpretation to the numerical analysis results presented at the end of the section. In order to match the realistic kinematic cuts at LHC, we integrate the coefficients over the phase space for two final-state objects and keep fixed the rapidity interval, Y, between the hadron and the jet:

$$C_n = \int_{y_H^{\min}}^{y_H^{\max}} dy_H \int_{y_J^{\min}}^{y_J^{\max}} dy_J \int_{k_H^{\min}}^{k_H^{\max}} dk_H \int_{k_J^{\min}}^{k_J^{\max}} dk_J\, \delta\left(y_H - y_J - Y\right)\, \mathscr{C}_n\left(y_H, y_J, k_H, k_J\right)\ . \tag{2.26}$$

We consider two distinct ranges for the final-state objects:

- **CMS-jet**: both the hadron and the jet tagged by the CMS detector in their typical kinematic configurations, *i.e.*: 5 GeV $< k_H <$ 21.5 GeV, 35 GeV $< k_J <$ 60 GeV, $|y_H| \leq$ 2.4, $|y_H| \leq$ 4.7;
- **CASTOR-jet**: a hadron always tagged inside CMS, together with a very backward jet detected by CASTOR in the range: 5 GeV $< k_J \lesssim$ 17.68 GeV, -6.6 $< y_J <$ -5.2.

2.2.3 Results and discussion

In Fig. 2.3 we present results for the Y-dependence of ϕ-summed cross section C_0 in $\overline{\text{MS}}$ scheme at $\sqrt{s} = 13,7$ TeV in the *CMS-jet* kinematic configuration; in this case we choose for the factorization scale $(\mu_F)_{H,J} = |\overrightarrow{k}_{H,J}|$, and keep fixing the natural values for the renormalization scale $\mu_R = \mu_N = \sqrt{|\overrightarrow{k}_H||\overrightarrow{k}_J|}$. We can see that the expected BFKL pattern is manifest, where the NLO corrections become larger with the increasing Y. As a matter of fact, these corrections are very large in absolute value, thus making the perturbative series highly unstable. For this reason we need some optimization procedure to make reliable predictions.

In Figs. 2.4 and 2.5, we report predictions with the BLM scale optimization for C_0 and several R_{nm} ratios with the jet tagged inside the CMS detector for $\sqrt{s} = 7$ and 13 TeV, respectively. Here, we can see that, as a result of using BLM optimization, the LLA and NLA predictions for C_0 are now comparable, which a sign of stability in the BFKL series. For the ratios R_{n0}, the NLA predictions appear to be above the LLA ones, as observed in Mueller-Navelet jets and in the hadron-hadron [107–109] case. The ratios R_{21} and R_{32}, show insensitivity to the NLO corrections.

Panels in Fig. 2.6 show results for C_0 and several R_{nm} ratios in the *CASTOR-jet* configuration at $\sqrt{s} = 13$ TeV. Here the following behaviour is observed: (i) the two parametrizations for the FFs lead to clearly distinct predictions, (ii) $\langle \cos\phi \rangle$ exceeds one at the smaller values for Y. The reason for these phenomena could be, due to the lower values for rapidity range provided by CASTOR-jet configuration, where both jet and hadron are backward.

Finally, for the sake of completeness, in Fig. 2.7 we compare the ϕ-summed cross section C_0 in different NLA BFKL processes: Mueller-Navelet jet, hadron-jet and hadron-hadron production, for $\mu_F = \mu_R^{\text{BLM}}$, at $\sqrt{s} = 7$ and 13 TeV, and $Y \leq 7.1$ in the *CMS-jet* case. The hadron-hadron cross section, with the kinematical cuts adopted, dominates over the jet-jet one by an order of magnitude, with the hadron-jet cross

section lying, as expected, in-between.

The above C_n expression 2.25 contains two sources of uncertainties, originated from the NLO corrections to both, the impact factors and the BFKL kernel. Using the same BLM optimization discussed in the previous section we will eliminate these ambiguities. Performing a finite renormalization from the modified minimal subtraction scheme ($\overline{\rm MS}$) to the physical momentum subtraction scheme (MOM), which is related to the 3-gluon vertex by definition. In order to find the values of the BLM scales, we introduce the ratios $m_R = \mu_R^{\rm BLM}/\mu_N$, where $\mu_N = \sqrt{|\vec{k}_H||\vec{k}_J|}$ is the "natural" scale suggested by the kinematic of the process. We look here for the values of m_R that solve Eq. (2.11), the final expression for the integrated coefficients in the BLM scheme:

$$C_n = \int_{y_H^{\rm min}}^{y_H^{\rm max}} dy_H \int_{y_J^{\rm min}}^{y_J^{\rm max}} dy_J \int_{k_H^{\rm min}}^{k_H^{\rm max}} dk_H \int_{k_J^{\rm min}}^{k_J^{\rm max}} dk_J \int_{-\infty}^{\infty} d\nu \tag{2.27}$$

$$\frac{e^Y}{s}\, e^{Y\bar{\alpha}_s^{\rm MOM}(\mu_R^{\rm BLM})\left[\chi(n,\nu)+\bar{\alpha}_s^{\rm MOM}(\mu_R^{\rm BLM})\left(\bar{\chi}(n,\nu)+\frac{T^{\rm conf}}{3}\chi(n,\nu)\right)\right]}\left(\alpha_s^{\rm MOM}(\mu_R^{\rm BLM})\right)^2$$

$$\times c_H(n,\nu)[c_J(n,\nu)]^* \left\{1+\bar{\alpha}_s^{\rm MOM}(\mu_R^{\rm BLM})\left[\frac{\bar{c}_H^{(1)}(n,\nu)}{c_H(n,\nu)}+\left[\frac{\bar{c}_J^{(1)}(n,\nu)}{c_J(n,\nu)}\right]^*+\frac{2T^{\rm conf}}{3}\right]\right\}.$$

The coefficient C_0 gives the ϕ-summed cross section, while the ratios $R_{n0} \equiv C_n/C_0 = \langle\cos(n\phi)\rangle$ determine the values of the mean cosines, or azimuthal correlations, of the produced hadron and jet.

We set the factorization scale μ_F equal to the renormalization scale μ_R, as assumed by the MMHT 2014 PDF.

All calculations are done in the MOM scheme. For comparison, we present results for the ϕ-averaged cross section C_0 in the $\overline{\rm MS}$ scheme. In the latter case, we choose natural values for μ_R, *i.e.* $\mu_R = \mu_N \equiv \sqrt{|\vec{k}_H||\vec{k}_J|}$, and two different values of the factorization scale, $(\mu_F)_{1,2} = |\vec{k}_{H,J}|$, depending on which of the two vertices is considered. We checked that the effect of using natural values also for μ_F, *i.e.* $\mu_F = \mu_N$, is

negligible with respect to our two-value choice.

2.3 Used tools

All numerical calculations were done using JETHAD [106], a promising standard software recently developed, suited for the computation of cross sections and related observables for semi-hard reactions. A two-loop running coupling setup with $\alpha_s(M_Z) = 0.11707$ and five quark flavors was chosen. All PDF sets and the NNFF1.0 FF parametrization were used via the Les Houches Accord PDF Interface (LHAPDF) 6.2.1 [124]. We selected the MMHT 2014 PDF set, together with the AKK 2008 [125] and HKNS 2007 [126] FF interfaces.

2.4 Closing statements

The lower cutoff for the hadron's transverse momentum k_H, allows to explore additional kinematic range with respect to jet case. In Hadron-jet production process we observe that, just as in the case of Mueller-Navelet jets decorrelation reduced with the increasing rapidity intervals, by the inclusion of NLO correction. And the predicted cross-sections for Hadron-jet process, as expected, are laying in the middle with respect to the Mueller-Navelet jets and investigated dihadron production [107–109], since that, this process is a hybridization between these two investigated processes, which are sharing the same theoretical description.

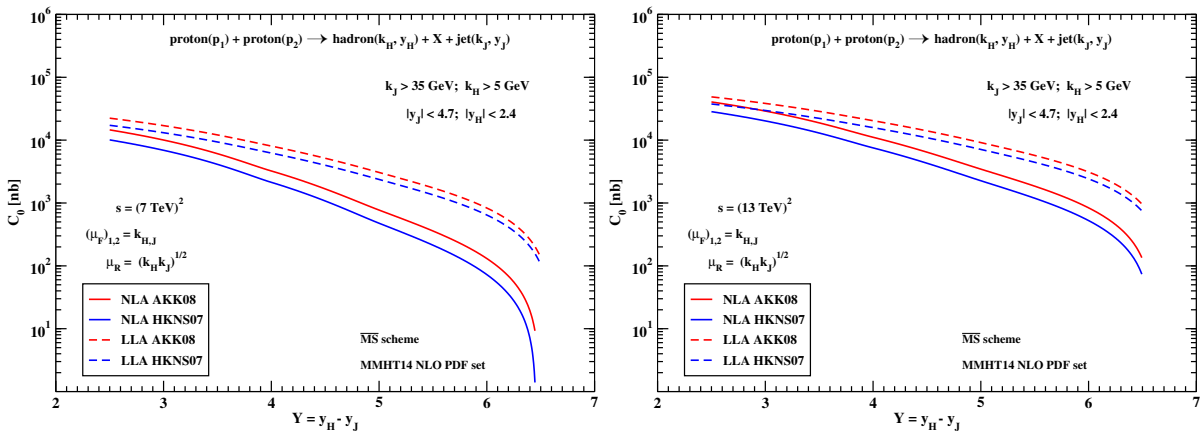

Figure 2.3: Y-dependence of C_0 for $\mu_R = \mu_N = \sqrt{|\vec{k}_H||\vec{k}_J|}$, $(\mu_F)_{1,2} = |\vec{k}_{H,J}|$, for $\sqrt{s}$ = 7 TeV (left) and $\sqrt{s}$ = 13 TeV (right), and $Y \leq 7.1$ (*CMS-jet* configuration).

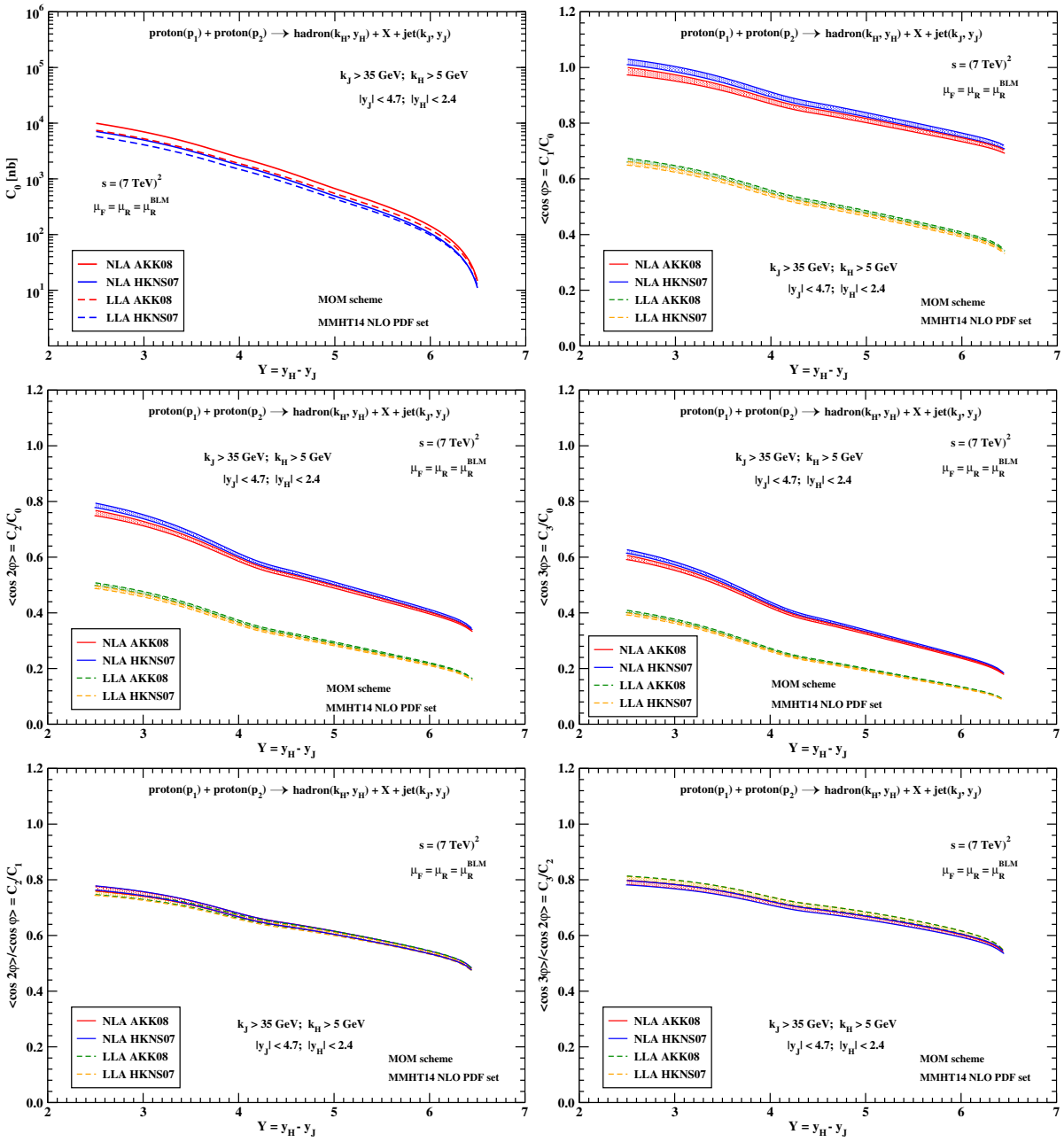

Figure 2.4: Y-dependence of C_0 and of several ratios C_m/C_n for $\mu_F = \mu_R^{\rm BLM}$, $\sqrt{s} = 7$ TeV, and $Y \leq 7.1$ (*CMS-jet* configuration).

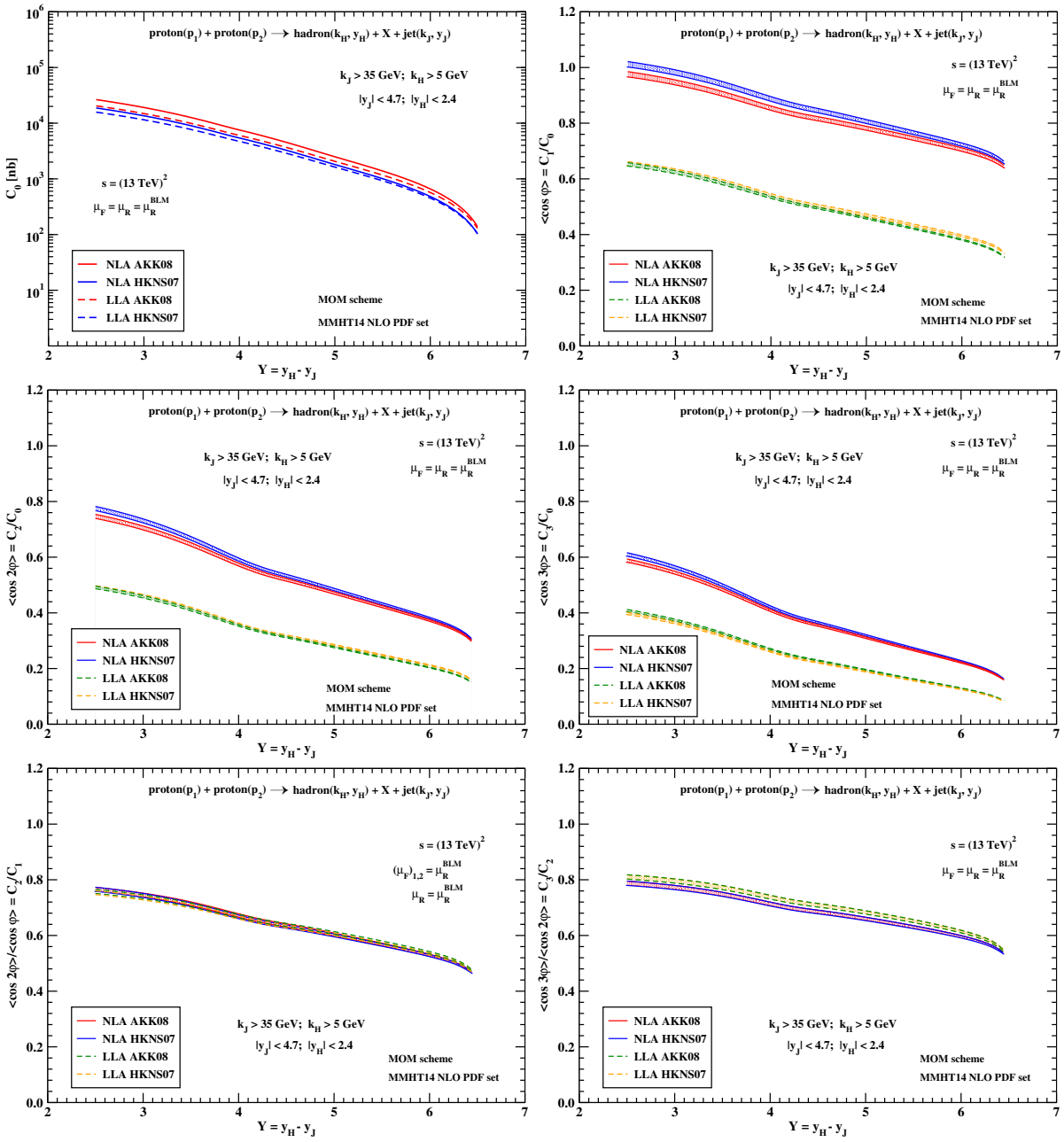

Figure 2.5: Y-dependence of C_0 and of several ratios C_m/C_n for $\mu_F = \mu_R^{\mathrm{BLM}}$, $\sqrt{s}$ = 13 TeV, and $Y \leq 7.1$ (*CMS-jet* configuration).

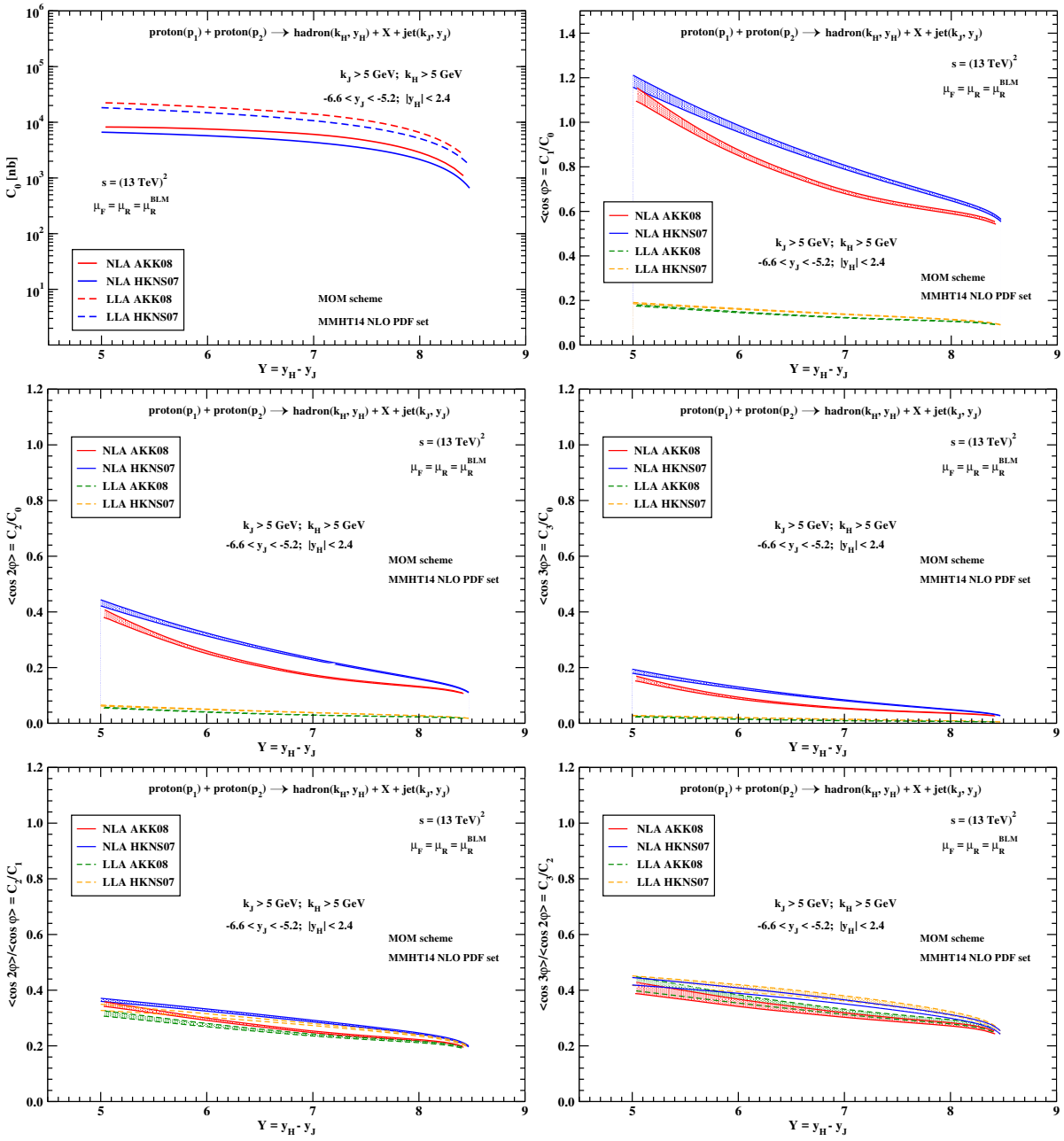

Figure 2.6: Y-dependence of C_0 and of several ratios C_m/C_n for $\mu_F = \mu_R^{\mathrm{BLM}}$, $\sqrt{s}$ = 13 TeV, and $Y \leq 9$ (*CASTOR-jet* configuration).

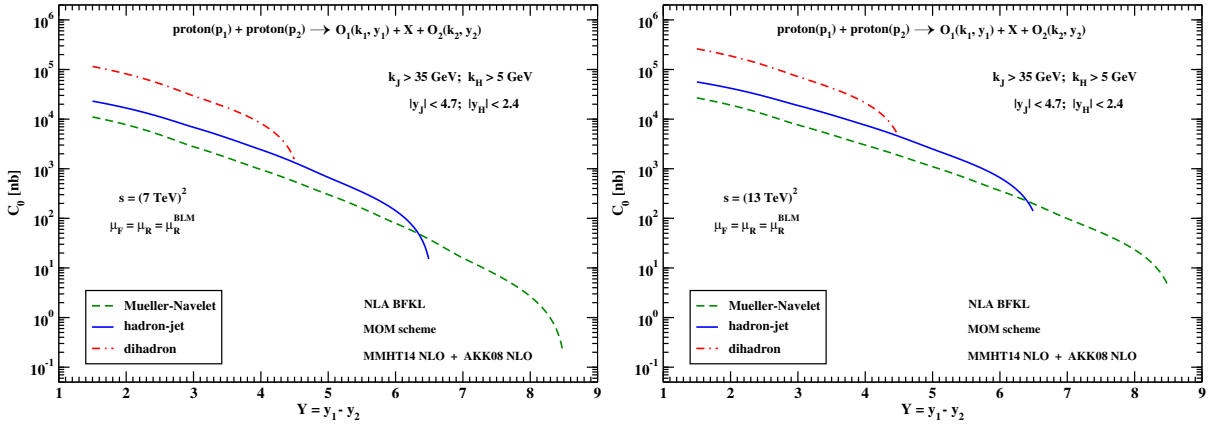

Figure 2.7: Comparison of the ϕ-averaged cross section C_0 in different NLA BFKL processes: Mueller-Navelet jet, hadron-jet and dihadron production, for $\mu_F = \mu_R^{\rm BLM}$, $\sqrt{s}$ = 7 and 13 TeV, and $Y \leq 7.1$ (*CMS-jet* configuration).

Chapter 3

Proposed stabilizers of the high-energy resummation

3.1 Inclusive Higgs-plus-jet production

With more data to be collected at the LHC, studying the Higgs boson plus multijet processes will allow us to further test the perturbative QCD on the Higgs boson production, contributing to a better understanding the dynamic of strong interactions in the high-energy limit. In this section, we present recent BFKL phenomenological results for the inclusive production of a Higgs in association with a jet, as a possible testfield for the semi-hard regime of QCD. We show how the large energy scales provided by the emission of a Higgs boson stabilize the BFKL series, and discuss the possible extension of this work in the full NLA BFKL analysis, by including the NLO jet impact factor, with a realistic implementation of the jet selection function, and the NLO forward-Higgs impact factor.

In this work we introduce and study with NLA BFKL accuracy a novel semi-hard reaction [65, 66], *i.e.* the concurrent inclusive production of a Higgs boson and a jet (depicted in Fig. 3.1):

$$\text{proton}(p_1) \;+\; \text{proton}(p_2) \;\to\; H(\vec{p}_H, y_H) \;+\; \text{X} \;+\; \text{jet}(\vec{p}_J, y_J)\,, \tag{3.1}$$

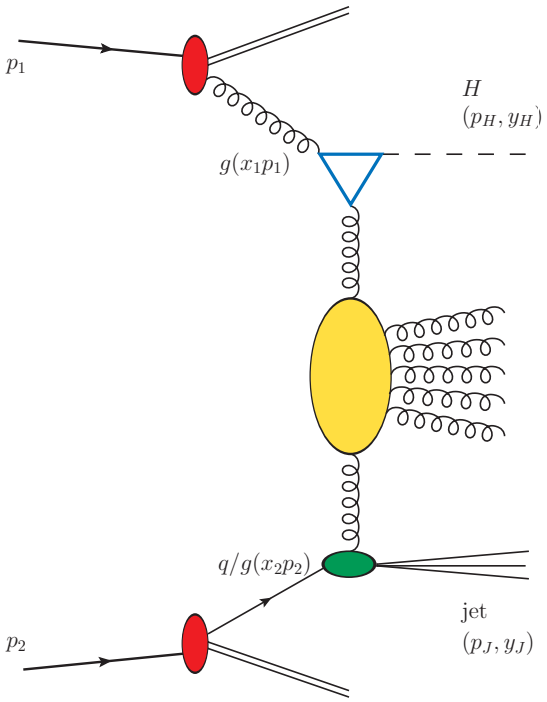

Figure 3.1: Schematic representation of the inclusive Higgs-jet hadroproduction.

emitted with large transverse momenta, $\vec{p}_{H,J} \gg \Lambda_{\rm QCD}$, and separated by a large rapidity gap, $\Delta Y = y_H - y_J$, where the Higgs boson and the jet are tagged in the forward and backward rapidity region, respectively. The tagged jet in the final state insure the existence of a large rapidity intervals, $\Delta Y = y_H - y_J \simeq \ln(s/Q^2)$, with Q^2 a typical hard-scale value. In our proposal, following Ref. [127], we adopt a kinematics which strictly respects the semi-hard regime, with suitable cuts on transverse momenta to single out only the high-energy logarithms[1].

3.1.1 Theoretical framework

As anticipated, the Higgs and the jet are expected to feature large transverse momenta, $|\vec{p}_H|^2 \sim |\vec{p}_J|^2 \gg \Lambda^2_{\rm QCD}$. The four-momenta of the parent protons, $p_{1,2}$, are taken as

[1] However, when $p^2_{H,J} \equiv p^2_T \ll M^2_H$, double logarithmic terms $\ln^2(M^2_H/p^2_T)$ appear, which are belong to back-to-back region of the phase space.

Sudakov vectors satisfying $p_{1,2}^2 = 0$ and $p_1 p_2 = s/2$, so that the final-state transverse momenta can be decomposed in the following way:

$$\begin{aligned} p_H &= x_H p_1 + \frac{M_{H,\perp}^2}{x_H s} p_2 + p_{H\perp} \,, \quad p_{H\perp}^2 = -|\vec{p}_H|^2 \,, \\ p_J &= x_J p_2 + \frac{|\vec{p}_J|^2}{x_J s} p_1 + p_{J\perp} \,, \quad p_{J\perp}^2 = -|\vec{p}_J|^2 \,, \end{aligned} \tag{3.2}$$

with the spacial part of the four-vector $p_{1\parallel}$ being taken positive; $M_{H,\perp} = \sqrt{M_H^2 + |\vec{p}_H|^2}$ is the Higgs-boson transverse mass.

The longitudinal-momentum fractions, $x_{H,J}$, for the Higgs and jet are related to the corresponding rapidities in the center-of-mass frame via the relations

$$y_H = \frac{1}{2} \ln \frac{x_H^2 s}{M_{H,\perp}^2} \,, \qquad y_J = \frac{1}{2} \ln \frac{|\vec{p}_J|^2}{x_J^2 s} \,, \qquad dy_{H,J} = \pm \frac{dx_{H,J}}{x_{H,J}} \,. \tag{3.3}$$

As for the rapidity distance, one has

$$\Delta Y = y_H - y_J = \ln \frac{x_H x_J s}{M_{H,\perp} |\vec{p}_J|} \,. \tag{3.4}$$

The BFKL cross section can be presented (see Ref. [20] for the derivation) as the Fourier series of the so-called *azimuthal coefficients*, $\mathscr{C}_n$,

$$\frac{d\sigma}{dy_H dy_J \, d|\vec{p}_H| \, d|\vec{p}_J| d\varphi_H d\varphi_J} = \frac{1}{(2\pi)^2} \left[\mathscr{C}_0 + \sum_{n=1}^{\infty} 2\cos(n\varphi) \, \mathscr{C}_n \right] \,, \tag{3.5}$$

where $\varphi = \varphi_H - \varphi_J - \pi$, with $\varphi_{H,J}$ the Higgs and the jet azimuthal angles. A comprehensive formula for the φ-averaged cross section, $\mathscr{C}_0$, and the other coefficients, $\mathscr{C}_{n>0}$, reads

$$\mathscr{C}_n \equiv \int_0^{2\pi} d\varphi_H \int_0^{2\pi} d\varphi_J \, \cos(n\varphi) \, \frac{d\sigma}{dy_H dy_J \, d|\vec{p}_H| \, d|\vec{p}_J| d\varphi_H d\varphi_J}$$

$$= \frac{e^{\Delta Y}}{s} \frac{M_{H,\perp}}{|\vec{p}_H|}$$

$$\times \int_{-\infty}^{+\infty} d\nu \left(\frac{x_J x_H s}{s_0}\right)^{\bar{\alpha}_s(\mu_{R_c})\left\{\chi(n,\nu)+\bar{\alpha}_s(\mu_{R_c})\left[\bar{\chi}(n,\nu)+\frac{\beta_0}{8N_c}\chi(n,\nu)\left[-\chi(n,\nu)+\frac{10}{3}+4\ln\left(\frac{\mu_{R_c}}{\sqrt{\vec{p}_H\vec{p}_J}}\right)\right]\right]\right\}}$$

$$\times \left\{\alpha_s^2(\mu_{R_1}) c_H(n,\nu,|\vec{p}_H|,x_H)\right\}\left\{\alpha_s(\mu_{R_2})[c_J(n,\nu,|\vec{p}_J|,x_J)]^*\right\}$$

$$\times \left\{1+\alpha_s(\mu_{R_1})\frac{c_H^{(1)}(n,\nu,|\vec{p}_H|,x_H)}{c_H(n,\nu,|\vec{p}_H|,x_H)}+\alpha_s(\mu_{R_2})\left[\frac{c_J^{(1)}(n,\nu,|\vec{p}_J|,x_J)}{c_J(n,\nu,|\vec{p}_J|,x_J)}\right]^*\right\}, \qquad (3.6)$$

where $\bar{\alpha}_s \equiv N_c/\pi\,\alpha_s$, with N_c the QCD color number, β_0 the first coefficient in the expansion of the QCD β-function (n_f is the active-flavor number), and $\chi(n,\nu)$ the eigenvalue of the LO BFKL kernel defined in Eq. 1.19, and $c_{H,J}(n,\nu)$ are the Higgs and the jet LO impact factors in the (ν,n)-space, given by

$$c_H(n,\nu,|\vec{p}_H|,x_H) = \frac{1}{v^2}\frac{|\mathscr{F}(\vec{p}_H^{\,2})|^2}{128\pi^3\sqrt{2(N_c^2-1)}}\left(\vec{p}_H^{\,2}\right)^{i\nu+1/2} f_g(x_H,\mu_{F_1})\,, \qquad (3.7)$$

$$c_J(n,\nu,|\vec{p}_J|,x_J) = 2\sqrt{\frac{C_F}{C_A}}\left(\vec{p}_J^{\,2}\right)^{i\nu-1/2}\left(\frac{C_A}{C_F}f_g(x_J,\mu_{F_2})+\sum_{a=q,\bar{q}} f_a(x_J,\mu_{F_2})\right)\,. \qquad (3.8)$$

The energy-scale parameter, s_0, is arbitrary within NLA accuracy and will be fixed in our analysis at $s_0 = M_{H,\perp}|\vec{p}_J|$. The remaining quantities are the NLO impact-factor corrections, $c_{H,J}^{(1)}(n,\nu,|\vec{p}_{H,J}|,x_{H,J})$. The expression for the Higgs NLO impact factor at the time of studying this process was not available, recently it has been calculated in the infinite top-mass limit within Lipatov's high-energy effective action [31, 32]. It is possible, however, to include some "universal" NLO contributions to the Higgs impact factor, which can be expressed through the corresponding LO impact factor, and are fixed by the requirement of stability within the NLO under variations of the

energy scale s_0, the renormalization scale μ_R and of the factorization scale μ_F, getting

$$\alpha_s c_H^{(1)}(n,\nu,|\vec{p}_H|,x_H) \to \bar{\alpha}_s \tilde{c}_H^{(1)}(n,\nu,|\vec{p}_H|,x_H)\,, \tag{3.9}$$

with

$$\begin{aligned}\tilde{c}_H^{(1)}(n,\nu,|\vec{p}_H|,x_H) = c_H(n,\nu,|\vec{p}_H|,x_H) \Bigg\{ & \frac{\beta_0}{4N_c}\left(2\ln\frac{\mu_{R_1}}{|\vec{p}_H|}+\frac{5}{3}\right)+\frac{\chi\,(n,\nu)}{2}\ln\left(\frac{s_0}{M_{H,\perp}^2}\right) \\ & +\frac{\beta_0}{4N_c}\left(2\ln\frac{\mu_{R_1}}{M_{H,\perp}}\right) \\ & -\frac{1}{2N_c f_g(x_H,\mu_{F_1})}\ln\frac{\mu_{F_1}^2}{M_{H,\perp}^2}\int_{x_H}^1\frac{dz}{z}\left[P_{gg}(z)f_g\left(\frac{x_H}{z},\mu_{F_1}\right)+\sum_{a=q,\bar{q}}P_{ga}(z)f_a\left(\frac{x_H}{z},\mu_{F_1}\right)\right]\Bigg\}\,.\end{aligned} \tag{3.10}$$

The jet impact factor is known at the NLO [19, 21, 22], nonetheless we treated it on the same ground as the Higgs one, including only the NLO corrections fixed by the renormalization group and leading to

$$\begin{aligned}\tilde{c}_J^{(1)}(n,\nu,|\vec{p}_J|,x_J) = c_J(n,\nu,|\vec{p}_J|,x_J) \Bigg\{ & \frac{\beta_0}{4N_c}\left(2\ln\frac{\mu_{R_2}}{|\vec{p}_J|}+\frac{5}{3}\right)+\frac{\chi\,(n,\nu)}{2}\ln\left(\frac{s_0}{|\vec{p}_J|^2}\right) \\ & -\frac{1}{2N_c\left(\frac{C_A}{C_F}f_g(x_J,\mu_{F_2})+\sum_{a=q,\bar{q}}f_a(x_J,\mu_{F_2})\right)}\ln\frac{\mu_{F_2}^2}{|\vec{p}_J|^2} \\ & \times\Bigg(\frac{C_A}{C_F}\int_{x_J}^1\frac{dz}{z}\left[P_{gg}(z)f_g\left(\frac{x_J}{z},\mu_{F_2}\right)+\sum_{a=q,\bar{q}}P_{ga}(z)f_a\left(\frac{x_J}{z},\mu_{F_2}\right)\right] \\ & +\sum_{a=q,\bar{q}}\int_{x_J}^1\frac{dz}{z}\left[P_{ag}(z)f_g\left(\frac{x_J}{z},\mu_{F_2}\right)+P_{aa}(z)f_a\left(\frac{x_J}{z},\mu_{F_2}\right)\right]\Bigg)\Bigg\}\,.\end{aligned} \tag{3.11}$$

Combining all the ingredients, we can write our master formula for the azimuthal coefficients,

$$\mathscr{C}_n = \frac{e^{\Delta Y}}{s}\frac{M_{H,\perp}}{|\vec{p}_H|}$$

$$\times \int_{-\infty}^{+\infty} d\nu \left(\frac{x_J x_H s}{s_0}\right)^{\bar{\alpha}_s(\mu_{R_c})\left\{\chi(n,\nu)+\bar{\alpha}_s(\mu_{R_c})\left[\bar{\chi}(n,\nu)+\frac{\beta_0}{8N_c}\chi(n,\nu)\left[-\chi(n,\nu)+\frac{10}{3}+4\ln\left(\frac{\mu_{R_c}}{\sqrt{\vec{p}_H\vec{p}_J}}\right)\right]\right]\right\}}$$

$$\times \left\{\alpha_s^2(\mu_{R_1}) c_H(n,\nu,|\vec{p}_H|,x_H)\right\}\left\{\alpha_s(\mu_{R_2})[c_J(n,\nu,|\vec{p}_J|,x_J)]^*\right\} \tag{3.12}$$

$$\times \left\{1+\bar{\alpha}_s(\mu_{R_1})\frac{\tilde{c}_H^{(1)}(n,\nu,|\vec{p}_H|,x_H)}{c_H(n,\nu,|\vec{p}_H|,x_H)}+\bar{\alpha}_s(\mu_{R_2})\left[\frac{\tilde{c}_J^{(1)}(n,\nu,|\vec{p}_J|,x_J)}{c_J(n,\nu,|\vec{p}_J|,x_J)}\right]^*\right\} .$$

The renormalization scales ($\mu_{R_{1,2,c}}$) and the factorization ones ($\mu_{F_{1,2}}$) can, in principle, be chosen arbitrarily, since their variation produces effects beyond the NLO. It is however advisable to relate them to the physical hard scales of the process. We chose to fix them differently from each other, depending on the subprocess to which they are related: $\mu_{R_1} \equiv \mu_{F_1} = C_\mu M_{H,\perp}$, $\mu_{R_2} \equiv \mu_{F_2} = C_\mu |\vec{p}_J|$, $\mu_{R_c} = C_\mu \sqrt{M_{H,\perp}|\vec{p}_J|}$, where C_μ is a variation parameter introduced to gauge the effect of a change of the scale (see the discussion at the end of Section 3.1.3).

3.1.2 Phenomenological analysis

In order to fit realistic kinematic cuts adopted by the current experimental analyses at the LHC, we constrain the Higgs emission inside the rapidity acceptances of the CMS barrel detector, *i.e.* $|y_H| < 2.5$, while we allow for a larger rapidity range of the jet [128], which can be detected also by the CMS endcaps, namely $|y_J| < 4.7$. Moreover, three distinct configurations for the final-state transverse momenta are considered:

a) ***symmetric*** configuration, fit to the pursuit of pure BFKL effects, where both the Higgs and the jet transverse momenta lie in the range: 20 GeV $< |\vec{p}_{H,J}| <$ 60 GeV;

b) ***asymmetric*** selection, typical of the ongoing LHC phenomenology, where the Higgs transverse momentum runs from 10 GeV to $2M_t$, where the jet is tagged inside its typical CMS configuration, from 20 to 60 GeV;

c) ***disjoint windows***, which allows for the maximum exclusiveness in the final state (to possibly discriminate BFKL from other resummation approaches): 35 GeV $< |\vec{p}_J| <$ 60 GeV and 60 GeV $< |\vec{p}_H| < 2M_t$.

Observables:

- The first observables of our consideration are the azimuthal-angle coefficients *integrated* over the phase space for two final-state particles, while the rapidity interval, ΔY, between the Higgs boson and the jet is kept fixed:

$$C_n(\Delta Y, s) = \int_{p_H^{\min}}^{p_H^{\max}} d|\vec{p}_H| \int_{p_J^{\min}}^{p_J^{\max}} d|\vec{p}_J| \int_{y_H^{\min}}^{y_H^{\max}} dy_H \int_{y_J^{\min}}^{y_J^{\max}} dy_J \, \delta\left(y_H - y_J - \Delta Y\right) \mathscr{C}_n \,. \tag{3.13}$$

  We study the φ-averaged cross section (*alias* the ΔY-distribution), $C_0(\Delta Y, s)$, the azimuthal-correlation moments, $R_{n0}(\Delta Y, s) = C_n/C_0 \equiv \langle \cos n\varphi \rangle$, and their ratios, $R_{nm} = C_n/C_m$ [120, 121] as functions of the Higgs-jet rapidity distance, ΔY.

- The second observable of our interest is the p_H-distribution for a given value of ΔY:

$$\frac{d\sigma(|\vec{p}_H|, \Delta Y, s)}{d|\vec{p}_H| d\Delta Y} = \int_{p_J^{\min}}^{p_J^{\max}} d|\vec{p}_J| \int_{y_H^{\min}}^{y_H^{\max}} dy_H \int_{y_J^{\min}}^{y_J^{\max}} dy_J \, \delta\left(y_H - y_J - \Delta Y\right) \mathscr{C}_0 \,, \tag{3.14}$$

  the Higgs and jet rapidity ranges being given above and 35 GeV $< |\vec{p}_J| <$ 60 GeV.

3.1.3 Results and discussion

In Fig. 3.2 we present results for the ΔY-dependence of the $\phi - summed$ cross section, C_0, in the three considered kinematic configurations. Here, the usual onset of BFKL effects comes easily into play. The rise with energy of the purely partonic cross section is quenched by the convolution with PDFs, this leading to decrease the total cross

section as ΔY of hadronic distributions increases. Notably, NLA predictions (red) are almost entirely contained inside LLA uncertainty bands (blue), this could be an evidence of the stabilizing effects of the BFKL series under NLO corrections, due to the large energy scales provided by the emission of a Higgs boson. For all the considered R_{nm} cases (Figs. 3.3), NLA corrections show a milder discrepancy with respect to pure LLA ones. This reflects the fact that in the Higgs-jet hadroproduction process, the renormalization scale needs not to be too large as for other processes where BLM optimization had to be used [41, 43, 44].

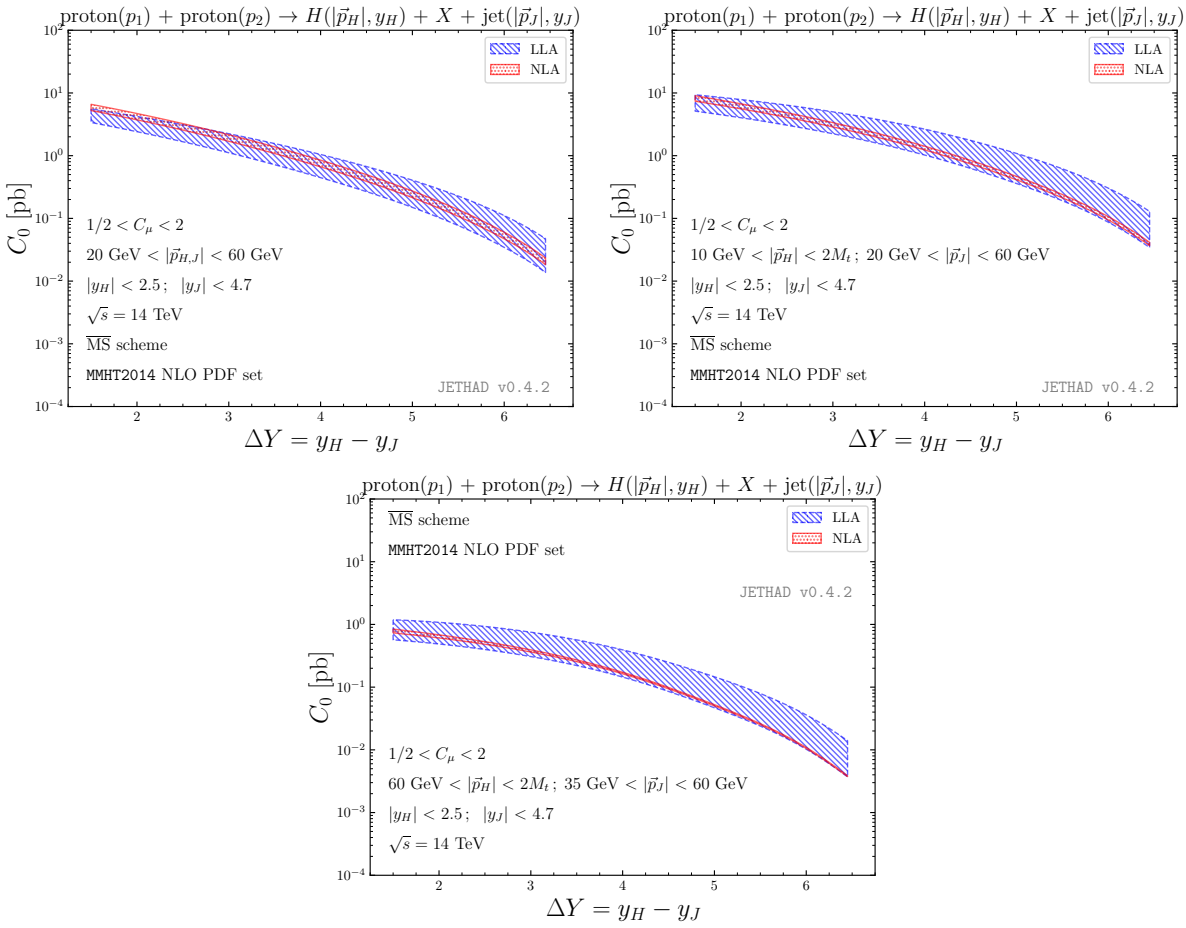

Figure 3.2: ΔY-dependence of the φ-averaged cross section, C_0, for the inclusive Higgs-jet hadroproduction in the three considered p_T-ranges and for $\sqrt{s}$ = 14 TeV.
.

The predictions for the p_H-distribution are reported in Fig. 3.6, in the range 10 GeV $< |\vec{p}_H| < 2M_t$, for two fixed values of ΔY = 3, 5. Here, the Born contribution (green), which describes the back-to-back emission of the Higgs and of the jet with no additional gluon radiation, obtained by switching off the BFKL green function, reads

$$\frac{d\sigma^{\rm Born}(|\vec{p}_H|,\Delta Y,s)}{d|\vec{p}_H|d\Delta Y} = \pi\frac{e^{\Delta Y}}{s}M_{H,\perp}\int_{y_H^{\rm min}}^{y_H^{\rm max}}dy_H\int_{y_J^{\rm min}}^{y_J^{\rm max}}dy_J\,\delta\left(y_H-y_J-\Delta Y\right)$$

$$\times\,\alpha_s^2(\mu_{R_1})\,\frac{1}{v^2}\frac{|\mathscr{F}(\vec{p}_H^{\,2})|^2}{128\pi^3\sqrt{2(N_c^2-1)}}f_g(x_H,\mu_{F_1}) \tag{3.15}$$

$$\times\,\alpha_s(\mu_{R_2})\,2\sqrt{\frac{C_F}{C_A}}\left(\frac{C_A}{C_F}f_g(x_J,\mu_{F_2})+\sum_{a=q,\bar{q}}f_a(x_J,\mu_{F_2})\right).$$

In our study, an upper cut-off in the $|\vec{p}_H|$-range, say around 125 GeV, is introduced to avoid the $x_J > 1$ limits for large jet transverse momenta.

In Fig. 3.6, both NLA and LLA corrections show a peak around $|\vec{p}_H|$= 40 GeV for the two fixed values of ΔY, and a decreasing behavior at large $|\vec{p}_H|$. Here, we distinguish three kinematic ranges, the first is the low-$|\vec{p}_H|$ region, *i.e.* $|\vec{p}_H| <$ 10 GeV, which is dominated by large transverse-momentum logarithms, need resummation formalism not accounted by our approach. The second subregion is the intermediate-$|\vec{p}_H|$ region, where $|\vec{p}_H| = |\vec{p}_J|$ and ranges from 35 to 60 GeV. It is essentially the peak region plus the first part of the decreasing tail, where NLA uncertainty bands are entirely contained inside the LLA ones. Here, our description at the hand of the BFKL resummation is validated by the impressive stability behavior of the perturbative series. The third region is the large-$|\vec{p}_H|$ represented by the long tail, where the NLA distributions start to decouple from LLA ones and exhibit an increasing sensitivity to scale variation. Here, collinear logarithms together with *threshold* effects [129] start to become relevant, thus the convergence of the high-energy series is not guaranteed. With the aim of providing a comparison between fixed-order calculations and BFKL predic-

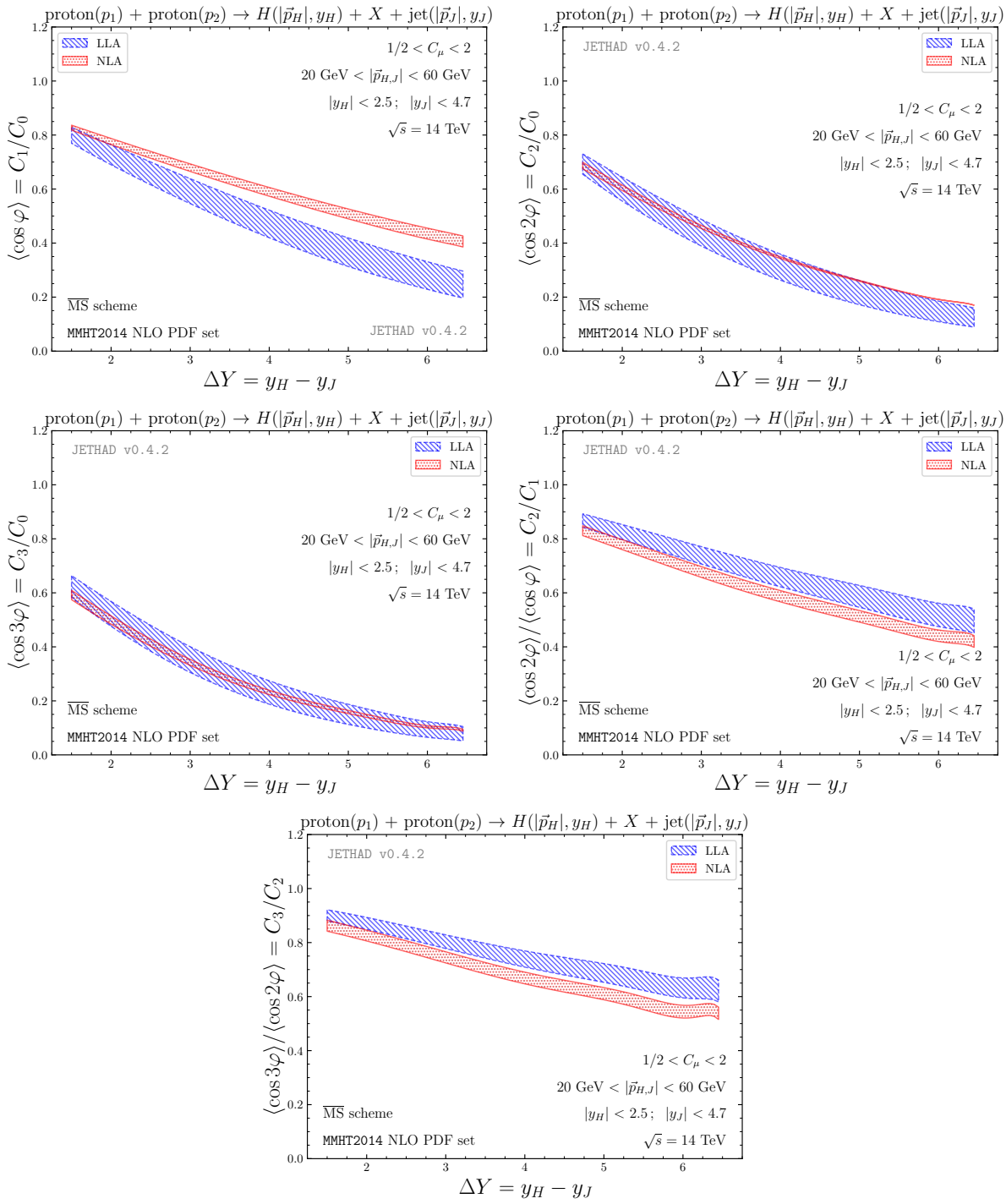

Figure 3.3: ΔY-dependence of several ratios $R_{nm} \equiv C_n/C_m$, for the inclusive Higgs-jet hadroproduction in the *p_T-symmetric* configuration and for $\sqrt{s}$ = 14 TeV.

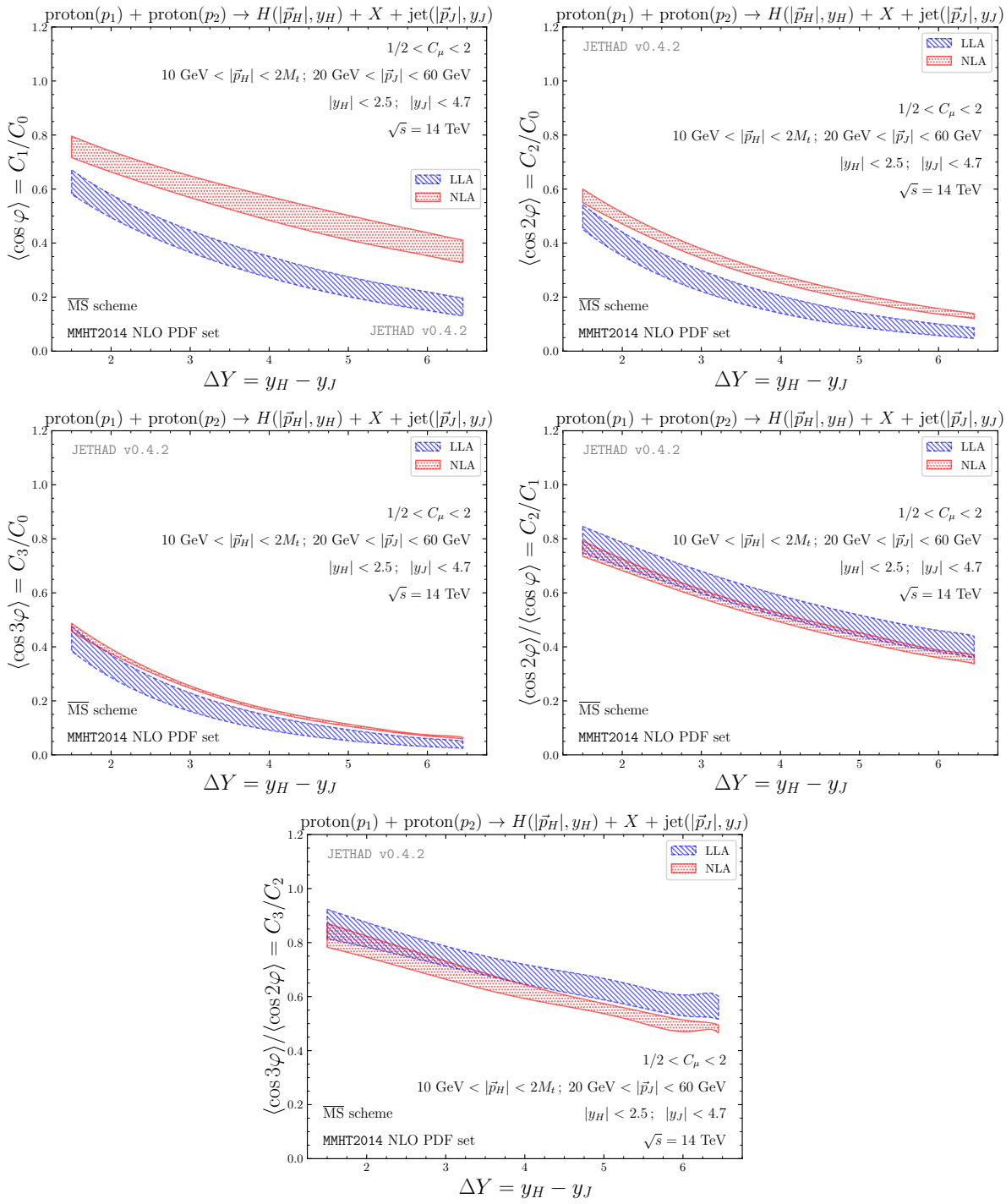

Figure 3.4: ΔY-dependence of several ratios $R_{nm} \equiv C_n/C_m$, for the inclusive Higgs-jet hadroproduction in the *p_T-asymmetric* configuration and for $\sqrt{s}$ = 14 TeV.

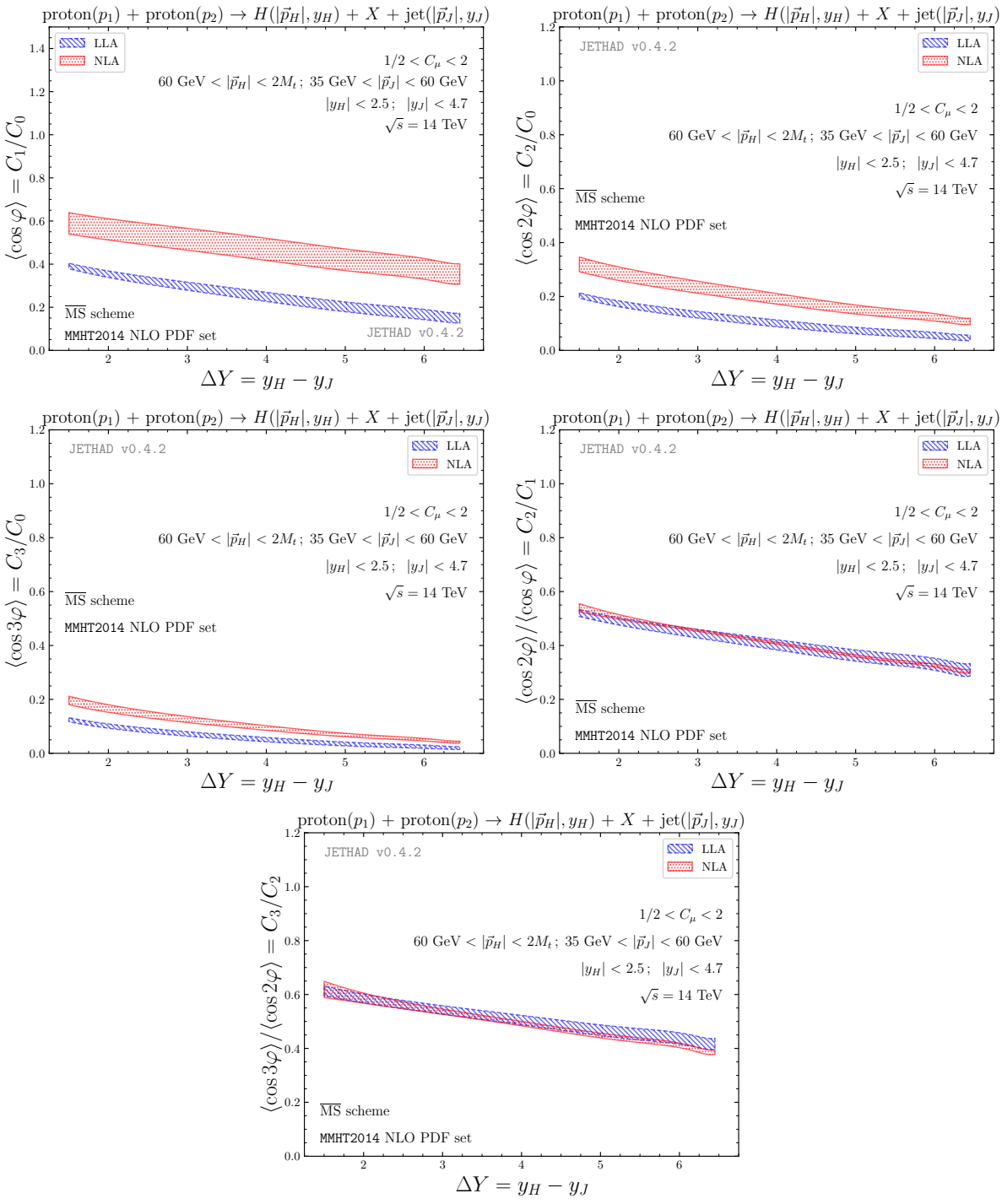

Figure 3.5: ΔY-dependence of several ratios $R_{nm} \equiv C_n/C_m$, for the inclusive Higgs-jet hadroproduction in the *disjoint* p_T-windows configuration and for $\sqrt{s}$ = 14 TeV.

tions, in Fig. 3.6 we present also the p_H-distributions at $\Delta Y = 3$ and 5, as obtained by a fixed-order NLO calculation implemented according to the POWHEG method [130], for this implementation we have adopted the subroutines dedicated to the inclusive Higgs plus jet final state [131]. It is interesting to observe that the NLO fixed-order prediction is systematically lower in comparison to the LLA- and NLA-BFKL ones, and this is more visible at the larger ΔY, where the effect of resummation is expected to be more important. Finally, we compared the distributions presented above with the corresponding ones obtained in the large top-mass limit, $M_t \to +\infty$. We noted that, when this limit is taken, cross sections become at most $5 \div 7\,\%$ larger, whereas the effect on azimuthal correlations is very small or negligible[2]. The impact on the p_H -distribution reported in Fig. 3.7, which is also quite small in the $|p_H| \sim |p_J|$ range, while it become more manifest at larger values of $|p_H|$.

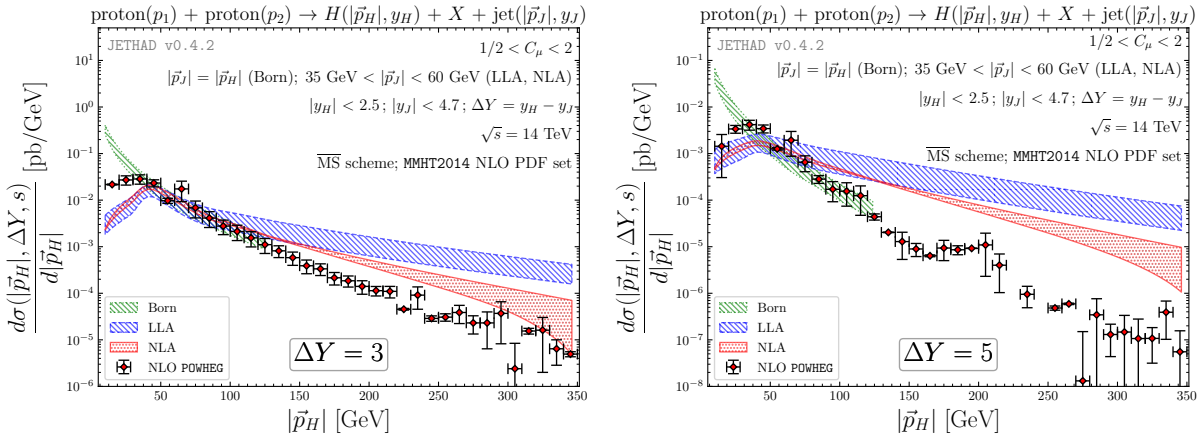

Figure 3.6: p_T-dependence of the cross section for the inclusive Higgs-jet hadroproduction for 35 GeV $< p_T <$ 60 GeV, $\sqrt{s} = 14$ TeV and for $\Delta Y = 3, 5$.

All these considerations brace the message that an a comprehensive investigation of the $|\vec{p}_H|$-distribution would depend on a brought together formalism where distinct resummations are simultaneously exemplified. Specifically, the effect of the BFKL re-

[2]Here, the bands related to the large top-mass limit are hardly distinguishable from the ones with physical top mass, thus we do not show figures for this comparison.

summation could rely on the delicate interplay among the Higgs transverse mass, the Higgs transverse momentum and the jet transverse momentum entering, in logarithmic form, the expressions of partial NLO corrections to impact factors (see Eqs. (3.10) and (3.11)). Future investigations including full higher-order corrections will permit us to additional check the strength of our estimations.

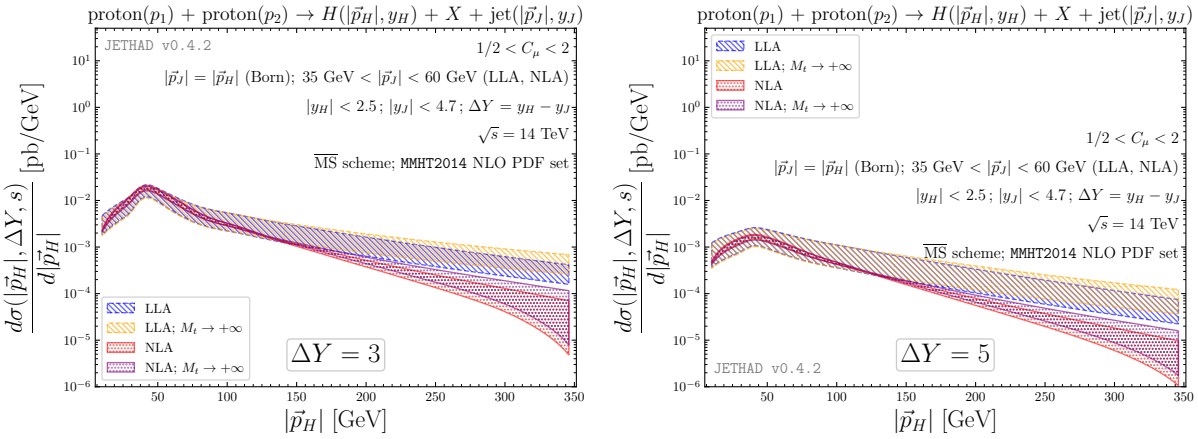

Figure 3.7: p_T-dependence of the cross section for the inclusive Higgs-jet hadroproduction in the large top-mass limit, for 35 GeV $< p_T <$ 60 GeV, $\sqrt{s}$ = 14 TeV and for $\Delta Y = 3, 5$.

3.1.4 Numerical specifics and uncertainty estimation

All the numerical studies were completed making use the previous mentioned tool JETHAD [106]. An auxiliary, independent MATHEMATICA interface allowed us to test the numerical reliability of our results. Quark and gluon PDFs were calculated through the MMHT2014 NLO PDF set [132] as provided by the LHAPDFv6.2.1 interpolator [124], whereas we selected a two-loop running coupling setup with $\alpha_s(M_Z) = 0.11707$ and with dynamic-flavor threshold.

All the relevant sources of numerical uncertainty, coming from the multidimensional integration over the final-state phase space and from the one-dimensional inte-

gral over the longitudinal momentum fraction ζ in the NLO impact factor corrections (Eqs. (3.10) and (3.11)), were directly estimated by the JETHAD integration tools.

Furthermore, we gauged the effect of concurrently varying the renormalization scales ($\mu_{R_{1,2,c}}$) and the factorization ones ($\mu_{F_{1,2}}$) of them around their *natural* values in the range 1/2 to two.

3.1.5 Summary

We have proposed the inclusive hadroproduction of a Higgs boson and of a jet featuring high transverse momenta and separated by a large rapidity distance as another diffractive semi-hard channel to test the BFKL resummation. At variance with previously discussed analyses, the Higgs + jet production channel exhibit quite a fair stability under higher-order corrections, so that the renormalization scale needs not to be too large as for other processes where BLM optimization had to be used. The obtained results for the distributions differential in the Higgs transverse momentum, provided an evidence that a high-energy treatment is valid and can be afforded in the region where Higgs p_T and the jet one are of the same order. Beyond that, the description for Higgs momentum distribution should rely on many-sided resummation formalism unifying different approaches. A possible extension of this work consists in the full NLA BFKL analysis, including the NLO jet impact factor, with a realistic implementation of the jet selection function, and the NLO forward-Higgs impact factor[3].

3.2 Bottom-flavored inclusive emissions

In this section, we present the inclusive semi-hard production, in proton-proton collisions, of two bottomflavored hadrons, as well as of a single bottom-flavored hadron

[3]See Appendix A.3.

accompanied by a light jet (depicted in Fig. 3.8), as novel probes for investigating the stabilization effects of the high-energy resummation under NLO corrections.

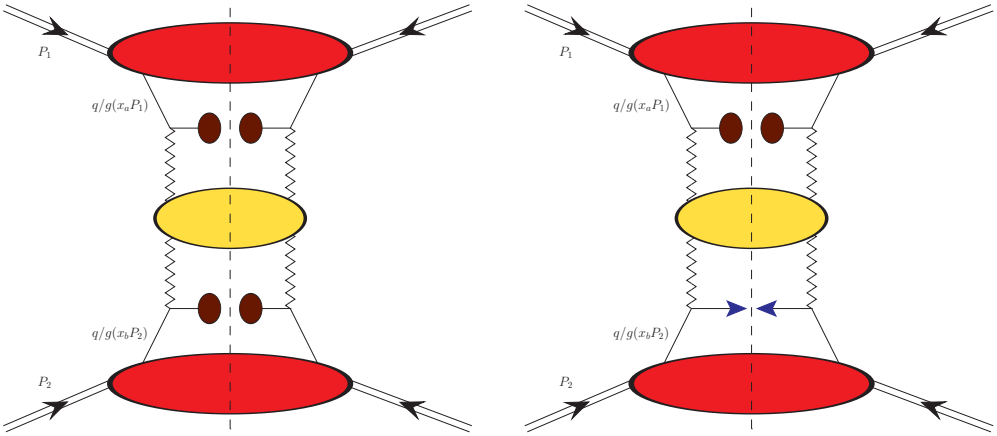

a) Double H_b b) H_b + jet

Figure 3.8: Schematic representation of the two inclusive processes under investigation.

3.2.1 Cross section in the NLA BFKL

The final state configurations of the inclusive processes under consideration is schematically represented in Fig. 3.8, where a b-hadron (p_1, y_1) is emitted along with another b-hadron or a jet (p_2, y_2), featuring a large rapidity separation, together with an undetected system of hadrons. For the sake of definiteness, we will consider the case where the rapidity for first detected final state object y_1 is larger than the second one y_2, so that $\Delta Y \equiv y_1 - y_2$ is always positive, which requires, for most considered values of ΔY, that the first object is forward and the second is backward.

The final-state objects are also required to possess large transverse momenta, $\vec{p}_1^{\,2} \sim \vec{p}_2^{\,2} \gg \Lambda^2_{QCD}$. The colliding protons' momenta P_1 and P_2 are taken as Sudakov basis vectors satisfying $P_1^2 = P_2^2 = 0$ and $2(P_1 \cdot P_2) = s$, so that the momenta of detected

objects can be decomposed as

$$p_{1,2} = x_{1,2}P_{1,2} + \frac{\vec{p}_{1,2}^{\,2}}{x_{1,2}s}P_{2,1} + p_{1,2\perp} \ , \quad p_{1,2\perp}^2 = -\vec{p}_{1,2}^{\,2} \tag{3.16}$$

The parton momentum fractions $x_{1,2}$ in the large rapidity limit are connected to the respective rapidities through the relation $y_{1,2} = \pm\frac{1}{2}\ln\frac{x_{1,2}^2 s}{\vec{p}_{1,2}^{\,2}}$, so that $dy_{1,2} = \pm\frac{dx_{1,2}}{x_{1,2}}$, and $\Delta Y = y_1 - y_2 = \ln\frac{x_1 x_2 s}{|\vec{p}_1||\vec{p}_2|}$, here the spatial part of the four-vector $p_{1\parallel}$ being taken positive.

In QCD collinear factorization, the processes can be viewed as started by two protons each emitting one parton, according to its parton distribution function (PDF) and ended with the detected b-hadron in the final state according to that its fragmentation functions (FFs). Within the collinear factorization LO cross section is given as a convolution of the (PDFs) and (FFs) with the subsequent partonic hard scattering as follows

$$\begin{aligned}\frac{d\sigma^{pp\to H_b H_b}}{dx_H dx_J d^2k_H d^2k_J} &= \sum_{r,s=q,\bar{q},g}\int_0^1 dx_1\int_0^1 dx_2\ f_r\left(x_1,\mu_F\right)\ f_s\left(x_2,\mu_F\right)\\ \times\int_{x_1}^1\frac{d\beta_1}{\beta_1}\int_{x_2}^1\frac{d\beta_2}{\beta_2}D_r^{H_b}\left(\frac{x_1}{\beta_1}\right)D_s^{H_b}\left(\frac{x_2}{\beta_2}\right)&\frac{d\hat{\sigma}_{r,s}\left(\hat{s},\mu_F\right)}{dx_1 dx_2 d\beta_1 d\beta_2 d^2\vec{p}_1 d^2\vec{p}_2}\ ,\end{aligned} \tag{3.17}$$

for the H_b channel, and similarly

$$\begin{aligned}\frac{d\sigma^{pp\to H_b jet}}{dx_H dx_J d^2k_H d^2k_J} &= \sum_{r,s=q,\bar{q},g}\int_0^1 dx_1\int_0^1 dx_2\ f_r\left(x_1,\mu_F\right)\ f_s\left(x_2,\mu_F\right)\\ &\times\int_{x_1}^1\frac{d\beta_1}{\beta_1}D_r^{H_b}\left(\frac{x_1}{\beta_1}\right)\frac{d\hat{\sigma}_{r,s}\left(\hat{s},\mu_F\right)}{dx_1 dx_2 d\beta_1 d\beta_2 d^2\vec{p}_1 d^2\vec{p}_2}\ .\end{aligned} \tag{3.18}$$

in the H_b plus jet channel.

Here the r,s indices specify the parton types (quarks $q = u,d,s,c,b$; antiquarks $\bar{q} = \bar{u},\bar{d},\bar{s},\bar{c},\bar{b}$; or gluon g), $f_{r,s}\left(x,\mu_F\right)$ and $D_{r,s}^{H_b}\left(x/\beta,\mu_F\right)$ denote the initial proton PDFs and the final detected baryon FFs, respectively; $x_{1,2}$ are the longitudinal fractions of

the partons involved in the hard subprocess, while μ_F is the factorization scale; $d\hat{\sigma}_{r,s}\,(\hat{s})$ is the partonic cross section and $\hat{s} \equiv x_1 x_2 s$ is the squared center-of-mass energy of the parton-parton collision subprocess.

In the BFKL approach the cross section of the hard subprocesses can be presented as the Fourier sum of the azimuthal coefficients $\mathscr{C}_n$, having so

$$\frac{d\sigma}{dy_1 dy_2\, d|\vec{p}_1|\, d|\vec{p}_2| d\phi_1 d\phi_2} = \frac{1}{(2\pi)^2}\left[\mathscr{C}_0 + \sum_{n=1}^{\infty} 2\cos(n\phi)\,\mathscr{C}_n\right], \tag{3.19}$$

where $\phi = \phi_1 - \phi_2 - \pi$, with $\phi_{1,2}$ the baryon/jet azimuthal angles, while $y_{1,2}$ and $\vec{p}_{1,2}$ are their rapidities and transverse momenta, respectively. The ϕ-averaged cross section $\mathscr{C}_0$ and the other coefficients $\mathscr{C}_{n\neq 0}$ are given by

$$\begin{aligned}
\mathscr{C}_n &\equiv \int_0^{2\pi} d\phi_1 \int_0^{2\pi} d\phi_2\, \cos[n(\phi_1 - \phi_2 - \pi)]\, \frac{d\sigma}{dy_1 dy_2\, d|\vec{p}_1|\, d|\vec{p}_2| d\phi_1 d\phi_2} \\
&= \frac{e^{\Delta Y}}{s}\int_{-\infty}^{+\infty} d\nu \left(\frac{x_1 x_2 s}{s_0}\right)^{\bar{\alpha}_s(\mu_R)\left\{\chi(n,\nu)+\bar{\alpha}_s(\mu_R)\left[\bar{\chi}(n,\nu)+\frac{\beta_0}{8N_c}\chi(n,\nu)\left[-\chi(n,\nu)+\frac{10}{3}+2\ln\left(\frac{\mu_R^2}{\sqrt{\vec{p}_1^{\,2}\vec{p}_2^{\,2}}}\right)\right]\right]\right\}} \\
&\quad \times \alpha_s^2(\mu_R) c_1(n,\nu,|\vec{p}_1|,x_1)[c_2(n,\nu,|\vec{p}_2|,x_2)]^* \\
&\quad \times \left\{1 + \alpha_s(\mu_R)\left[\frac{c_1^{(1)}(n,\nu,|\vec{p}_1|,x_1)}{c_1(n,\nu,|\vec{p}_1|,x_1)} + \left[\frac{c_2^{(1)}(n,\nu,|\vec{p}_2|,x_2)}{c_2(n,\nu,|\vec{p}_2|,x_2)}\right]^*\right]\right. \\
&\quad \left. + \bar{\alpha}_s^2(\mu_R)\ln\left(\frac{x_1 x_2 s}{s_0}\right)\frac{\beta_0}{4N_c}\chi(n,\nu) f(\nu)\right\}.
\end{aligned} \tag{3.20}$$

3.2.2 Phenomenological analysis

We give results in the full NLA of cross sections, azimuthal correlations and double differential distributions in the transverse momenta of final-state particles, the latter is proposed as a common basis to investigate the interplay of distinct resummations mechanisms. In our analysis, the light-flavored jet is always tagged in its typical CMS ranges [128], *i.e.* $|y_J|< 4.7$ and 35 GeV $< p_J <$ 60 GeV For our hadron, we admit a tagging of b-hadrons on a slightly wider range, $|y_H|< 2.4$ and 20 GeV $< p_H <$ 60 GeV. For the non-perturbative ingredients in our formalism, we employed the MMHT14 PDF set, and for the fragmentation of our hadrons we use the KKSS07 NLO FFs.

Observables:

- ΔY*-distribution*: The first observable we take into our account is the ϕ-averaged contribution to the cross section, also known as ΔY-distribution or simply C_0:

$$C_0 = \int_{y_1^{\min}}^{y_1^{\max}} dy_1 \int_{y_2^{\min}}^{y_2^{\max}} dy_2 \int_{p_1^{\min}}^{p_1^{\max}} d|\vec{p}_1| \int_{p_2^{\min}}^{p_2^{\max}} d|\vec{p}_2|\ \delta(\Delta Y - (y_1 - y_2))\ \mathscr{C}_0\,. \tag{3.21}$$

- *Azimuthal correlations*: Analogously to C_0, we define the phase-space integrated higher azimuthal coefficients, $C_{n\neq 0}$, to build their ratios

$$R_{nm} \equiv \frac{C_n}{C_m} = \frac{\int_{y_1^{\min}}^{y_1^{\max}} dy_1 \int_{y_2^{\min}}^{y_2^{\max}} dy_2 \int_{p_1^{\min}}^{p_1^{\max}} d|\vec{p}_1| \int_{p_2^{\min}}^{p_2^{\max}} d|\vec{p}_2|\ \delta(\Delta Y - (y_1 - y_2))\ \mathscr{C}_n}{\int_{y_1^{\min}}^{y_1^{\max}} dy_1 \int_{y_2^{\min}}^{y_2^{\max}} dy_2 \int_{p_1^{\min}}^{p_1^{\max}} d|\vec{p}_1| \int_{p_2^{\min}}^{p_2^{\max}} d|\vec{p}_2|\ \delta(\Delta Y - (y_1 - y_2))\ \mathscr{C}_m}\,. \tag{3.22}$$

  The R_{n0} ratios determine the values of the mean cosines $\langle \cos n\varphi \rangle$, while the ones without zero indices represent ratios of correlations. We study the behavior of the R_{nm} moments as functions of ΔY and in the kinematic ranges defined above.

- *Double differential p_T-distribution*: The transverse-momentum double differential

cross section given as

$$\frac{d\sigma(|\vec{p}_{1,2}|,\Delta Y,s)}{d|\vec{p}_1|d|\vec{p}_2|d\Delta Y} = \int_{y_1^{\min}}^{y_1^{\max}} \mathrm{d}y_1 \int_{y_2^{\min}}^{y_2^{\max}} \mathrm{d}y_2\, \delta(\Delta Y - (y_1 - y_2))\, \mathscr{C}_0\left(|\vec{p}_1|,|\vec{p}_2|,y_1,y_2\right) . \tag{3.23}$$

3.2.3 Results and discussion

In Fig. 3.9 we report in the upper panel the C_0 results for the double H_b production, and for the H_b + jet reaction the C_0 results are presented in the lower one. Predictions using natural scales present in the left panel of the figure, while the BLM results shown in the right one. Here the decreasing behavior of both LLA and NLA with the increasing intervals of rapidity is a usual BFKL pattern observed in previous semi-hard processes. Although the resummation of high-energy logs leads to a growth with energy of the pure hard cross section, the total effect is downtrend by the convoluted PDFs and FFs. We observe that NLA uncertainty bands are almost contained inside LLA one at BLM scale, and decouple form each other at natural scale. This decoupling behavior is a manifestation of the fact that NLA series is stable under varying scale. Moreover in the case of double H_b the LLA bands tend to shrink, while getting wider in H_b+ jet one.

In Figs. 3.10 and 3.11 we present the $R_{nm} \equiv C_n/C_m$ moments results for the double H_b probe channel at natural and BLM scales, respectively. The notable observation here is that the natural scale predictions are closely in shape to the corresponding optimized (BLM) ones. The reason of the increased stability for $R_{n0} \equiv C_n/C_0$, is due to the relatively small uncertainty on C_0.

In Figs. 3.12 we present results for azimuthal ratios in the H_b+ jet reaction at natural scales. Here, the NLA R_{n0} correlations appear to be strongly sensitive to scale variation[4]. Corresponding results for R_{n0} moments at BLM scale (shown in Fig 3.13)

[4]In semi-hard processes with emitted jet, such as Mueller–Navelet dijet or Hadron + jet, whenever

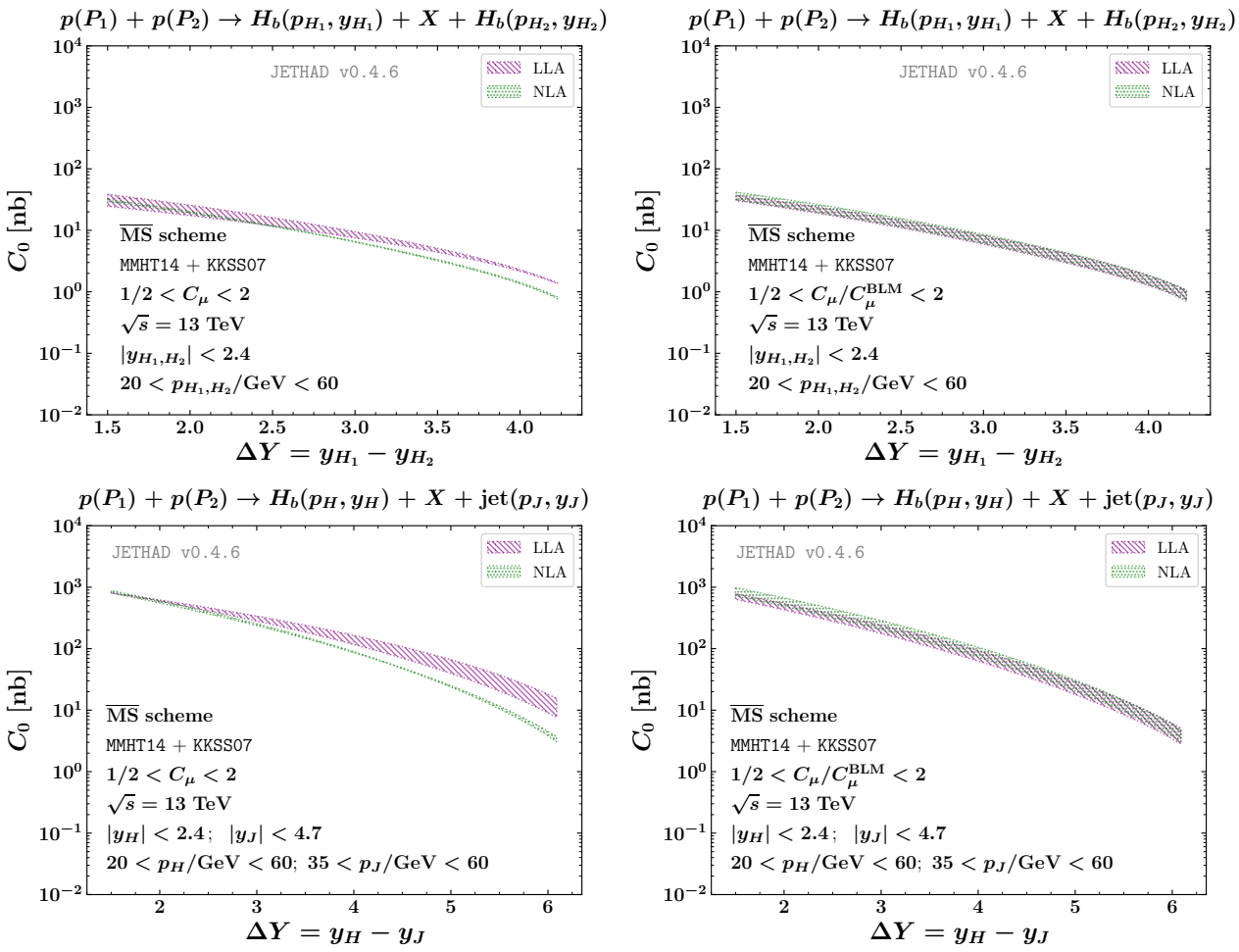

Figure 3.9: ΔY-shape of C_0 in the double H_b (upper) and in the H_b + jet channel (lower), at natural (left) and BLM-optimized scales (right), and for $\sqrt{s}$ = 13 TeV .

have a similar shape to predictions of the double H_b channel.

In Figs 3.14 and 3.15 we report p_T-distributions results in H_b+ jet channel at ΔY = 3 and 5, without employing any scale optimization. We observe that results fall rapidly at larger values of transverse momenta, $|\vec{p}_H|$ and $|\vec{p}_J|$. Here NLA predictions (right panels) are lower than LLA ones (left panels) as expected. The scale variation effect shows pertinent with respect to what happens for the rapidity distribution and

instabilities emerging at natural scales are so strong, these probes cannot be studied at natural scales.

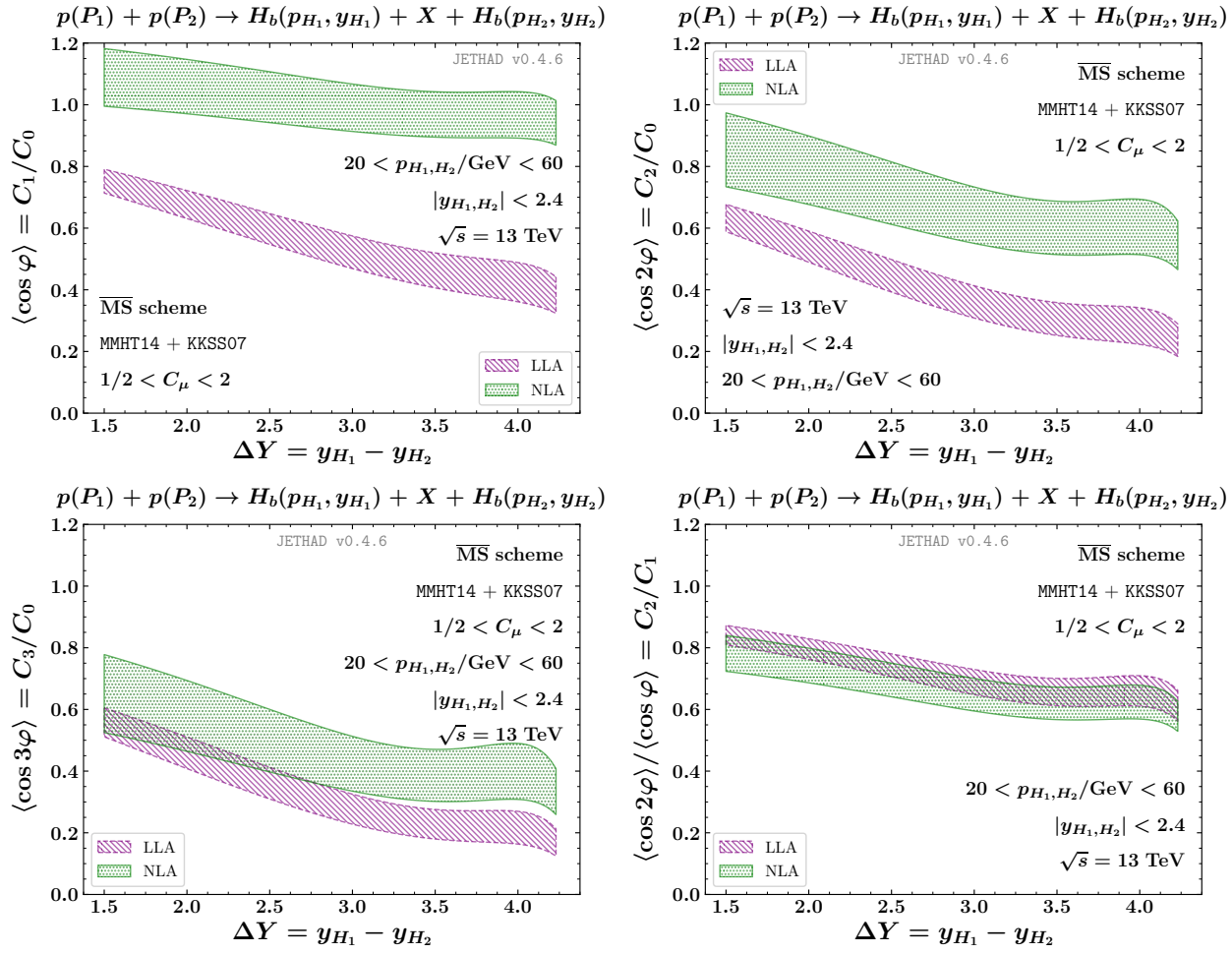

Figure 3.10: ΔY-shape of azimuthal correlations, $R_{nm} \equiv C_n/C_m$, in the double H_b channel, at natural scales, and for $\sqrt{s}$ = 13 TeV .

azimuthal correlations.

Tables 3.1 and 3.2 give us explicit quantitative information, by presenting numerical values of our distributions for a representative sample of $(|\vec{p}_H|, |\vec{p}_J|)$ pairs. We observe that moving away from the symmetric p_T-region, $|\vec{p}_H| \simeq |\vec{p}_J|$, the sensitivity on scale variation of all the predictions increases. Furthermore, for almost all the considered p_T-pairs in Tables 3.1 and 3.2, LLA results fall off when the C_μ scale parameter increase, while NLA prediction tend to oscillate around $C_\mu = 1$, which appears to act

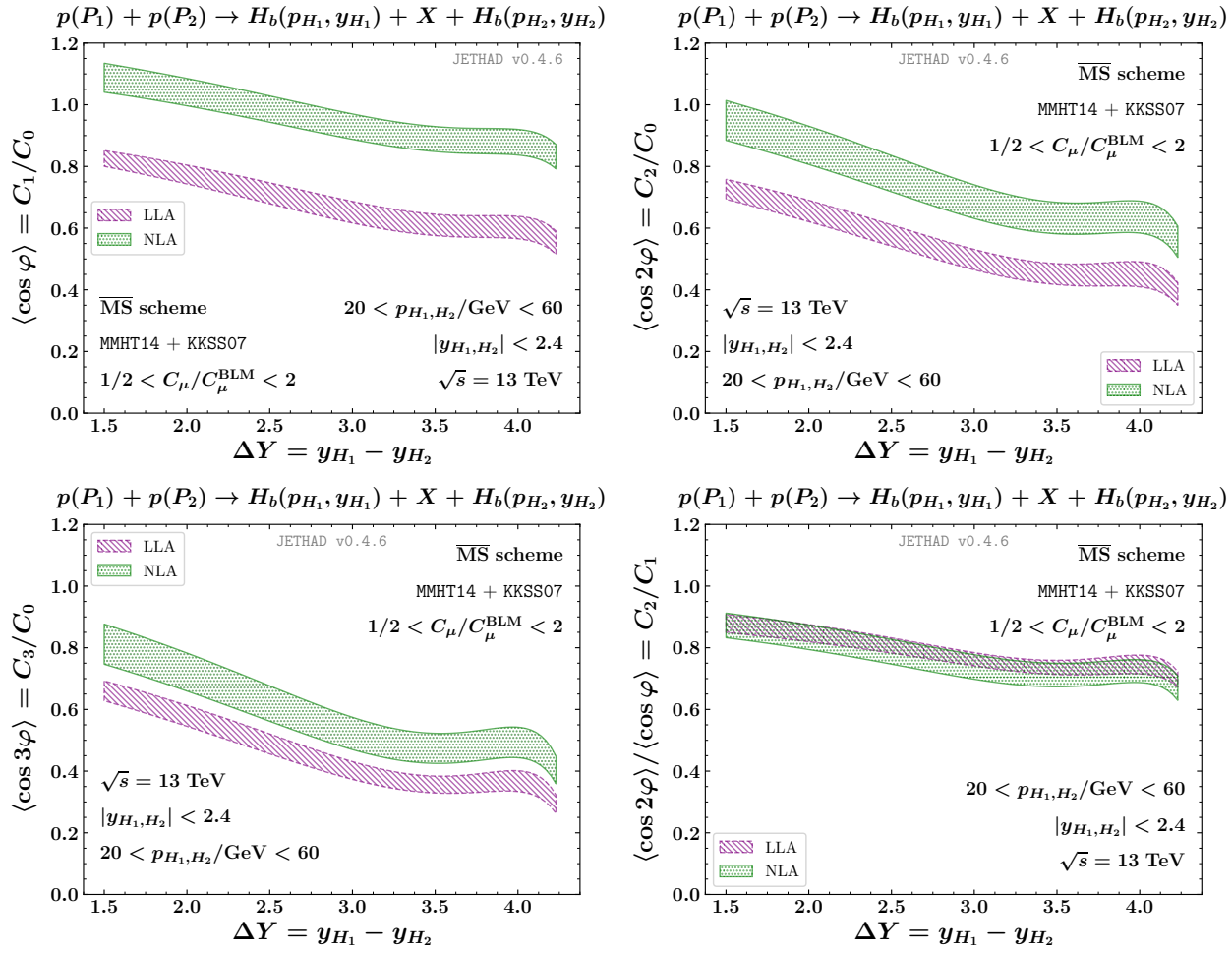

Figure 3.11: ΔY-shape of azimuthal correlations, $R_{nm} \equiv C_n/C_m$, in the double H_b channel, at BLM scales, and for $\sqrt{s}$ = 13 TeV .

as a critical point for them.

This clearly indicates that our distributions are more stable on scale variation when higher-order corrections are included. At the same time for ΔY = 3 (Table 3.1), their sensitivity on C_μ is almost of the same order (up to 45%) for both LLA and NLA cases, while it is roughly halved when passing from LLA (up to 50%) to NLA (up to 25%) for ΔY = 5 (Table 3.2). This reflects the fact that the stabilizing effect of higher-order corrections is more pronounced when we go through the BFKL-sensitive region, *i.e.*

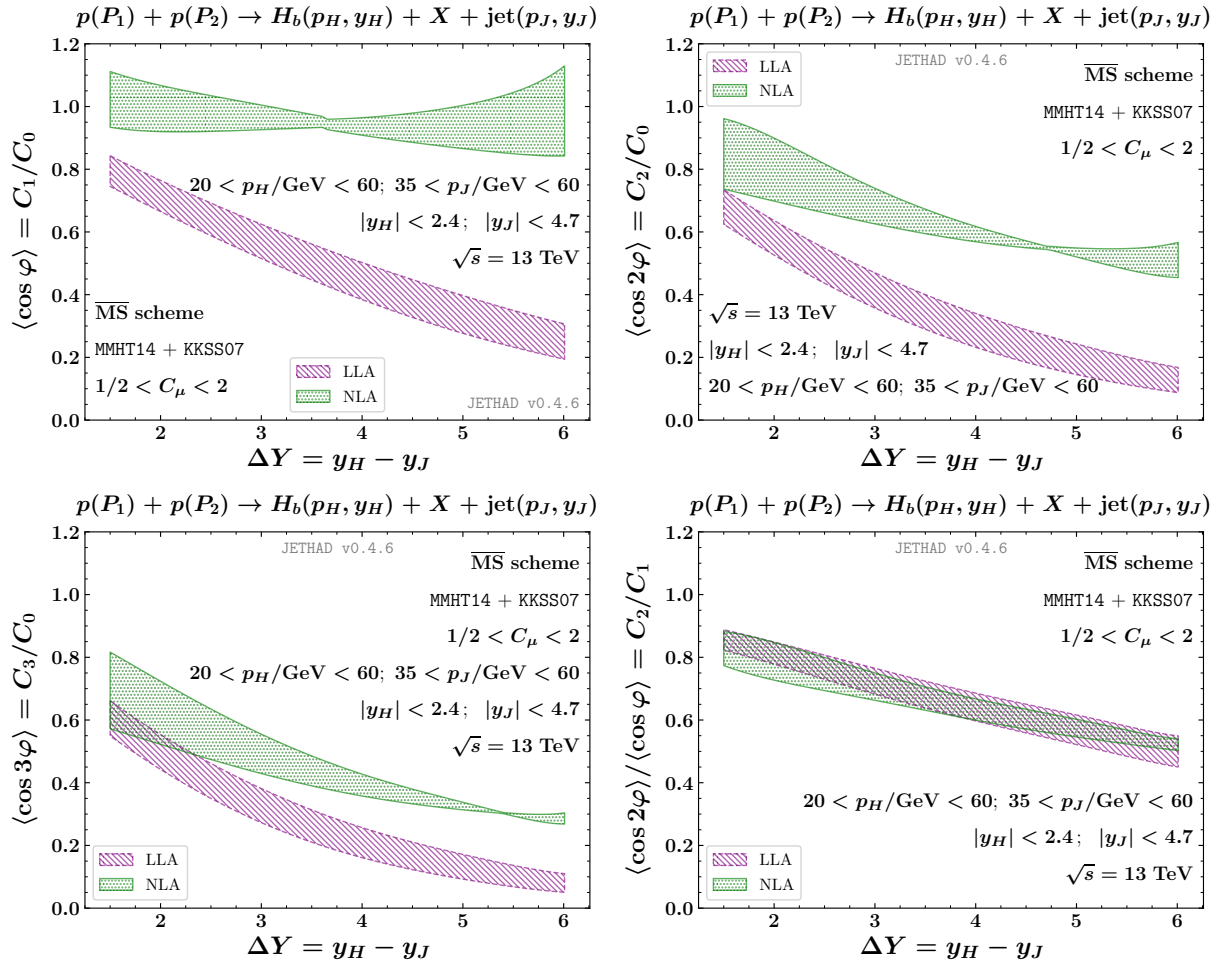

Figure 3.12: ΔY-shape of azimuthal correlations, $R_{nm} \equiv C_n/C_m$, in the H_b + jet channel, at natural scales, and for $\sqrt{s}$ = 13 TeV .

when ΔY grows. Finally, we observe that our distributions are much smaller when $|\vec{p}_H| > |\vec{p}_J|$ than when $|\vec{p}_H| < |\vec{p}_J|$. Actually, it becomes more and more difficult to produce a b-flavored bound state than a light jet when the transverse momentum grows.

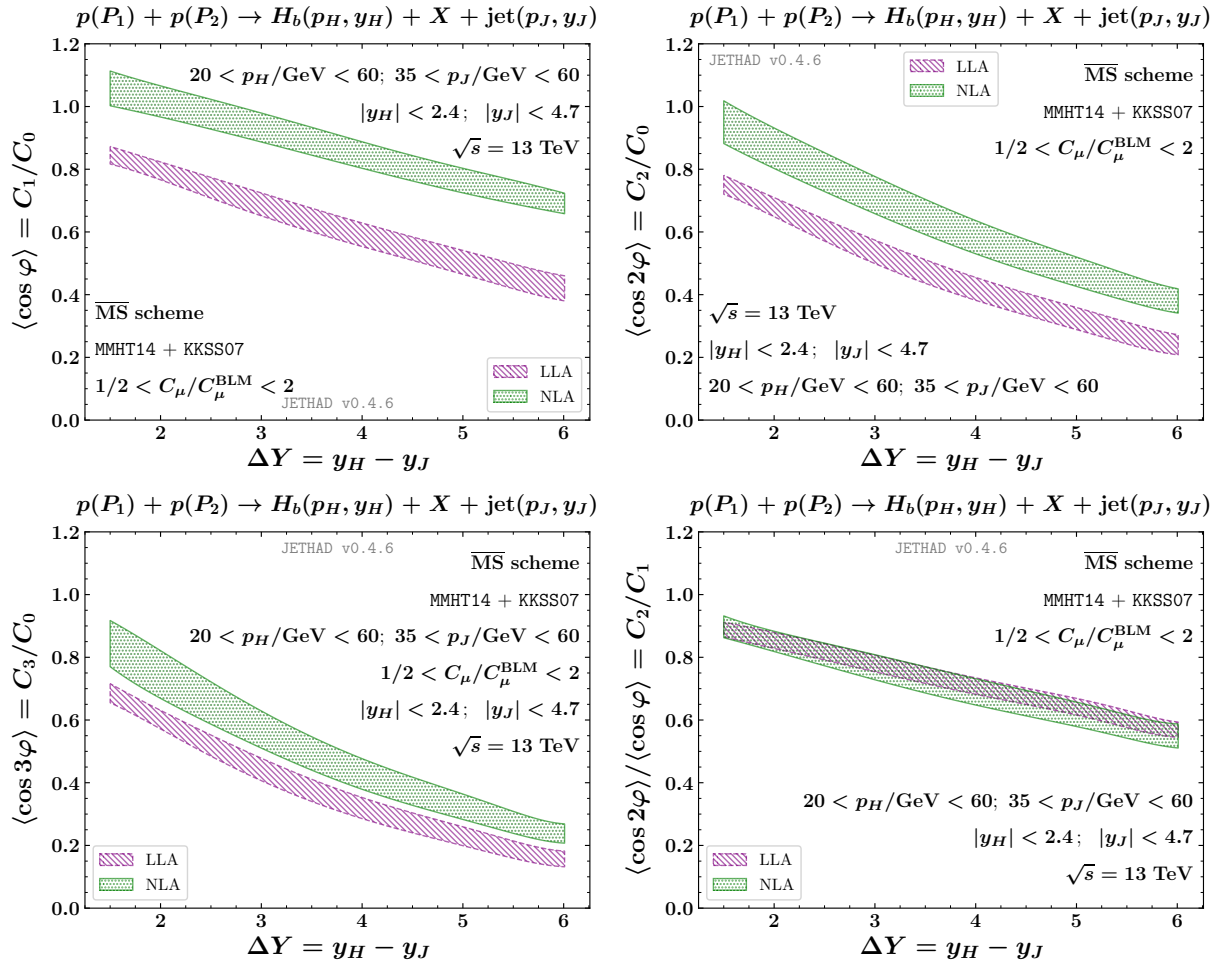

Figure 3.13: ΔY-shape of azimuthal correlations, $R_{nm} \equiv C_n/C_m$, in the H_b + jet channel, at BLM scales, and for $\sqrt{s}$ = 13 TeV .

3.2.4 Summary

In this proposed probes, motivated by looking for signals of stabilization of the high-energy resummation under higher-order corrections and under scale variation, we found that these effects are present and allow for the description or BFKL-sensitive observables at natural scales, moreover, study azimuthal moments at natural scales also when jet emissions are allowed, which is a novel feature which corroborates the statement that heavy-flavored emissions of bound states act as fair stabilizers of the

Table 3.1: Representative values of the double differential p_T-distribution [nb/GeV^2] for the H_b + jet channel, at $\Delta Y = 3$ and $\sqrt{s} = 13$ TeV.

$\lvert\vec{p}_H\rvert$ [GeV]	$\lvert\vec{p}_J\rvert$ [GeV]	LLA $C_\mu = 1/2$	LLA $C_\mu = 1$	LLA $C_\mu = 2$	NLA $C_\mu = 1/2$	NLA $C_\mu = 1$	NLA $C_\mu = 2$
12.5	12.5	54.505(11)	110.673(20)	119.483(22)	59.87(26)	96.16(11)	107.02(21)
20	20	9.5523(18)	10.8676(20)	9.9592(17)	9.679(11)	9.845(16)	9.604(28)
20	30	4.2318(11)	4.7487(10)	4.5908(10)	3.516(11)	3.564(12)	3.816(13)
30	20	2.45567(87)	2.35844(71)	1.97517(80)	1.404(19)	1.028(19)	0.851(20)
30	30	1.31402(33)	1.22764(28)	1.03082(27)	1.2051(14)	1.0995(28)	1.0184(38)
30	50	0.37493(11)	0.357939(83)	0.31849(10)	0.2780(11)	0.2648(12)	0.2706(12)
50	30	0.20170(11)	0.166163(72)	0.129175(83)	0.0481(18)	0.0326(14)	0.0309(14)
50	50	0.079078(22)	0.064566(20)	0.050412(21)	0.06287(15)	0.05511(21)	0.04978(25)
75	75	0.0069684(20)	0.0053265(11)	0.0039949(12)	0.00489(19)	0.004310(22)	0.003885(23)

Table 3.2: Representative values of the double differential p_T-distribution [nb/GeV^2] for the H_b + jet channel, at $\Delta Y = 5$ and $\sqrt{s} = 13$ TeV.

$\lvert\vec{p}_H\rvert$ [GeV]	$\lvert\vec{p}_J\rvert$ [GeV]	LLA $C_\mu = 1/2$	LLA $C_\mu = 1$	LLA $C_\mu = 2$	NLA $C_\mu = 1/2$	NLA $C_\mu = 1$	NLA $C_\mu = 2$
12.5	12.5	23.0020(29)	36.3534(77)	33.2496(52)	11.979(44)	15.952(19)	18.320(25)
20	20	3.01358(59)	2.82293(18)	2.25985(22)	1.4016(17)	1.3654(18)	1.4063(26)
20	30	1.02761(16)	0.91503(13)	0.74331(11)	0.44181(85)	0.43683(93)	0.47148(95)
30	20	0.89192(16)	0.721321(96)	0.530710(87)	0.2406(21)	0.2053(20)	0.2079(21)
30	30	0.322595(57)	0.256804(29)	0.19209(3)	0.13595(17)	0.12690(23)	0.12645(29)
30	50	0.0671327(66)	0.052709(11)	0.0402854(42)	0.024583(87)	0.024557(86)	0.026155(76)
50	30	0.056804(16)	0.040257(10)	0.0277934(41)	0.00681(16)	0.00685(15)	0.00820(15)
50	50	0.0136641(35)	0.009805(20)	0.0069481(15)	0.004873(15)	0.004708(15)	0.004682(14)
75	75	0.000847907(94)	0.00057898(48)	0.000397990(32)	0.0002501(15)	0.0002620(12)	0.0002661(10)

high-energy series.

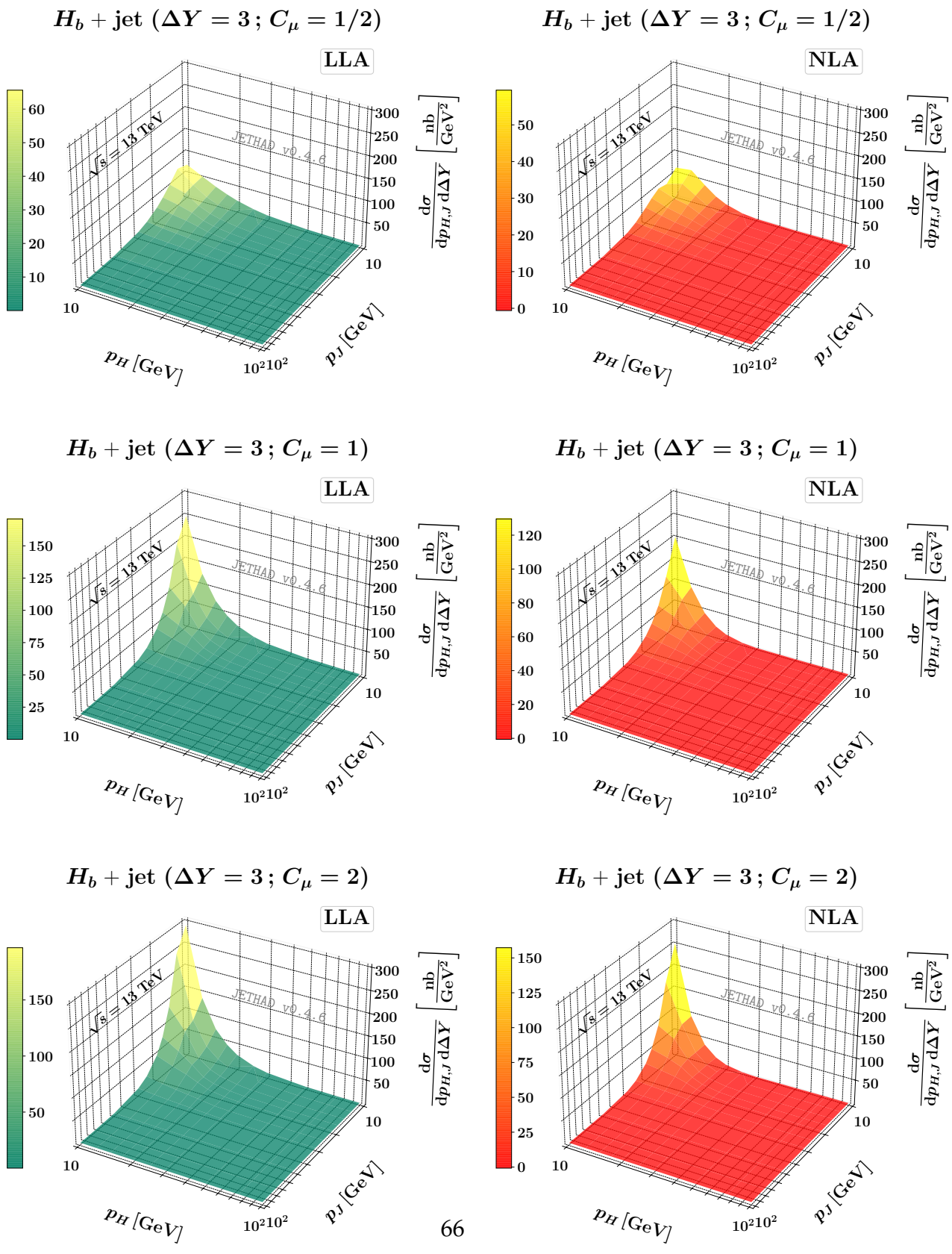

Figure 3.14: Double differential p_T-distribution for the H_b + jet channel at $\Delta Y = 3$, $\sqrt{s} = 13$ TeV, and in the LLA (left) and NLA (right) resummation accuracy .

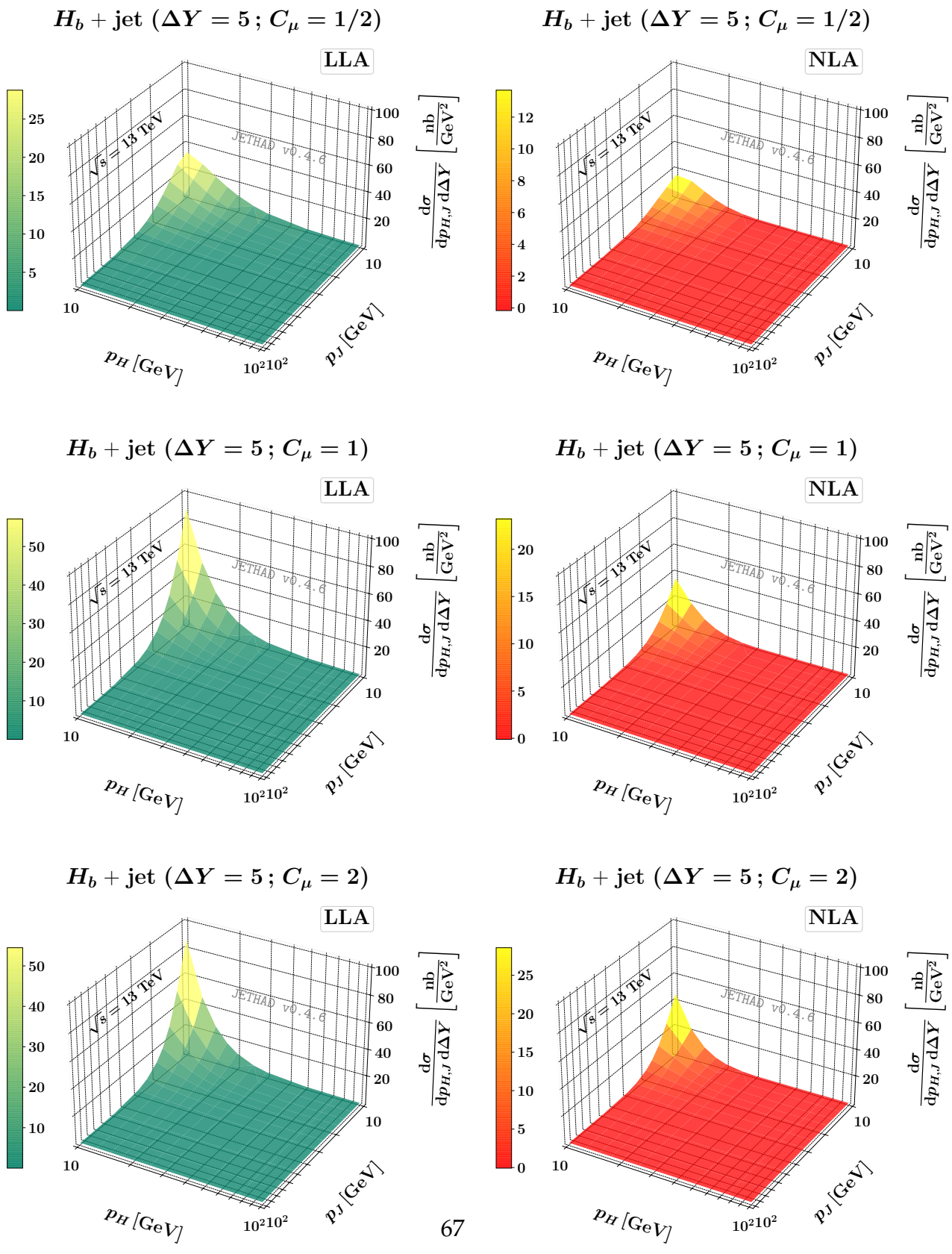

Figure 3.15: Double differential p_T-distribution for the H_b + jet channel at $\Delta Y = 5$, $\sqrt{s} = 13$ TeV, and in the LLA (left) and NLA (right) resummation accuracy .

Chapter 4

Conclusions and Outlook

4.1 Conclusions

We pursued the goal of following the phenomenological paths toward hunting signals of stabilization of the high-energy resummation under higher-order corrections and energy-scale variation, in order to perform a precision calculations via BFKL formalism. The BFKL theoretical key ingredients have been introduced in chapter 1. Chapter 2 was devoted to describe a proposed candidate probe of BFKL dynamics at the LHC in the channel of inclusive production of an identified charged light hadron and a jet, separated by a large rapidity gap. We have given some general arguments that this reaction, though being a simple hybridization of two already well studied ones, presents some own features which can make it worthy of consideration in future analyses at the LHC. In view of that, we gave some theoretical predictions, with next-to-leading accuracy, for the cross section averaged over the azimuthal-angle between the identified jet and hadron and for ratios of the azimuthal coefficients, employing the BLM optimization approach for fixing the renormalization scale μ_R. The trends observed in the distributions over the rapidity interval between the jet and the hadron are not different from the cases of Mueller-Navelet jets (see, Refs. [20, 22, 39–50]), and hadron-hadron [107–109], when the jet is detected by CMS, and due to the different nature of the objects produced in this channel, asymmetric cuts were naturally con-

sidered, thus enhancing the BFKL effects, whereas some new features have appeared when the jet is seen by CASTOR, which deserve further investigation.

We have followed in chapter 3 the new direction toward hunting signals for the stability of the BFKL series at natural scales; section 3.1 was dictated to investigate the inclusive hadroproduction of a Higgs boson and of a jet featuring high transverse momenta and separated by a large rapidity distance. In this process the large transverse mass of the emitted Higgs boson suppresses the higher-order corrections, thus affording us a peerless opportunity to study energy scales around their natural values. Furthermore, we have extended this study to distributions differential in the Higgs transverse momentum, providing evidence that a high-energy treatment is valid and can be afforded in the region where Higgs p_T and the jet one are of the similar size, and beyond, the description for Higgs momentum distribution would be relied on a multi-lateral resummation formalism unifying different approaches. The stability effects that allow for the description or BFKL-sensitive observables at natural scales have been spotted in section 3.2, where we have proposed the inclusive emission, in proton-proton collisions, of a forward bottom-flavored hadron accompanied by another backward bottom-flavored hadron or a backward light-flavored jet in semi-hard regimes that can be studied at current LHC energies. In the H_b + jet channel it was possible to study azimuthal moments at natural scales although previous studies on Mueller–Navelet dijet or ligther-hadron + jet production have shown that instabilities emerge when jet emissions are studied at natural scales, so strong to prevent any realistic analysis. All that would support the recent assumption, that heavy-flavored emissions of bound states act as fair stabilizers of the high-energy series. Here, the stability of our predictions motivates our interest in proposing the hybrid high-energy and collinear factorization as an additional tool to improve the fixed-order description. Moreover we believe that future, exhaustive studies of the inclusive exclusive observables, such as the double differential transverse-momentum

distributions, would benefit from the inclusion of high-energy effects in a unified formalism where distinct resummations are concurrently embodied.

4.2 Outlook

Future studies are needed to unveil the connection between the sensitivity of some observable, such as R_{n0} ratio, on scale variation and other potential sources of uncertainty, as the jet algorithm selection. For the Higgs + jet program, an obvious extension consists in the full NLA BFKL analysis, including a NLO jet impact factor and the NLO Higgs impact factor, the latter one was calculated quite recently in the large top-mass limit, and a full calculation in the so-called (ν, n)-representation (projected on the eigenfunctions of the BFKL kernel) which can be easily implemented in numerical calculations, is underway. The next step in our program of investigating semi-hard phenomenology relies on a two-fold strategy: first, we plan to compare observables sensitive to heavy-flavor production in regimes where either the light-flavored quarks and gluons are accounted for by proton collinear parton densities (PDFs) or in case when all flavors are present in the initial state and are taken massless, and possibly do a match between the two descriptions. The inclusion of quarkonium production channels will certainly enrich our phenomenology. The second step is extending our studies on heavy flavor by considering wider kinematic ranges.

Appendix A

Forward Jet, Hadron, and Higgs impact factors

In this Appendix the expressions for the LO and NLO corrections to both jet and an identified hadron impact factors are given.

A.1 Jet impact factor

In this subsection the expressions for the LO forward jet impact factor and the NLO correction in the small-cone limit are given, (for more details about the latter see Ref. [21])
For the jet vertex at LO it reads:

$$c_1(n,\nu,|\overrightarrow{k}|,x) = 2\sqrt{\frac{C_F}{C_A}}(\overrightarrow{k}^2)^{-i\nu-1/2}\left\{\frac{C_A}{C_F}f_g(x)+\sum_{a=q,\bar{q}}f_a(x)\right\}, \tag{A.1}$$

where the functions $f(x)$ are the parton distribution functions (PDFs), and $C_A = N$, $C_F = (N^2 - 1/2N)$.

$$c_2(n,\nu,|\overrightarrow{k}|,x) = \left[c_1(n,\nu,|\overrightarrow{k}|,x)\right]^*. \tag{A.2}$$

The NLO correction to the forward jet impact factor in the small-cone limit $c_2^{(1)}(n,\nu,|\overrightarrow{k}|,x)$ has following expression

$$c_1^{(1)}(n,\nu,|\overrightarrow{k}|,x) = \frac{1}{\pi}\sqrt{\frac{C_F}{C_A}}(\overrightarrow{k})^{i\nu-1/2}\int_x^1 \frac{d\zeta}{\zeta}\zeta^{-\bar{\alpha}_s(\mu_R)\chi(n,\nu)}\Big\{\sum_{\alpha=q,\bar{q}} f_a(\frac{x}{\zeta})$$
$$\times\Big[\Big(P_{qq}(\zeta)+\frac{C_A}{C_F}P_{gq}(\zeta)\Big)\ln\frac{\overrightarrow{k}^2}{\mu_F^2} - 2\zeta^{-2\gamma}\ln R(P_{qq}(\zeta)+P_{gq}(\zeta)) - \frac{\beta_0}{2}\ln\frac{\overrightarrow{k}^2}{\mu_R^2}\delta(1-\zeta)$$
$$+C_A\delta(1-\zeta)\Big(\chi(n,\gamma)\ln\frac{s_0}{\overrightarrow{k}^2}+\frac{85}{18}+\frac{\pi^2}{2}+\frac{1}{2}\Big(\psi'(1+\gamma+\frac{n}{2})-\psi'(\frac{n}{2}-\gamma)-\chi^2(n,\gamma)\Big)\Big)$$
$$+(1+\zeta^2)\Big[C_A\Big(\frac{1+\zeta^{-2\gamma}\chi(n,\gamma)}{2(1-\zeta)_+}-\zeta^{-2\gamma}\Big(\frac{\ln(1-\zeta)}{1-\zeta}\Big)_+\Big)+(C_F-\frac{C_A}{2})\Big[\frac{\bar{\zeta}}{\zeta^2}I_2-\frac{2\ln\zeta}{1-\zeta}$$
$$+2\Big(\frac{\ln(1-\zeta)}{1-\zeta}\Big)_+\Big]\Big]+\delta(1-\zeta)(C_F(3\ln 2-\frac{\pi^2}{3}-\frac{9}{2})-\frac{5n_f}{9})$$
$$C_A\zeta+C_F\bar{\zeta}+\frac{1+\bar{\zeta}^2}{\zeta}\Big(C_A\frac{\bar{\zeta}}{\zeta}I_1+2C_A\ln\frac{\bar{\zeta}}{\zeta}+C_F\zeta^{-2\gamma}(\chi(n,\gamma)-2\ln\bar{\zeta})\Big)\Big]+f_g\Big(\frac{x}{\zeta}\Big)\frac{C_A}{C_F}$$
$$\times\Big[\Big(P_{gg}(\zeta)+2n_f\frac{C_A}{C_F}P_{qg}(\zeta)\Big)\ln\frac{\overrightarrow{k}^2}{\mu_F^2} - 2\zeta^{-2\gamma}\ln R(P_{gg}(\zeta)+2n_fP_{qg}(\zeta)) - \frac{\beta_0}{2}\ln\frac{\overrightarrow{k}^2}{4\mu_R^2}\delta(1-\zeta)$$
$$+C_A\delta(1-\zeta)\Big(\chi(n,\gamma)\ln\frac{s_0}{\overrightarrow{k}^2}+\frac{1}{12}+\frac{\pi^2}{6}+\frac{1}{2}\Big(\psi'(1+\gamma+\frac{n}{2})-\psi'(\frac{n}{2}-\gamma)-\chi^2(n,\gamma)\Big)\Big)$$
$$+2C_A(1-\zeta^{-2\gamma})\Big(\Big(\frac{1}{\zeta}-2+\zeta\bar{\zeta}\Big)\ln\bar{\zeta}+\frac{(1-\zeta)}{1-\zeta}\Big)$$
$$+C_A\Big[\frac{1}{\zeta}+\frac{1}{(1-\zeta)_+}-2\zeta\bar{\zeta}\Big]\Big((1+\zeta^{-2\gamma})\chi(n,\gamma)-2\ln\zeta+\frac{\bar{\zeta}^2}{\zeta^2}I_2\Big)$$
$$+n_f\Big[2\zeta\bar{\zeta}\frac{C_F}{C_A}+(\zeta^2+\bar{\zeta}^2)\Big(\frac{C_F}{C_A}\chi(n,\gamma)+\frac{\bar{\zeta}}{\zeta}I_3\Big)-\frac{1}{12}\delta(1-\zeta)\Big]\Big]\Big\}, \tag{A.3}$$

$$c_2^{(1)}(n,\nu,|\overrightarrow{k}|,x) = \Big[c_1^{(1)}(n,\nu,|\overrightarrow{k}|,x)\Big] \tag{A.4}$$

where $\bar{\zeta}=1-\zeta$, $\gamma=i\nu-1/2$, and $P_{ij}(\zeta)$ are the LO DGLAP kernels defined as follows:

$$P_{qq}(\zeta) = C_F\Big(\frac{1+\zeta^2}{(1-\zeta)_+}+\frac{3}{2}\delta(1-\zeta)\Big),$$
$$P_{gq}(\zeta) = C_F\frac{1+(1-\zeta)^2}{\zeta},$$

$$P_{gg}(\zeta) = 2C_A\Big\{\frac{1}{(1-\zeta)_+} + \frac{1}{\zeta} - 2 + \zeta(1-\zeta) + \Big(\frac{11}{6}C_A - \frac{n_f}{3}\Big)\delta(1-\zeta)\Big\},$$

$$P_{qg}(\zeta) = T_R\Big(\zeta^2 + (1-\zeta)^2\Big),$$

where C_F is the Casimir operator associated with gluon emission from a quark, $C_F = (N_c^2 - 1)/2N_c$ and $T_R = 1/2$ is the colour factor associated with the splitting of a gluon into a quark-antiquark pair.
For the $I_{1,2,3}$ functions we have the results:

$$I_2 = \frac{\zeta^2}{\bar{\zeta}^2}\Big\{\zeta\left(\frac{2F_1(1, 1+\gamma-\frac{n}{2}, 2+\gamma-\frac{n}{2}, \zeta)}{\frac{n}{2}-\gamma-1} - \frac{2F_1(1, 1+\gamma+\frac{n}{2}, 2+\gamma+\frac{n}{2}, \zeta)}{\frac{n}{2}+\gamma+1}\right)$$
$$+ \zeta^{-2\gamma}\left(\frac{2F_1(1, -\gamma-\frac{n}{2}, 1-\gamma-\frac{n}{2}, \zeta)}{\frac{n}{2}+\gamma} - \frac{2F_1(1, -\gamma+\frac{n}{2}, 1-\gamma+\frac{n}{2}, \zeta)}{\frac{n}{2}-\gamma}\right)$$
$$+ (1+\zeta^{-2\gamma})(\chi(n,\gamma) - 2\ln\bar{\zeta}) + 2\ln\zeta\Big\}, \quad \text{(A.5)}$$

$$I_1 = \frac{\bar{\zeta}}{2\zeta}I_2 + \frac{\zeta}{\bar{\zeta}}\left[\ln\zeta + \frac{1-\zeta^{-2\gamma}}{2}(\chi(n,\gamma) - 2\ln\bar{\zeta})\right], \quad \text{(A.6)}$$

$$I_3 = \frac{\bar{\zeta}}{2\zeta}I_2 - \frac{\zeta}{\bar{\zeta}}\left[\ln\zeta + \frac{1-\zeta^{-2\gamma}}{2}(\chi(n,\gamma) - 2\ln\bar{\zeta})\right]. \quad \text{(A.7)}$$

7) Using the following property of the hypergeometric function,

$$2F_1(1, a+1, \zeta) = a\sum_{n=0}^{\infty}\frac{(a)_n}{n!}\left[\psi(n+1) - \psi(a+n) - \ln\bar{\zeta}\right], \quad \text{(A.8)}$$

one can easily see that $\zeta \to 1$

$$I_2 = O(\ln\bar{\zeta}), \qquad I_1 = O(\ln\bar{\zeta}), \qquad I_3 = O(\ln\bar{\zeta}), \quad \text{(A.9)}$$

which implies that the integral over ζ in (A.3) is convergent on the upper limit.

A.2 Hadron impact factor

Here the expressions for the LO and NLO to the identified hadron impact factor in ν -representation is given (see Ref. [23] for further details).
The LO impact factor case, written in expression contains the PDFs of the gluon and of the different quark/anti-quark flavors in the proton, and the FFs of the detected

hadron, reads:

$$c_1(n,\nu,|\overrightarrow{k}|,\alpha) = 2\sqrt{\frac{C_F}{C_A}}(\overrightarrow{k}_1^2)^{i\nu-1/2}\int_\alpha^1 \frac{dx}{x}\left(\frac{x}{\alpha}\right)^{2i\nu-1} \times\left\{\frac{C_A}{C_F}f_g(x)D_g^h(\frac{\alpha}{x})+\sum_{a=q,\bar{q}}f_a(x)D_a^h(\frac{\alpha}{x})\right\}, \quad \text{(A.10)}$$

where D_i^h are parton fragmentation functions.

$$c_2(n,\nu,|\overrightarrow{k}|,\alpha) = \left[c_1(n,\nu,|\overrightarrow{k}|,\alpha)\right]^* \quad \text{(A.11)}$$

The NLO impact factor corrections in (ν,n)-representation $c_1^{(1)}(n,\nu,|\overrightarrow{k}|,\alpha)$, have the form

$$\begin{aligned} c_1^{(1)}(n,\nu,|\overrightarrow{k}|,\alpha) = 2\sqrt{\frac{C_F}{C_A}}(\overrightarrow{k}^2)^{i\nu-1/2}\frac{1}{2\pi}\int_\alpha^1\frac{dx}{x}\int_{\frac{\alpha}{x}}^1\frac{d\zeta}{\zeta}\left(\frac{x\zeta}{\alpha}\right)^{2i\nu-1} \\ \times\Big\{\frac{C_A}{C_F}f_g(x)D_g^h(\frac{\alpha}{x\zeta})C_{gg}(x,\zeta)+\sum_{a=q,\bar{q}}f_a(x)D_a^h(\frac{\alpha}{x\zeta})C_{qq}(x,\zeta) \\ + D_g^h(\frac{\alpha}{x\zeta})\sum_{a=q,\bar{q}}f_a(x)C_{qg}(x,\zeta)+\frac{C_A}{C_F}f_g(x)\sum_{a=q,\bar{q}}D_g^h(\frac{\alpha}{x\zeta})C_{gq}(x,\zeta)\Big\}. \quad \text{(A.12)} \end{aligned}$$

The expressions for the coefficient functions $C_{gg}, C_{qq}, C_{qg} and C_{gq}$, are given in Ref [23].

A.3 Higgs impact factor

We can define LO impact factor for the production of the Higgs in gluon-gluon fusion, as follow:

$$V^{(0)}_{gg\to H}(\overrightarrow{q}) = \sum_{\{f\}}\int\frac{ds_{gH}}{2\pi}\overline{|\mathscr{M}|^2}dP.S.^{(f)}. \quad \text{(A.13)}$$

The integration here is over the standard phase space $dP.S.^{(f)}$ of an intermediate state $\{f\}$ as well as over its squared invariant mass s_{gR}. The LO impact factors in our case take contribution only from a one-particle intermediate state in the gluon-Reggeon collision, and then the phase space integration simply gives

$$P.S^{(1)} = \int\frac{d^4P_H}{(2\pi)^3}\delta(P_H^2-M_H^2)(2\pi)^4\delta(k+q-P_H) = 2\pi\delta(s_{gR}-M_H^2), \quad \text{(A.14)}$$

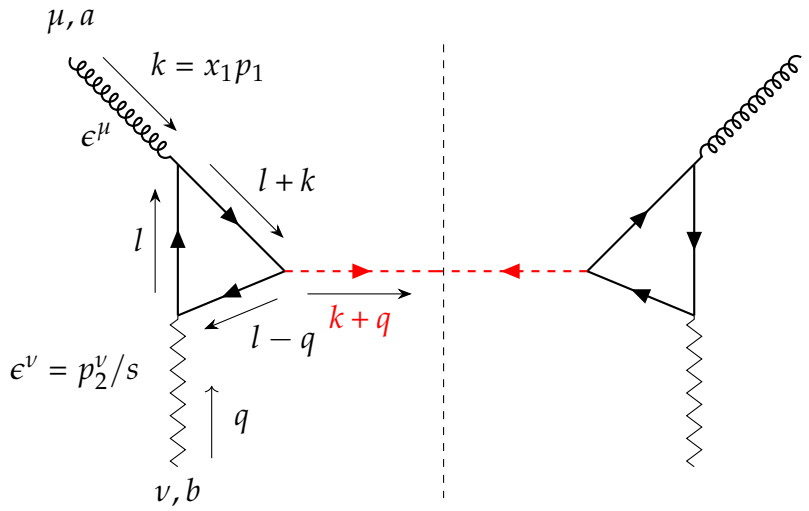

Figure A.1: Optical theorem: Representative Feynman diagram for the process $gg^* \longrightarrow H$.

where P_H is the Higgs boson momentum, using this result we end up with

$$V^{(0)}_{gg\to H}(\overrightarrow{q}) = \frac{\alpha_s^2}{v^2}\frac{1}{128\pi^2\sqrt{N_c^2-1}}|q_\perp^2||\mathscr{F}(|q_\perp^2|)|^2, \tag{A.15}$$

satisfying $V^{(0)}_{gg\to H}(\overrightarrow{q})|_{\overrightarrow{q}=0} \longrightarrow 0$, which will guarantee the infra-red finiteness of the BFKL amplitude. Applying the large top mass limit ($I_1 \to \frac{1}{3}$), our LO impact factor reads

$$V^{(0)}_{gg\to H}(\overrightarrow{q}) = \frac{\alpha_s^2}{v^2}\frac{1}{72\pi^2\sqrt{N_c^2-1}}|q_\perp^2|, \tag{A.16}$$

which is in agreement with what has been computed in section B of Ref [133].
Now after inclusion of PDF of the gluon, Eq.(A.15) becomes

$$V^{(0)}_{gg\to H}(\overrightarrow{q}) = \frac{\alpha_s^2}{v^2}\frac{|\mathscr{F}(|q_\perp^2|)|^2}{128\pi^2\sqrt{N_c^2-1}}|q_\perp^2|\int_0^1 dx_1 f_g(x_1) \tag{A.17}$$

In order to establish the proper normalization for our impact factor, we insert into (A.17) a delta function depends on the produced Higgs boson transverse momentum $\overrightarrow{P_H}$, then the LO result for the impact factor reads

$$\frac{dV^{(0)}_{gg\to H}(\overrightarrow{q})}{\overrightarrow{q}^2} = \frac{\alpha_s^2}{v^2}\frac{|\mathscr{F}(|q_\perp^2|)|^2}{128\pi^2\sqrt{N_c^2-1}}|q_\perp^2|\int_0^1 dx_1 f_g(x_1)\frac{d^2\overrightarrow{P_H}}{\overrightarrow{P_H}^2}\delta^{(2)}(\overrightarrow{P_H}-\overrightarrow{q}). \tag{A.18}$$

This will simplify the calculation of the impact factors when we project them into the so called (ν, n)-representation, i.e. the eigenfunctions of LO BFKL kernel. The transfer to (ν, n)-space is done as follows:

$$dV^{(0)}_{gg\to H}(\nu, n) = \int d^2\overrightarrow{q}\, \frac{dV^{(0)}_{gg\to H}(\overrightarrow{q})}{\overrightarrow{q}^2} \frac{(\overrightarrow{q}^2)^{i\nu-1/2}}{\pi\sqrt{2}} e^{in\phi}. \tag{A.19}$$

Using (A.18) and absorbing our inserted delta function we get the following differential expression for our LO impact factor in the azimuth symmetric $n = 0$ sector

$$\frac{dV^{(0)}_{gg\to H}(\nu, n=0)}{dx_1 d^2\overrightarrow{P_H}} = \frac{\alpha_s^2}{v^2} \frac{|\mathscr{F}(|q_\perp^2|)|^2}{128\pi^3\sqrt{2(N_c^2-1)}} (\overrightarrow{P_H}^2)^{i\nu-1/2} f_g(x_1). \tag{A.20}$$

Higher-order corrections

Going to higher order, we have to calculate the virtual and real emission corrections, which both of them contain infrared divergences canceling each other, moreover, the real corrections could contain a collinear divergences, which can be handled by taken into account the Altarelli–Parisi splitting functions up to the appropriate order. The next-to-leading order calculations involve the computation of two-loop triangular diagrams with massive quarks, which complicate the process, but fortunately, the large quarks mass limit ($m_t \to \infty$) allows us to replace the coupling of Higgs with the two gluon via the quarks loop by an effective vertex, which is help to reduce the number of loops appear in any given diagram by one, moreover it can serves as a valuable check of the complete two-loop calculations for the gluonic radiative corrections. The coupling vertex between the two gluons and the produced Higgs can be obtained from the following effective Lagrangian[1],

$$\mathscr{L}_{eff} = -\frac{g_H}{4} H G^a_{\mu\nu} G_a^{\mu\nu}, \tag{A.21}$$

where $G^a_{\mu\nu}$ is the gluon field strength tensor , H is the Higgs filed, and the effective coupling g_H given by

$$g_H = \frac{\alpha_s}{3\pi v}\left(1 + \alpha_s \frac{11}{4\pi}\right).$$

Using this effective Lagrangian we can generate all the building blocks vertices which involve the two, three and four gluons with the Higgs.

[1]Which can be derived from the top-quark contribution to gluon self-energy by taking the derivative of the gluon propagator with respect to the bare quark mass.

1-loop Virtual corrections to $gg^* \to H$

Before we proceed to the virtual correction, it will be useful to rewrite our previous LO (Born)-amplitude at large quarks mass limit in ($d = 4 - 2\epsilon$) dimensions, considering this, there is only one extra ϵ term appears due to averaging over the different possible polarization and color states of the incoming gluons,

$$\mathscr{M}^{(B)}_{gg^*\to H} = i g_H \delta^{ab} \left(g^{\mu\nu}(k_1 \cdot q) - k_1^\nu q^\mu\right) \frac{k_2^\nu}{s} \epsilon_\mu(k_1),$$

$$|\mathscr{M}^{(B)}_{gg^*\to H}|^2 = \frac{\alpha_s^2}{72\pi^2} \frac{|q_\perp^2|}{v^2} \frac{1}{(1-\epsilon).} \tag{A.22}$$

There are several diagrams appearing at one-loop, few of them giving null contri-

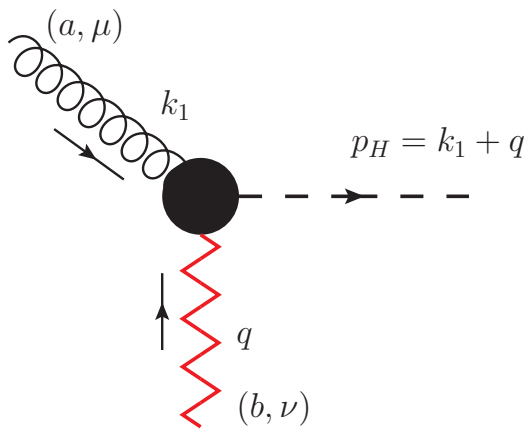

Figure A.2: Diagrammatic representation for $gg^* \to H$ tree level amplitude at HEFT

butions, and the only non-zero contribution to $gg^* \to H$, comes from six different diagrams shown in Fig.A.3. These diagram could be classified according to the type of the correction into three contributed groups of diagrams, the first group represents the one-gluon exchange contribution, the second and third contributions are those from the Riggezed gluon loop correction and the two-gluon exchange diagrams respectively.

Real correction

The real correction contains two different contribution comes from both gluon initiated processes, and only one initial quark process contribute to the total real cor-

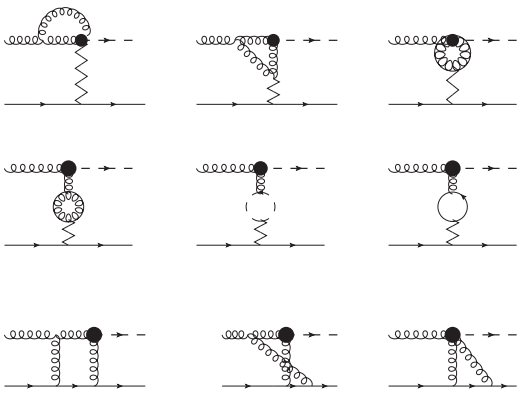

Figure A.3: Feynman diagrams giving non-zero contribution to $gg^* \to H$ at one-loop.

rection. we can simply read the Feynman amplitudes of our processes one by one directly from their corresponding diagrams.

Quark initiated process

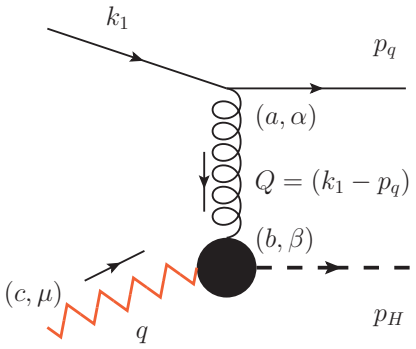

Figure A.4: Feynman diagram for $qg^* \to Hq$ process.

Gluon initiated process

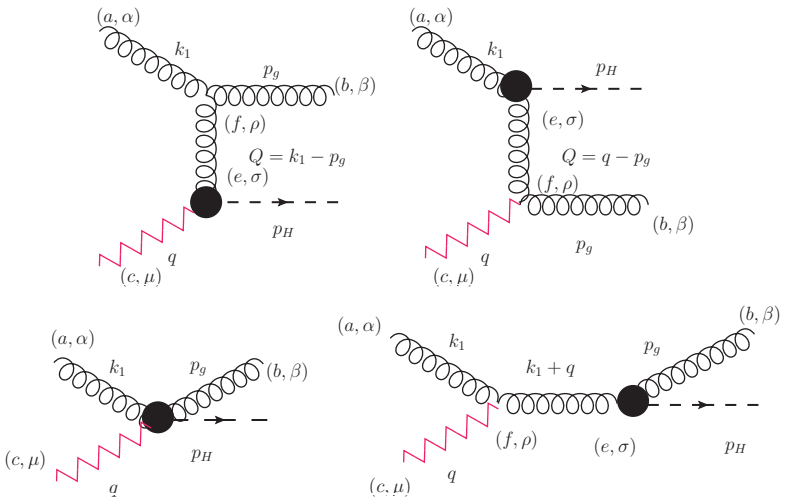

Figure A.5: Feynman diagram for $gg^* \to Hq$ process.

Bibliography

[1] G. Aad *et al.*, *Observation of a new particle in the search for the Standard Model Higgs boson with the ATLAS detector at the LHC*, Phys. Lett. B **716**, 1 (2012), doi:10.1016/j.physletb.2012.08.020, 1207.7214. (Cited on page 1.)

[2] S. Chatrchyan *et al.*, *Observation of a New Boson at a Mass of 125 GeV with the CMS Experiment at the LHC*, Phys. Lett. B **716**, 30 (2012), doi:10.1016/j.physletb.2012.08.021, 1207.7235. (Cited on page 1.)

[3] L. V. Gribov, E. M. Levin and M. G. Ryskin, *Semihard Processes in QCD*, Phys. Rept. **100**, 1 (1983), doi:10.1016/0370-1573(83)90022-4. (Cited on page 1.)

[4] L. N. Lipatov, *The Bare Pomeron in Quantum Chromodynamics*, Sov. Phys. JETP **63**, 904 (1986). (Cited on page 1.)

[5] V. S. Fadin, E. A. Kuraev and L. N. Lipatov, *On the Pomeranchuk Singularity in Asymptotically Free Theories*, Phys. Lett. B **60**, 50 (1975), doi:10.1016/0370-2693(75)90524-9. (Cited on pages 1 and 6.)

[6] E. Kuraev, L. Lipatov and V. S. Fadin, *Multi-reggeon processes in yang-milles theory*, Soviet Physics-JETP **43**(3), 443 (1976). (Cited on pages 1 and 6.)

[7] E. Kuraev, L. Lipatov and V. S. Fadin, *The Pomeranchuk Singularity in Nonabelian Gauge Theories*, Sov. Phys. JETP **45**, 199 (1977). (Cited on page 1.)

[8] L. N. Lipatov, *Reggeization of the Vector Meson and the Vacuum Singularity in Nonabelian Gauge Theories*, Sov. J. Nucl. Phys. **23**, 338 (1976). (Cited on pages 1 and 6.)

[9] I. I. Balitsky and L. N. Lipatov, *The Pomeranchuk Singularity in Quantum Chromodynamics*, Sov. J. Nucl. Phys. **28**, 822 (1978). (Cited on page 1.)

[10] V. S. Fadin and L. N. Lipatov, *BFKL pomeron in the next-to-leading approximation*, Phys. Lett. B **429**, 127 (1998), doi:10.1016/S0370-2693(98)00473-0, hep-ph/9802290. (Cited on pages 1 and 2.)

[11] M. Ciafaloni and G. Camici, *Energy scale(s) and next-to-leading BFKL equation*, Phys. Lett. B **430**, 349 (1998), doi:10.1016/S0370-2693(98)00551-6, hep-ph/9803389. (Cited on pages 1 and 2.)

[12] V. S. Fadin, R. Fiore and A. Papa, *The Quark part of the nonforward BFKL kernel and the 'bootstrap' for the gluon Reggeization*, Phys. Rev. D **60**, 074025 (1999), doi:10.1103/PhysRevD.60.074025, hep-ph/9812456. (Cited on page 2.)

[13] V. S. Fadin and R. Fiore, *Non-forward BFKL pomeron at next-to-leading order*, Phys. Lett. B **610**, 61 (2005), doi:10.1016/j.physletb.2005.06.074, [Erratum: Phys.Lett.B 621, 320 (2005)], hep-ph/0412386. (Cited on page 2.)

[14] V. S. Fadin and R. Fiore, *Non-forward NLO BFKL kernel*, Phys. Rev. D **72**, 014018 (2005), doi:10.1103/PhysRevD.72.014018, hep-ph/0502045. (Cited on page 2.)

[15] V. S. Fadin, R. Fiore, M. I. Kotsky and A. Papa, *The Gluon impact factors*, Phys. Rev. D **61**, 094005 (2000), doi:10.1103/PhysRevD.61.094005, hep-ph/9908264. (Cited on pages 2 and 12.)

[16] V. S. Fadin, R. Fiore, M. I. Kotsky and A. Papa, *The Quark impact factors*, Phys. Rev. D **61**, 094006 (2000), doi:10.1103/PhysRevD.61.094006, hep-ph/9908265. (Cited on pages 2 and 12.)

[17] J. Bartels, D. Colferai and G. P. Vacca, *The NLO jet vertex for Mueller-Navelet and forward jets: The Quark part*, Eur. Phys. J. C **24**, 83 (2002), doi:10.1007/s100520200919, hep-ph/0112283. (Cited on pages 2 and 12.)

[18] J. Bartels, D. Colferai and G. P. Vacca, *The NLO jet vertex for Mueller-Navelet and forward jets: The Gluon part*, Eur. Phys. J. C **29**, 235 (2003), doi:10.1140/epjc/s2003-01169-5, hep-ph/0206290. (Cited on pages 2 and 12.)

[19] F. Caporale, D. Yu. Ivanov, B. Murdaca, A. Papa and A. Perri, *The next-to-leading order jet vertex for Mueller-Navelet and forward jets revisited*, JHEP **02**, 101 (2012), doi:10.1007/JHEP02(2012)101, 1112.3752. (Cited on pages 2, 12, and 44.)

[20] F. Caporale, D. Yu. Ivanov, B. Murdaca and A. Papa, *Mueller-Navelet small-cone jets at LHC in next-to-leading BFKL*, Nucl. Phys. B **877**, 73 (2013), doi:10.1016/j.nuclphysb.2013.09.013, 1211.7225. (Cited on pages 2, 12, 24, 42, and 68.)

[21] D. Yu. Ivanov and A. Papa, *The next-to-leading order forward jet vertex in the small-cone approximation*, JHEP **05**, 086 (2012), doi:10.1007/JHEP05(2012)086, 1202.1082. (Cited on pages 2, 12, 44, and 71.)

[22] D. Colferai and A. Niccoli, *The NLO jet vertex in the small-cone approximation for kt and cone algorithms*, JHEP **04**, 071 (2015), doi:10.1007/JHEP04(2015)071, 1501.07442. (Cited on pages 2, 12, 44, and 68.)

[23] D. Yu. Ivanov and A. Papa, *Inclusive production of a pair of hadrons separated by a large interval of rapidity in proton collisions*, JHEP **07**, 045 (2012), doi:10.1007/JHEP07(2012)045, 1205.6068. (Cited on pages 2, 12, 24, 73, and 74.)

[24] D. Yu. Ivanov, M. I. Kotsky and A. Papa, *The Impact factor for the virtual photon to light vector meson transition*, Eur. Phys. J. C **38**, 195 (2004), doi:10.1140/epjc/s2004-02039-4, hep-ph/0405297. (Cited on pages 2 and 12.)

[25] J. Bartels, S. Gieseke and C. F. Qiao, *The (gamma* —> q anti-q) Reggeon vertex in next-to-leading order QCD*, Phys. Rev. D **63**, 056014 (2001), doi:10.1103/PhysRevD.63.056014, [Erratum: Phys.Rev.D 65, 079902 (2002)], hep-ph/0009102. (Cited on pages 2 and 12.)

[26] J. Bartels, S. Gieseke and A. Kyrieleis, *The Process gamma*(L) + q —> (q anti-q g) + q: Real corrections to the virtual photon impact factor*, Phys. Rev. D **65**, 014006 (2002), doi:10.1103/PhysRevD.65.014006, hep-ph/0107152. (Cited on pages 2 and 12.)

[27] J. Bartels, D. Colferai, S. Gieseke and A. Kyrieleis, *NLO corrections to the photon impact factor: Combining real and virtual corrections*, Phys. Rev. D **66**, 094017 (2002), doi:10.1103/PhysRevD.66.094017, hep-ph/0208130. (Cited on pages 2 and 12.)

[28] J. Bartels and A. Kyrieleis, *NLO corrections to the gamma* impact factor: First numerical results for the real corrections to gamma*(L)*, Phys. Rev. D **70**, 114003 (2004), doi:10.1103/PhysRevD.70.114003, hep-ph/0407051. (Cited on pages 2 and 12.)

[29] V. S. Fadin, D. Yu. Ivanov and M. I. Kotsky, *Photon Reggeon interaction vertices in the NLA*, Phys. Atom. Nucl. **65**, 1513 (2002), doi:10.1134/1.1501664, hep-ph/0106099. (Cited on pages 2 and 12.)

[30] I. Balitsky and G. A. Chirilli, *Photon impact factor and k_T-factorization for DIS in the next-to-leading order*, Phys. Rev. D **87**(1), 014013 (2013), doi:10.1103/PhysRevD.87.014013, 1207.3844. (Cited on pages 2 and 12.)

[31] M. Hentschinski, K. Kutak and A. van Hameren, *Forward Higgs production within high energy factorization in the heavy quark limit at next-to-leading order accuracy*, Eur. Phys. J. C **81**(2), 112 (2021), doi:10.1140/epjc/s10052-021-08902-6, [Erratum: Eur.Phys.J.C 81, 262 (2021)], 2011.03193. (Cited on pages 2, 12, and 43.)

[32] M. A. Nefedov, *Computing one-loop corrections to effective vertices with two scales in the EFT for Multi-Regge processes in QCD*, Nucl. Phys. B **946**, 114715 (2019), doi: 10.1016/j.nuclphysb.2019.114715, 1902.11030. (Cited on pages 2, 12, and 43.)

[33] B. Pire, L. Szymanowski and S. Wallon, *Double diffractive rho-production in gamma* gamma* collisions*, Eur. Phys. J. C **44**, 545 (2005), doi:10.1140/epjc/s2005-02386-6, hep-ph/0507038. (Cited on page 2.)

[34] M. Segond, L. Szymanowski and S. Wallon, *Diffractive production of two rho0(L) mesons in e+e- collisions*, Eur. Phys. J. C **52**, 93 (2007), doi:10.1140/epjc/s10052-007-0365-9, hep-ph/0703166. (Cited on page 2.)

[35] R. Enberg, B. Pire, L. Szymanowski and S. Wallon, *BFKL resummation effects in gamma* gamma* —> rho rho*, Eur. Phys. J. C **45**, 759 (2006), doi:10.1140/epjc/s10052-007-0375-7, [Erratum: Eur.Phys.J.C 51, 1015 (2007)], hep-ph/0508134. (Cited on pages 2 and 20.)

[36] D. Yu. Ivanov and A. Papa, *Electroproduction of two light vector mesons in the next-to-leading approximation*, Nucl. Phys. B **732**, 183 (2006), doi:10.1016/j.nuclphysb.2005.10.028, hep-ph/0508162. (Cited on page 2.)

[37] D. Yu. Ivanov and A. Papa, *Electroproduction of two light vector mesons in next-to-leading BFKL: Study of systematic effects*, Eur. Phys. J. C **49**, 947 (2007), doi:10.1140/epjc/s10052-006-0180-8, hep-ph/0610042. (Cited on page 2.)

[38] A. H. Mueller and H. Navelet, *An Inclusive Minijet Cross-Section and the Bare Pomeron in QCD*, Nucl. Phys. B **282**, 727 (1987), doi:10.1016/0550-3213(87)90705-X. (Cited on pages 2 and 20.)

[39] D. Colferai, F. Schwennsen, L. Szymanowski and S. Wallon, *Mueller Navelet jets at LHC - complete NLL BFKL calculation*, JHEP **12**, 026 (2010), doi:10.1007/JHEP12(2010)026, 1002.1365. (Cited on pages 2 and 68.)

[40] B. Ducloué, L. Szymanowski and S. Wallon, *Confronting Mueller-Navelet jets in NLL BFKL with LHC experiments at 7 TeV*, JHEP **05**, 096 (2013), doi:10.1007/JHEP05(2013)096, 1302.7012. (Cited on pages 2 and 68.)

[41] B. Ducloué, L. Szymanowski and S. Wallon, *Evidence for high-energy resummation effects in Mueller-Navelet jets at the LHC*, Phys. Rev. Lett. **112**, 082003 (2014), doi:10.1103/PhysRevLett.112.082003, 1309.3229. (Cited on pages 2, 47, and 68.)

[42] F. Caporale, B. Murdaca, A. Sabio Vera and C. Salas, *Scale choice and collinear contributions to Mueller-Navelet jets at LHC energies*, Nucl. Phys. B **875**, 134 (2013), doi:10.1016/j.nuclphysb.2013.07.005, 1305.4620. (Cited on pages 2 and 68.)

[43] F. Caporale, D. Yu. Ivanov, B. Murdaca and A. Papa, *Mueller–Navelet jets in next-to-leading order BFKL: theory versus experiment*, Eur. Phys. J. C **74**(10), 3084 (2014), doi:10.1140/epjc/s10052-015-3754-5, [Erratum: Eur.Phys.J.C 75, 535 (2015)], 1407.8431. (Cited on pages 2, 47, and 68.)

[44] F. Caporale, D. Yu. Ivanov, B. Murdaca and A. Papa, *Brodsky-Lepage-Mackenzie optimal renormalization scale setting for semihard processes*, Phys. Rev. D **91**(11), 114009 (2015), doi:10.1103/PhysRevD.91.114009, 1504.06471. (Cited on pages 2, 24, 25, 47, and 68.)

[45] B. Ducloué, L. Szymanowski and S. Wallon, *Evaluating the double parton scattering contribution to Mueller-Navelet jets production at the LHC*, Phys. Rev. D **92**(7), 076002 (2015), doi:10.1103/PhysRevD.92.076002, 1507.04735. (Cited on pages 2 and 68.)

[46] F. G. Celiberto, D. Yu. Ivanov, B. Murdaca and A. Papa, *Mueller–Navelet Jets at LHC: BFKL Versus High-Energy DGLAP*, Eur. Phys. J. C **75**(6), 292 (2015), doi:10.1140/epjc/s10052-015-3522-6, 1504.08233. (Cited on pages 2 and 68.)

[47] F. G. Celiberto, D. Yu. Ivanov, B. Murdaca and A. Papa, *Mueller–Navelet Jets at the LHC: Discriminating BFKL from DGLAP by Asymmetric Cuts*, Acta Phys. Polon. Supp. **8**, 935 (2015), doi:10.5506/APhysPolBSupp.8.935, 1510.01626. (Cited on pages 2 and 68.)

[48] F. G. Celiberto, D. Yu. Ivanov, B. Murdaca and A. Papa, *Mueller–Navelet jets at 13 TeV LHC: dependence on dynamic constraints in the central rapidity region*, Eur. Phys. J. C **76**(4), 224 (2016), doi:10.1140/epjc/s10052-016-4053-5, 1601.07847. (Cited on pages 2 and 68.)

[49] F. G. Celiberto, D. Yu. Ivanov, B. Murdaca and A. Papa, *BFKL effects and central rapidity dependence in Mueller-Navelet jet production at 13 TeV LHC*, PoS **DIS2016**, 176 (2016), doi:10.22323/1.265.0176, 1606.08892. (Cited on pages 2 and 68.)

[50] F. Caporale, F. G. Celiberto, G. Chachamis, D. Gordo Gómez and A. Sabio Vera, *Inclusive dijet hadroproduction with a rapidity veto constraint*, Nucl. Phys. B **935**, 412 (2018), doi:10.1016/j.nuclphysb.2018.09.002, 1806.06309. (Cited on pages 2 and 68.)

[51] F. G. Celiberto, D. Yu. Ivanov, B. Murdaca and A. Papa, *High energy resummation in dihadron production at the LHC*, Phys. Rev. D **94**(3), 034013 (2016), doi:10.1103/PhysRevD.94.034013, 1604.08013. (Cited on page 2.)

[52] F. G. Celiberto, D. Yu.. Ivanov, B. Murdaca and A. Papa, *Dihadron Production at LHC: BFKL Predictions for Cross Sections and Azimuthal Correlations*, AIP Conf.

Proc. **1819**(1), 060005 (2017), doi:10.1063/1.4977161, 1611.04811. (Cited on page 2.)

[53] F. G. Celiberto, D. Yu. Ivanov, B. Murdaca and A. Papa, *Dihadron production at the LHC: full next-to-leading BFKL calculation*, Eur. Phys. J. C **77**(6), 382 (2017), doi:10.1140/epjc/s10052-017-4949-8, 1701.05077. (Cited on page 2.)

[54] F. Caporale, G. Chachamis, B. Murdaca and A. Sabio Vera, *Balitsky-Fadin-Kuraev-Lipatov Predictions for Inclusive Three Jet Production at the LHC*, Phys. Rev. Lett. **116**(1), 012001 (2016), doi:10.1103/PhysRevLett.116.012001, 1508.07711. (Cited on pages 2, 20, and 27.)

[55] F. Caporale, F. G. Celiberto, G. Chachamis and A. Sabio Vera, *Multi-Regge kinematics and azimuthal angle observables for inclusive four-jet production*, Eur. Phys. J. C **76**(3), 165 (2016), doi:10.1140/epjc/s10052-016-3963-6, 1512.03364. (Cited on pages 2, 20, and 27.)

[56] F. Caporale, F. G. Celiberto, G. Chachamis, D. Gordo Gómez and A. Sabio Vera, *BFKL azimuthal imprints in inclusive three-jet production at 7 and 13 TeV*, Nucl. Phys. B **910**, 374 (2016), doi:10.1016/j.nuclphysb.2016.07.012, 1603.07785. (Cited on pages 2, 20, and 27.)

[57] F. Caporale, F. G. Celiberto, G. Chachamis and A. Sabio Vera, *Inclusive four-jet production: a study of Multi-Regge kinematics and BFKL observables*, PoS **DIS2016**, 177 (2016), doi:10.22323/1.265.0177, 1610.01880. (Cited on pages 2 and 27.)

[58] F. Caporale, F. G. Celiberto, G. Chachamis, D. Gordo Gómez and A. Sabio Vera, *Inclusive Four-jet Production at 7 and 13 TeV: Azimuthal Profile in Multi-Regge Kinematics*, Eur. Phys. J. C **77**(1), 5 (2017), doi:10.1140/epjc/s10052-016-4557-z, 1606.00574. (Cited on pages 2, 20, and 27.)

[59] F. G. Celiberto, *BFKL phenomenology: resummation of high-energy logs in semi-hard processes at LHC*, Frascati Phys. Ser. **63**, 43 (2016), 1606.07327. (Cited on page 2.)

[60] F. Caporale, F. G. Celiberto, G. Chachamis, D. Gordo Gomez and A. Sabio Vera, *Inclusive three- and four-jet production in multi-Regge kinematics at the LHC*, AIP Conf. Proc. **1819**(1), 060009 (2017), doi:10.1063/1.4977165, 1611.04813. (Cited on pages 2 and 27.)

[61] F. Caporale, F. G. Celiberto, G. Chachamis, D. Gordo Gómez and A. Sabio Vera, *Probing the BFKL dynamics in inclusive three jet production at the LHC*, EPJ Web Conf. **164**, 07027 (2017), doi:10.1051/epjconf/201716407027, 1612.02771. (Cited on pages 2, 20, and 27.)

[62] F. Caporale, F. G. Celiberto, G. Chachamis, D. Gordo Gómez and A. Sabio Vera, *Stability of Azimuthal-angle Observables under Higher Order Corrections in Inclusive Three-jet Production*, Phys. Rev. D **95**(7), 074007 (2017), doi:10.1103/PhysRevD.95.074007, 1612.05428. (Cited on pages 2, 20, and 27.)

[63] R. Boussarie, B. Ducloué, L. Szymanowski and S. Wallon, *Forward J/ψ and very backward jet inclusive production at the LHC*, Phys. Rev. D **97**(1), 014008 (2018), doi:10.1103/PhysRevD.97.014008, 1709.01380. (Cited on pages 2 and 27.)

[64] A. D. Bolognino, F. G. Celiberto, D. Yu. Ivanov, M. M. A. Mohammed and A. Papa, *High-energy effects in forward inclusive dijet and hadron-jet production*, PoS **DIS2019**, 049 (2019), doi:10.22323/1.352.0049, 1906.11800. (Cited on pages 2 and 27.)

[65] F. G. Celiberto, D. Yu. Ivanov, M. M. A. Mohammed and A. Papa, *High-energy resummed distributions for the inclusive Higgs-plus-jet production at the LHC*, Eur. Phys. J. C **81**(4), 293 (2021), doi:10.1140/epjc/s10052-021-09063-2, 2008.00501. (Cited on pages 2, 3, and 40.)

[66] F. G. Celiberto, D. Yu. Ivanov, M. M. A. Mohammed and A. Papa, *High-energy resummation in inclusive hadroproduction of Higgs plus jet*, In *28th International Workshop on Deep Inelastic Scattering and Related Subjects* (2021), 2107.13037. (Cited on pages 2, 3, and 40.)

[67] A. D. Bolognino, F. G. Celiberto, M. Fucilla, D. Yu. Ivanov and A. Papa, *Inclusive production of a heavy-light dijet system in hybrid high-energy/collinear factorization*, Phys. Rev. D, in press (2021), 2103.07396. (Cited on page 3.)

[68] A. D. Bolognino, F. G. Celiberto, M. Fucilla, D. Yu. Ivanov and A. Papa, *Hybrid high-energy/collinear factorization in a heavy-light dijets system reaction*, In *28th International Workshop on Deep Inelastic Scattering and Related Subjects* (2021), 2107.12120. (Cited on page 3.)

[69] K. Golec-Biernat, L. Motyka and T. Stebel, *Forward Drell-Yan and backward jet production as a probe of the BFKL dynamics*, JHEP **12**, 091 (2018), doi:10.1007/JHEP12(2018)091, 1811.04361. (Cited on page 3.)

[70] F. G. Celiberto, M. Fucilla, D. Yu. Ivanov and A. Papa, *High-energy resummation in Λ_c baryon production*, Eur. Phys. J. C **81**(8), 780 (2021), doi:10.1140/epjc/s10052-021-09448-3, 2105.06432. (Cited on pages 3 and 20.)

[71] V. Barone and E. Predazzi, *High-energy particle diffraction*, Springer Science & Business Media (2002). (Cited on page 5.)

[72] J. R. Forshaw, J. R. Forshaw, D. Ross and D. A. Ross, *Quantum chromodynamics and the pomeron*, 9. Cambridge University Press (1997). (Cited on page 5.)

[73] B. L. Ioffe, V. S. Fadin and L. N. Lipatov, *Quantum chromodynamics: Perturbative and nonperturbative aspects*, 30. Cambridge University Press (2010). (Cited on page 5.)

[74] M. Gell-Mann and M. L. Goldberger, *Elementary Particles of Conventional Field Theory as Regge Poles*, Phys. Rev. Lett. **9**(6), 275 (1962), doi:10.1103/PhysRevLett.9.275. (Cited on page 6.)

[75] M. Gell-Mann, M. L. Goldberger, F. E. Low and F. Zachariasen, *Elementary particles of conventional field theory as regge poles - II*, Phys. Lett. **4**(5), 265 (1963), doi:10.1016/0031-9163(63)90592-4. (Cited on page 6.)

[76] M. Gell-Mann, M. L. Goldberger, F. E. Low, V. Singh and F. Zachariasen, *Elementary Particles of Conventional Field Theory as Regge Poles. IV*, Phys. Rev. **133**, B161 (1964), doi:10.1103/PhysRev.133.B161. (Cited on page 6.)

[77] S. Mandelstam, *Non-Regge Terms in the Vector-Spinor Theory*, Phys. Rev. **137**, B949 (1965), doi:10.1103/PhysRev.137.B949. (Cited on page 6.)

[78] M. T. Grisaru, H. J. Schnitzer and H.-S. Tsao, *Reggeization of yang-mills gauge mesons in theories with a spontaneously broken symmetry*, Phys. Rev. Lett. **30**, 811 (1973), doi:10.1103/PhysRevLett.30.811. (Cited on page 6.)

[79] M. T. Grisaru, H. J. Schnitzer and H.-S. Tsao, *Reggeization of elementary particles in renormalizable gauge theories: vectors and spinors*, Physical Review D **8**(12), 4498 (1973). (Cited on page 6.)

[80] V. S. Fadin and V. Sherman, *Fermion reggeization in nonabelian calibration theories*, Pisma Zh. Eksp. Teor. Fiz **23**, 599 (1976). (Cited on page 6.)

[81] V. S. Fadin and V. E. Sherman, *Processes Involving Fermion Exchange in Nonabelian Gauge Theories*, Zh. Eksp. Teor. Fiz. **72**, 1640 (1977). (Cited on page 6.)

[82] A. V. Bogdan, V. Del Duca, V. S. Fadin and E. W. N. Glover, *The Quark Regge trajectory at two loops*, JHEP **03**, 032 (2002), doi:10.1088/1126-6708/2002/03/032, `hep-ph/0201240`. (Cited on page 6.)

[83] V. S. Fadin and L. Lipatov, *Bfkl pomeron in the next-to-leading approximation*, Physics Letters B **429**(1-2), 127 (1998). (Cited on pages 9 and 11.)

[84] V. S. Fadin, R. Fiore and M. Kotsky, *Gluon reggeization in qcd in the next to leading order*, Physics Letters B **359**(1-2), 181 (1995). (Cited on page 9.)

[85] V. S. Fadin, R. Fiore and M. Kotsky, *Gluon Regge trajectory in the two-loop approximation*, Physics Letters B **387**(3), 593 (1996). (Cited on page 9.)

[86] V. S. Fadin and L. N. Lipatov, *Next-to-leading corrections to the BFKL equation from gluon and quark production*, Nuclear Physics B **477**(3), 767 (1996). (Cited on page 10.)

[87] V. Fadin, M. Kotsky and L. Lipatov, *One-loop correction to the bfkl kernel from two gluon production*, Physics Letters B **415**(1), 97 (1997). (Cited on page 10.)

[88] M. Kotsky, V. S. Fadin and L. Lipatov, *Two-gluon contribution to the kernel of the balitsky-fadin-kuraev-lipatov equation*, Physics of Atomic Nuclei **61**(4), 641 (1998). (Cited on page 10.)

[89] V. S. Fadin, R. Fiore, A. Flachi and M. Kotsky, *Quark-antiquark contribution to the BFKL kernel*, Physics Letters B **422**(1-4), 287 (1998). (Cited on page 10.)

[90] D. Ross, *The effect of higher order corrections to the BFKL equation on the perturbative pomeron*, Physics Letters B **431**(1-2), 161 (1998). (Cited on page 10.)

[91] M. Ciafaloni, D. Colferai, G. P. Salam and A. M. Staśto, *Renormalization group improved small-x Green's function*, Phys. Rev. D **68**, 114003 (2003), doi:10.1103/PhysRevD.68.114003. (Cited on page 10.)

[92] R. S. Thorne, *Nlo bfkl equation, running coupling, and renormalization scales*, Phys. Rev. D **60**, 054031 (1999), doi:10.1103/PhysRevD.60.054031. (Cited on page 10.)

[93] S. J. Brodsky, V. S. Fadin, V. T. Kim, L. N. Lipatov and G. B. Pivovarov, *The QCD pomeron with optimal renormalization*, Journal of Experimental and Theoretical Physics Letters **70**(3), 155 (1999). (Cited on page 10.)

[94] E. Levin, *The bfkl high energy asymptotic in the next-to-leading approximation*, Nuclear Physics B **545**(1-3), 481 (1999). (Cited on page 10.)

[95] G. P. Salam, *A resummation of large sub-leading corrections at small x*, Journal of High Energy Physics **1998**(07), 019 (1998). (Cited on page 10.)

[96] M. Ciafaloni, D. Colferai, G. Salam and A. Staśto, *Extending QCD perturbation theory to higher energies*, Physics Letters B **576**(1-2), 143 (2003). (Cited on page 10.)

[97] S. Donnachie, G. Dosch, P. Landshoff and O. Nachtmann, *Pomeron physics and QCD*, vol. 19, Cambridge University Press (2002). (Cited on page 11.)

[98] A. M. Mueller, *o*(2, 1) *analysis of single-particle spectra at high energy*, Phys. Rev. D **2**, 2963 (1970), doi:10.1103/PhysRevD.2.2963. (Cited on page 11.)

[99] K.-H. Wang, *Multi-regge expansions, the generalized optical theorem, and inclusive reactions*, Phys. Rev. D **6**, 2906 (1972), doi:10.1103/PhysRevD.6.2906. (Cited on page 11.)

[100] A. V. Kotikov and L. N. Lipatov, *NLO corrections to the BFKL equation in QCD and in supersymmetric gauge theories*, Nucl. Phys. B **582**, 19 (2000), doi:10.1016/S0550-3213(00)00329-1, hep-ph/0004008. (Cited on page 15.)

[101] V. S. Fadin and R. Fiore, *The Generalized nonforward BFKL equation and the 'bootstrap' condition for the gluon Reggeization in the NLLA*, Phys. Lett. B **440**, 359 (1998), doi:10.1016/S0370-2693(98)01099-5, hep-ph/9807472. (Cited on page 18.)

[102] D. Yu. Ivanov, M. I. Kotsky and A. Papa, *The impact factor for the virtual photonto light vector meson transition*, The European Physical Journal C **38**(2), 195–213 (2004), doi:10.1140/epjc/s2004-02039-4. (Cited on page 20.)

[103] D. Yu. Ivanov and A. Papa, *Electroproduction of two light vector mesons in the next-to-leading approximation*, Nuclear Physics B **732**(1-2), 183–199 (2006), doi:10.1016/j.nuclphysb.2005.10.028. (Cited on page 20.)

[104] D. Yu. Ivanov and A. Papa, *Electroproduction of two light vector mesons in next-to-leading BFKL: study of systematic effects*, The European Physical Journal C **49**(4), 947–955 (2007), doi:10.1140/epjc/s10052-006-0180-8. (Cited on page 20.)

[105] D. Yu. Ivanov, B. Murdaca and A. Papa, *The $\gamma^*\gamma^*$ total cross section in next-to-leading order BFKL and LEP2 data*, JHEP **10**, 058 (2014), doi:10.1007/JHEP10(2014)058, 1407.8447. (Cited on page 20.)

[106] F. G. Celiberto, *Hunting BFKL in semi-hard reactions at the LHC*, Eur. Phys. J. C **81**(8), 691 (2021), doi:10.1140/epjc/s10052-021-09384-2, 2008.07378. (Cited on pages 20, 34, and 53.)

[107] F. G. Celiberto, D. Yu. Ivanov, B. Murdaca and A. Papa, *High energy resummation in dihadron production at the LHC*, Physical Review D **94**(3) (2016), doi:10.1103/physrevd.94.034013. (Cited on pages 20, 32, 34, and 68.)

[108] F. G. Celiberto, D. Yu. Ivanov, B. Murdaca and A. Papa, *Dihadron production at LHC: BFKL predictions for cross sections and azimuthal correlations* (2017), doi:10.1063/1.4977161. (Cited on pages 20, 32, 34, and 68.)

[109] F. G. Celiberto, D. Yu. Ivanov, B. Murdaca and A. Papa, *Dihadron production at the LHC: full next-to-leading BFKL calculation*, The European Physical Journal C **77**(6) (2017), doi:10.1140/epjc/s10052-017-4949-8. (Cited on pages 20, 32, 34, and 68.)

[110] R. Boussarie, B. Ducloué, L. Szymanowski and S. Wallon, *Forward J/ψ and very backward jet inclusive production at the LHC*, Physical Review D **97**(1) (2018), doi:10.1103/physrevd.97.014008. (Cited on page 20.)

[111] A. D. Bolognino, F. G. Celiberto, D. Yu.. Ivanov, M. M. A. Mohammed and A. Papa, *Hadron-jet correlations in high-energy hadronic collisions at the LHC*, The European Physical Journal C **78**(9) (2018), doi:10.1140/epjc/s10052-018-6253-7. (Cited on page 20.)

[112] A. D. Bolognino, F. G. Celiberto, D. Yu. Ivanov, M. M. A. Mohammed and A. Papa, *Inclusive hadron-jet production at the LHC* (2019), 1902.04511. (Cited on page 20.)

[113] A. D. Bolognino, F. G. Celiberto, D. Yu. Ivanov, M. M. A. Mohammed and A. Papa, *High-energy effects in forward inclusive dijet and hadron-jet production* (2019), 1906.11800. (Cited on page 20.)

[114] F. G. Celiberto, D. Yu. Ivanov and A. Papa, *Diffractive production of Λ hyperons in the high-energy limit of strong interactions*, Phys. Rev. D **102**, 094019 (2020), doi:10.1103/PhysRevD.102.094019, 2008.10513. (Cited on page 20.)

[115] K. Golec-Biernat, L. Motyka and T. Stebel, *Forward Drell-Yan and backward jet production as a probe of the BFKL dynamics*, Journal of High Energy Physics **2018**(12) (2018), doi:10.1007/jhep12(2018)091. (Cited on page 20.)

[116] M. Deak, A. van Hameren, H. Jung, A. Kusina, K. Kutak and M. Serino, *Calculation of the Z+ jet cross section including transverse momenta of initial partons*, Physical Review D **99**(9) (2019), doi:10.1103/physrevd.99.094011. (Cited on page 20.)

[117] F. G. Celiberto, D. Yu. Ivanov, B. Murdaca and A. Papa, *High-energy resummation in heavy-quark pair photoproduction*, Phys. Lett. B **777**, 141 (2018), doi:10.1016/j.physletb.2017.12.020, 1709.10032. (Cited on page 20.)

[118] A. D. Bolognino, F. G. Celiberto, M. Fucilla, D. Yu. Ivanov, B. Murdaca and A. Papa, *Inclusive production of two rapidity-separated heavy quarks as a probe of BFKL dynamics*, PoS **DIS2019**, 067 (2019), doi:10.22323/1.352.0067, 1906.05940. (Cited on page 20.)

[119] A. D. Bolognino, F. G. Celiberto, M. Fucilla, D. Yu. Ivanov and A. Papa, *High-energy resummation in heavy-quark pair hadroproduction*, Eur. Phys. J. C **79**(11), 939 (2019), doi:10.1140/epjc/s10052-019-7392-1, 1909.03068. (Cited on page 20.)

[120] A. Sabio Vera, *The Effect of NLO conformal spins in azimuthal angle decorrelation of jet pairs*, Nucl. Phys. B **746**, 1 (2006), doi:10.1016/j.nuclphysb.2006.04.004, hep-ph/0602250. (Cited on pages 26 and 46.)

[121] A. Sabio Vera and F. Schwennsen, *The Azimuthal decorrelation of jets widely separated in rapidity as a test of the BFKL kernel*, Nucl. Phys. B **776**, 170 (2007), doi:10.1016/j.nuclphysb.2007.03.050, hep-ph/0702158. (Cited on pages 26 and 46.)

[122] A. D. Bolognino, F. G. Celiberto, D. Yu. Ivanov, M. M. Mohammed and A. Papa, *Hadron-jet correlations in high-energy hadronic collisions at the LHC*, Eur. Phys. J. C **78**(9), 772 (2018), doi:10.1140/epjc/s10052-018-6253-7, 1808.05483. (Cited on page 27.)

[123] A. D. Bolognino, F. G. Celiberto, D. Yu. Ivanov, M. M. Mohammed and A. Papa, *Inclusive hadron-jet production at the LHC*, Acta Phys. Polon. Supp. **12**(4), 773 (2019), doi:10.5506/APhysPolBSupp.12.773, 1902.04511. (Cited on page 27.)

[124] A. Buckley, J. Ferrando, S. Lloyd, K. Nordström, B. Page, M. Rüfenacht, M. Schönherr and G. Watt, *LHAPDF6: parton density access in the LHC precision era*, Eur. Phys. J. C **75**, 132 (2015), doi:10.1140/epjc/s10052-015-3318-8, 1412.7420. (Cited on pages 34 and 53.)

[125] S. Albino, B. A. Kniehl and G. Kramer, *AKK Update: Improvements from New Theoretical Input and Experimental Data*, Nucl. Phys. B **803**, 42 (2008), doi:10.1016/j.nuclphysb.2008.05.017, 0803.2768. (Cited on page 34.)

[126] M. Hirai, S. Kumano, T. H. Nagai and K. Sudoh, *Determination of fragmentation functions and their uncertainties*, Phys. Rev. D **75**, 094009 (2007), doi:10.1103/PhysRevD.75.094009, hep-ph/0702250. (Cited on page 34.)

[127] V. Del Duca and C. R. Schmidt, *Mini - jet corrections to Higgs production*, Phys. Rev. D **49**, 177 (1994), doi:10.1103/PhysRevD.49.177, hep-ph/9305346. (Cited on page 41.)

[128] V. Khachatryan *et al.*, *Azimuthal decorrelation of jets widely separated in rapidity in pp collisions at* $\sqrt{s}$ = 7 *TeV*, JHEP **08**, 139 (2016), doi:10.1007/JHEP08(2016)139, 1601.06713. (Cited on pages 45 and 58.)

[129] R. Bonciani, S. Catani, M. L. Mangano and P. Nason, *Sudakov resummation of multiparton QCD cross-sections*, Phys. Lett. B **575**, 268 (2003), doi:10.1016/j.physletb.2003.09.068, hep-ph/0307035. (Cited on page 48.)

[130] P. Nason, *A New method for combining NLO QCD with shower Monte Carlo algorithms*, JHEP **11**, 040 (2004), doi:10.1088/1126-6708/2004/11/040, hep-ph/0409146. (Cited on page 52.)

[131] J. M. Campbell, R. K. Ellis, R. Frederix, P. Nason, C. Oleari and C. Williams, *NLO Higgs Boson Production Plus One and Two Jets Using the POWHEG BOX, MadGraph4 and MCFM*, JHEP **07**, 092 (2012), doi:10.1007/JHEP07(2012)092, 1202.5475. (Cited on page 52.)

[132] L. Harland-Lang, A. Martin, P. Motylinski and R. Thorne, *Parton distributions in the LHC era: MMHT 2014 PDFs*, Eur. Phys. J. C **75**(5), 204 (2015), doi:10.1140/epjc/s10052-015-3397-6, 1412.3989. (Cited on page 53.)

[133] V. Del Duca, W. Kilgore, C. Oleari, C. R. Schmidt and D. Zeppenfeld, *Kinematical limits on Higgs boson production via gluon fusion in association with jets*, Phys. Rev. D **67**, 073003 (2003), doi:10.1103/PhysRevD.67.073003, hep-ph/0301013. (Cited on page 75.)